Department of Precision and Microsystems Engineering

Overhang constraint in topology optimisation for additive manufacturing: a density gradient based approach

A. M. Driessen

Report no : EM 2016.007
Coach : dr.ir. M. Langelaar
Professor : prof.dr.ir. A. van Keulen
Specialisation : Engineering Mechanics
Type of report : MSc thesis
Date : 9-2-2016

Overhang constraint in topology optimisation for additive manufacturing

a density gradient based approach

by

A.M. Driessen

to obtain the degree of Master of Science
at the Delft University of Technology,
to be defended publicly on Tuesday February 9, 2016 at 4:00 PM.

Thesis committee:	dr.ir. M. Langelaar,	TU Delft, supervisor
	prof.dr.ir. A. van Keulen,	TU Delft
	dr.ir. M.A.N. Hendriks,	TU Delft
	dr.ir. R.A.J. van Ostayen,	TU Delft

TU Delft

Abstract

This research aims at improving the synergy between 3D printing and topology optimisation. 3D printing, more formally known as additive manufacturing, forms an object by constructing successive layers on top of each other. This procedure of manufacturing offers new possibilities due to the improved design freedom. Topology optimisation is a mathematical design tool that finds the optimal material distribution for a specified problem. Usually the generated optimal designs have a complex shape which are difficult to produce with traditional manufacturing techniques, and post-processing of the design is necessary in order to obtain a manufacturable design. Additive manufacturing makes most of this post-processing redundant due to its unprecedented manufacturing abilities. However, despite the greatly improved design freedom, certain geometric restrictions are encountered in popular additive manufacturing techniques like selective laser melting (SLM). Amongst others, designs need to be self-supporting in order to guarantee a successful production. The best way to deal with this is to incorporate an overhang restriction directly into the topology optimisation, such that optimal designs are generated that also comply with this manufacturing constraint.

Existing work on eliminating overhang from topology optimised designs does not consider the orientation of the part in the build chamber of the SLM machine. The methods described in literature implicitly assume a fixed build orientation a priori, which makes them not very suitable for the consideration of this orientation. However, the build orientation is of great importance with respect to optimisation of overhang free designs, since a properly oriented part can be made free of overhang with less design modifications and thus corresponds more to the original optimum.

This research investigates an approach based on the gradient of the density field used in topology optimisation for the optimisation of self-supporting designs, which should also be suitable for the incorporation of the build direction during the optimisation. A strategy to approximate the density gradient is found and an overhang constraint is formulated. The constraint is implemented in a minimal compliance topology optimisation algorithm and tested on numerical examples. Different implementations of the overhang constraint are investigated.

As a first approach, the individual overhang constraints are directly imposed on the problem. This approach is extended by a relaxation method, and by a filtering and thresholding procedure in order to ease the problem at the initial stages of the optimisation. Furthermore, the complexity of the optimisation problem is reduced by considering aggregation of the individual constraints. Finally, a novel method for the inclusion of the optimal build orientation directly into the optimisation is devised and tested.

It is found that the many individual overhang constraints complicate the optimisation. As a consequence, convergence to a recognizable structure failed. The resulting final topologies consisted mainly of elements of intermediate density. The proposed relaxation method succeeded in mending the problem and clearer yet overhang-free designs were obtained. Also, the filtering and thresholding method resulted in distinguishable structures. However, for these methods carefully set up continuation schemes are indispensable which make the optimisation slow and fragile. The aggregation of the individual constraints into one global constraint also improved the results. Clearer structures were obtained without the need for continuation. On the density gradient based overhang constraint in general, it was discovered that this method has the weakness to allow support structures that become less dense in the vertical direction.

The novel method to include also the build orientation showed promising first results. The method is efficient and the numerical examples returned a combination of a structure and build orientation such that the overhang constraint is satisfied.

The density gradient based overhang constraint is shown to be suitable for the inclusion of optimal build orientation into the topology optimisation in an efficient way. Problems concerning the convergence, fully dense support structures and a more accurate density gradient remain a challenge. More research should be carried out to develop a fully satisfactory method.

Acknowledgements

This thesis is the final part of my study mechanical engineering at Delft university of technology. I would like to use this opportunity to express my appreciation for a few people.

First of all, I would like to thank my supervisor, Matthijs Langelaar, for your help, creative suggestions and useful feedback during my graduation project. Our regular meetings gave me renewed inspiration and motivation to continue.

I also want to thank my friends at the department of PME. A lot of time we have spent together at university. I could not have wished for better company during the lunch and coffee breaks. I feel lucky to have shared so many experiences with you the last two and a half years.

A special thanks goes out to my girlfriend, Kiki, for the encouragements and the welcome distraction you provided. Finally, I want to thank my family. In particular I am grateful to my parents, for all your support, the opportunities that you have given me, and the fact that I can always count on you.

Contents

1 Introduction

Additive manufacturing or 3D-printing is an emerging technology that opens many new possibilities. Additive manufacturing started about 30 years ago as a technology to rapidly produce prototypes. Since then, the developments followed each other quickly. Many different print techniques have been developed. Also, the developments resulted in a broad variety of materials suitable for additive manufacturing, such as: plastics, metals and ceramics. The improvements on the process and the better quality of the printed material made it possible to also print functional parts.

The additive manufacturing process is characterised by the layer-by-layer construction of the part. A 3D computer model is cut into thin slices and translated to patterns of the cross-sections. Starting from the bottom, the slices are printed on top of each other. This way of manufacturing allows very complex geometries to be made that are not possible to make with other techniques or at a much higher cost. Other advantages are the flexible production and individualisation of products [14]. Additive manufacturing is less suited for mass production because it is a relatively slow process. However, for small or medium batch production metal additive manufacturing can be economically competitive to traditional techniques [4].

Fields of application are for example the automotive, aviation and space industries, were complex shaped parts can be used for increased performance. In the medical field additive manufacturing is very well suited for the fabrication of prostheses, because these have typically a complex shape and are individual. The introduction of the desktop 3D-printer gave the wide public direct access to this new technology, allowing consumers to manufacture self-designed products or download designs from the internet to be printed at home. Although, so far 3D-printing at home seems to remain something for hobbyists. Unlike the domestic 3D-printers that use plastic as build material, industry is mostly interested in additive manufacturing techniques that print parts out of metal. One such process is selective laser melting (SLM).

For some applications additive manufacturing is already applied in industry. However, the technology is still far from fully matured. Academia and industry is conducting more research to develop the process ever further.

To benefit most from additive manufacturing, the products should be designed with the new possibilities kept in mind. A new design begins with specifying the requirements of the desired product. Always, there will be conflicting interests, and a trade-off needs to be made. Therefore, it is not straightforward what the optimal design is. Optimisation techniques are used to find the design that makes the best trade-off for optimal performance.

A relatively new but extremely rapidly expanding field of optimisation in structural and continuum mechanics is called topology optimisation. Topology optimisation is a mathematical design tool that finds the material distribution for the best performance. For example, the structure that gives the highest stiffness for a limited amount of available material. Topology optimisation is sometimes referred to as a free-from design technique due to the often natural-looking shapes it generates. Consequently, the optimal designs exhibit very complex geometries for manufacturing. The main advantage of topology optimisation is the little designers input that is required. No assumptions on the shape a priori are necessary. However, after optimisation manual post-processing of the design is usually necessary. Addi-

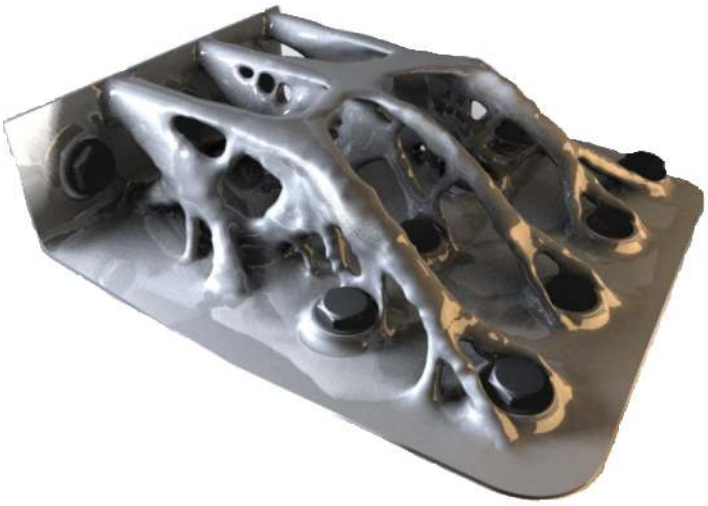

Figure 1.1: Example of a complex shaped part that is effortlessly produced with selective laser melting (SLM). The part is a topology optimised aerospace bracket and shows the match between topology optimisation and additive manufacturing. [8].

tional requirements on, for example, the manufacturability need to be incorporated. Post-processing of designs is disadvantageous because the changes to the optimal design lower its performance. Therefore, topology optimisation techniques are constantly improved to also incorporate post-processing steps directly in the optimisation.

The unprecedented manufacture abilities of additive manufacturing make most of the manufacturability issues of the complex shaped topology optimised designs redundant. Therefore, the post-processing can be significantly reduced, resulting in parts closer to the optimal design and thus a better performance. Design for additive manufacturing could use topology optimisation to benefit most from the advantages of additive manufacturing, because the natural-looking shapes are particularly suitable to be made with additive manufacturing. This synergy of additive manufacturing and topology optimisation was already recognized by many others, e.g. [8, 34]. In Figure 1.1 an additive manufactured aerospace bracket that was designed with topology optimisation is shown as an example. Research is performed to make the compatibility between topology optimisation and additive manufacturing even better.

One of the major manufacturing constraints of SLM is the inability to print unsupported material. Investigations to the selective laser melting process have identified that overhanging surfaces up to an angle of about 45° cannot be properly printed [33]. This project investigates methods to extend topology optimisation by incorporating this SLM-specific manufacturing constraint. The elimination of overhang should result in directly manufacturable designs. Thereby, reducing post-processing costs and increasing the performance by closer to optimal products.

In Figure 1.2 the structure of this report is captured in a schematic. The next chapter, Chapter 2, gives a study on relevant literature. In this chapter existing work on the topic is reviewed and topics for possible improvements identified. Based on the findings from literature, in Chapter 3 the research question and goals of this project are formulated. In Chapter 4 the basis for this report is laid down by introducing the basis for the new overhang restriction. Then, the different aspects of the research approach are described in Chapter 5. The report continues with the implementation of the manufacturing constraint using different formulations in Chapters 6 and 7. In Chapter 8 another very important aspect of the overhang constraint, the build direction, is considered. Each of these chapters contains the formulations, results and a discussion. A more general discussion on the proposed method is given in Chapter 9. Finally, in Chapter 10 the conclusions of the project are drawn and recommendations for future research are made.

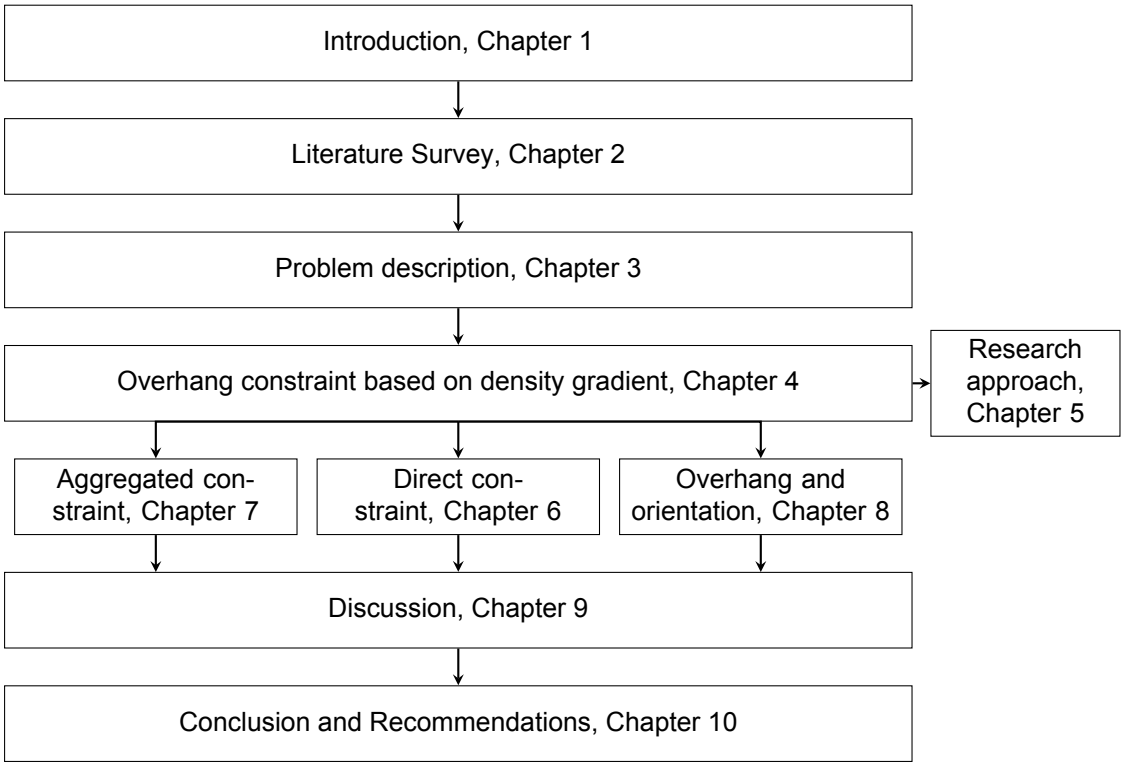

Figure 1.2: The structure of this report schematically represented.

2

Literature Survey

This chapter gives a condensed overview of concepts and techniques found in literature relevant to this thesis on topology optimisation and additive manufacturing. For a more in-depth discussion, readers are referred to the full literature review [12]. Readers familiar with these topics can move directly to Chapter 3.

2.1. Topology optimisation

Topology optimisation is a technique to find the optimal distribution of material in space and also involves the determination of features such as the number, location and shape of holes [6]. Different approaches to topology optimisation have been developed, of which the density based methods are most commonly used. In the density based approach the design domain is discretized using finite elements. Every finite element is assigned a design variable x_e that defines whether the element belongs to the material domain or not. The optimal topology is found by determining which elements should be in the material domain $x_e = 1$ and which should not $x_e = 0$. Typically, this discrete formulation is relaxed to attain a continuous form of the problem. Then, some kind of interpolation model is used to steer the solution to discrete values. These continuous design variables can be interpreted as the density of the material at the element.

A typical topology optimisation problem that is often used in research because of its relative simplicity is the minimisation of the compliance with a constraint on the available material. This problem is commonly solved with the SIMP (solid isotropic material with penalisation) material interpoloation, by Bendsøe and Sigmund [6]. It uses a penalised stiffness model for the interpolation of the elasticity modulus, as in Equation (2.1):

$$E_e(x) = x_e^p E_0. \tag{2.1}$$

Here, $E_e(x)$ is the elastic modulus in element e, x are the design variables or densities of the elements, E_0 is the elastic modulus of a solid element and p is the penalisation parameter. In SIMP the penalisation parameter is chosen larger than one, typically $p = 3$. This interpolation technique effectively makes intermediate densities unfavourable because of their relatively low stiffness compared to the density.

The described approach to topology optimisation is prone to problems of checker-boards and mesh-dependency. Much research has been performed on methods to deal with these issues. Checker-boarding refers to the appearance of alternating solid and void elements ordered in a checker-board like fashion. Overestimation of the stiffness of checker-boards due to bad numerical modelling was shown to be the reason [30]. Mesh-dependency is encountered at refining the mesh. Mesh refinement results in substantial different structures with smaller structural features, whereas only a more accurate finite element modelling and more detailed boundary information was intended. Many different prevention techniques to cope with these problems have been proposed in literature. Most of these methods can roughly be divided into one of two categories: mesh-independent filtering methods and constraint methods. The former group being the most popular due to efficiency and ease of implementation [29].

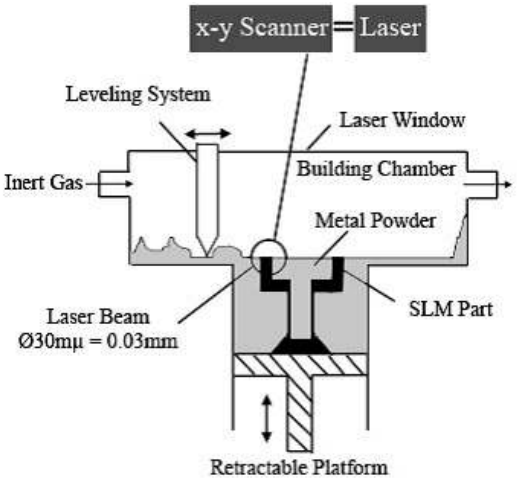

Figure 2.1: Schematic of the Working principle of the selective laser melting process [33].

2.2. Additive manufacturing

2.2.1. Operating principle

Additive manufacturing for functional metal parts is based on methods that work by fully melting a metal powder [16]. Examples of such processes are selective laser melting, electron beam melting and laser metal deposition. The basic working principle of the selective laser melting process is shown in Figure 2.1. The part is built on a vertically moveable platform or base plate. A layer of metal powder is deposited and spread out by a wiper or roller. Then, the high power laser scans the 2D pattern of the cross-section, obtained from the computer model, in the powder bed for it to melt. The melted powder solidifies and forms a slice of the part. After scanning, the platform is lowered by the height of one layer and the cycle repeats. The operating principle of the other two processes is very similar, the difference being the energy source and the layer creation method respectively. The high energetic sources are powerful enough to completely melt the powder, resulting in parts that are fully dense. The mechanical properties of the solidified material is found to be comparable to that of bulk material [16, 36]. Therefore, these additive manufacturing processes are well suited for the production of functional parts.

2.2.2. Restrictions

The main advantage of additive manufacturing is its superior ability to produce complex shaped structures. However, there are limitations to the process regarding the manufacturability. Identifying these limitations is a recurring topic in literature. The Direct Manufacturing Research Center (DMRC), collaboration between industry and the University Paderborn, published a catalogue of design rules for different additive manufacturing techniques, including SLM, which ensures a robust design for manufacturing [1]. In [33] a study on the manufacturing constraints specifically focused on the SLM process is performed. It can be concluded that currently the most prominent restrictions of the SLM process are the minimum feature size and overhanging surfaces.

The minimum feature size restriction of structural parts is mainly determined by the hardware of the machine, primarily laser beam diameter. The minimum size of slots and holes is dependent on both hardware and machine settings.

With overhanging surfaces are meant downward facing surfaces of the structure that have an angle relative to the base plate that is smaller than a certain critical angle. In literature different numbers for the critical angle are mentioned, ranging from $20°$ to $45°$ [19, 33, 36]. The differences in machines, process parameters and/or material properties are presumably the cause. Overhanging surfaces are said to be not self-supporting, and can therefore not be build without serious defects. The failure of overhanging surfaces is explained by the heat flow during the build. The energy of the high power laser is converted into heat in order to melt the metal powder. Sufficiently supported layers will transfer the heat into the bulk material mainly by conduction [5, 18, 26]. A powder supported layer is unable to dissipate the heat form the laser beam because the lower heat conductivity of the metal powder. The

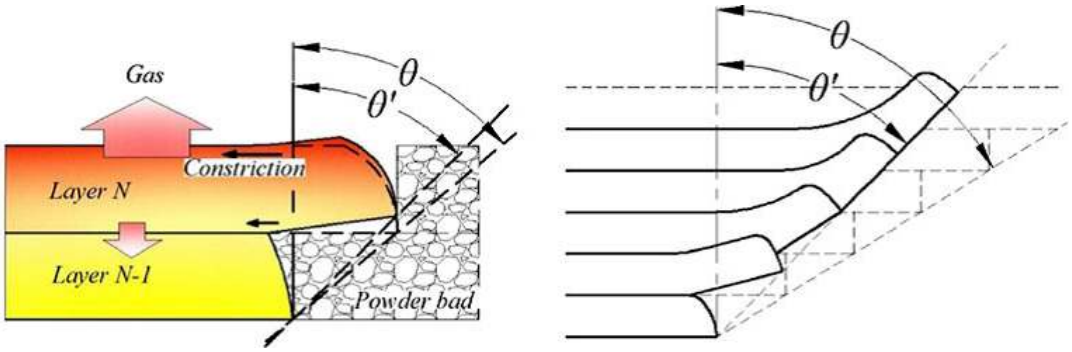

Figure 2.2: Due to the large temperature gradients during the SLM process, thermal streses cause the structure to deform. Left figure: The intended inclined angle θ is not accurately printed. Due to warp, the actual inclined angle is larger θ'. Right figure: Accumulation of warp can result in serious deformations and can even upset the operation of the machine. [38]

powder can have a thermal conductivity that is 100 times lower than solid material [38]. The energy of the laser cannot escape quickly enough, resulting in a larger melt pool and local overheating. Owing to the rapid heating of the upper surface by the laser beam and the rather slow heat conduction a steep temperature gradient develops. Local overheating and the large temperature gradients have negative effects on the porosity, surface roughness, micro-structure and residual stresses [35]. Gravity and capillary forces cause the large pool of melted metal to sink into the powder bed and dross will be formed underneath an overhanging slope [38]. Thermal stresses can cause deformation during the build, called warp. Due to warp, the designed angle is not accurately printed, see left image of Figure 2.2. The accumulation of warp, right image of Figure 2.2 might even upset the powder levelling system, forcing the operation to be terminated. Unwanted residual stresses can cause deformations or cracks when the part is disconnected from the base plate and affects the strength.

2.2.3. Current solution methods

The minimum feature size limitation is not specifically for additive manufacturing but is also encountered in milling and turning. Multiple methods already exists to deal with this issue in topology optimisation. The manufacturing constraint is incorporated directly in the topology optimisation problem, this is done in for example [15, 25, 29].

To avert the above described defects caused by insufficient heat conduction, support structures are commonly applied. A support structure is additional material that solely serves to prevent manufacturing errors. As it does not belong to the actual product, it has to be removed, often manually, after completion. The geometric freedom of designs is restricted because support material should be accessible for removal. Other negative effects of support material include the extra waste material and extended build time.

Research is conducted to apply support material in a smart manner. Support structures are designed to minimize material usage, reduce the build time or improve the structural support [11, 18]. Others also considered the influence of the build direction on the need for support material [9, 31]. The build direction refers to the orientation of the product in the build chamber. A smart rotation can strongly reduce the amount of overhang.

It is currently being investigated to improve the SLM process, such that is is capable of manufacturing overhanging structures and eliminate the need for support material. By regulating the machine settings, for example the laser power or scanning speed, more control over the process can be acquired. This possibility is investigated by modelling the manufacturing process [5, 17, 22, 37] and in practical studies [10, 11, 38, 39].

A different approach that is followed to eliminate the need for support material is to treat overhang as a manufacturing constraint and alter designs such that they comply with this constraint. Leary *et al.* [19] developed an automated process that first identifies critical regions in an optimised design and then, automatically designs additional members to make the design self-supporting.

Following the methods for the minimum feature size constraint, two studies have been published that incorporate overhang as a manufacturing constraint directly in the optimisation process [13, 28]. Serphos [28] defines overhang in a regular mesh of 4-node square elements, as an element that has

(a) Multiple objective (b) Global constraint (c) Filter

Figure 2.3: Results obtained from the different methods investigated in [28]. The test structure is the cantilever beam clamped at the left and loaded in the right lower corner. The multiple objective and global constriant method, subfigures a and b, did not successfully eliminate all overhang. The overhang filter did result in a self-supporting design, but cnvergence issues resulted in a greyish topology.

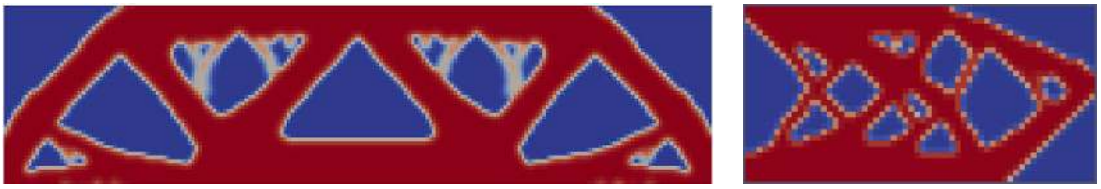

(a) MBB beam (b) Cantilever beam

Figure 2.4: Results of the anti-overhang projection method intorduced by [13]. The results show self-supporting optimal designs. However, the MBB beam shows support structures that are not fully dense.

a greater density than the maximum of the three adjacent elements in the row below. This definition is used in a multiple objective formulation, as a global constraint and by means of a filter operation. Results of the three methods are given in Figure 2.3. In the work of Gaynor and Guest [13] a projection scheme is set up to make the design self-supporting at every iteration. A wedge of underlying elements is considered to check for adequate support. Then, the density field is projected such that material at elements that are not supported is removed and the density of the supported elements remains. Figure 2.4 shows results from this method. The two studies are quite comparable, both use an underlying base of elements to check for adequate support and go through the rows of the density field sequentially. These methods give promising first results, design are found that largely eliminate the overhang. However, improvements are necessary. Both methods are reported to suffer from convergence issues. The sensitivity analysis in [28] was reported to be very computationally expensive, the multiple objective and global constraint were not able to fully eliminate all overhang and the filtering method gives designs that are made of intermediate densities. The results from [13] show support structures made of elements with intermediate densities. Furthermore, both methods only consider 2 dimensional problems. For applicability in real life the methods should be extended to 3D.

3

Problem description

From the literature survey, Chapter 2, the synergy between topology optimisation and additive manufacturing is confirmed. Additive manufacturing can be benefited from most when the design exploits the free-form build process. At the same time, topology optimised designs need significantly less post-processing in order to be manufacturable if additive manufacturing is used.

The process of metal additive manufacturing techniques that fully melts the powder, such as SLM, are suitable in industry for the production of functional parts. Although, SLM can print almost anything, some manufacturing constraints remain. One of the most prominent restrictions of these processes regarding manufacturability concerns overhanging surfaces. It is important to eliminate overhang from designs because currently it is not possible to correctly print them.

Sacrificial support structures are momentarily often used. Support structures however increase material usage and build time, introduce manual labour for removal and restrict geometric design freedom related to removal. Work on how to apply support structures in a smart manner aimed at reducing the negative effects by optimising the design of support structures and considering more favourable build directions help, although the need for support structures is in general not entirely resolved. Design modifications to critical regions, either manually or automated, are used to eliminate the need for sacrificial support material. Unlike the other approach, this method does completely avoid the use of sacrificial support material. However, post-optimisation design modifications result in a final component that does not correspond to the optimum design, leading to sub-optimal performance. Instead of modifying the design after optimisation, incorporating an overhang restriction method directly during the design optimisation is preferable. The final design will be optimal given the constraint on manufacturability. Some attempts to incorporate the overhang restriction directly into the optimisation process were already made by [13, 28]. These attempt showed promising first results. However, besides the reported issues concerning convergence and not completely supported designs, other improvements on these overhang restriction method are essential.

The method described in [28] utilises the properties of the regular mesh for the formulation of overhang. As such, this method is only applicable on this regular mesh and only suitable for a critical overhang angle of $45°$. In Chapter 2 it was shown that the critical overhang angle is very dependent on all kind of influences. An overhang restriction method should therefore ideally be suitable for an arbitrary critical angle. In [13] the mesh-dependency is overcome by using a mesh-independent wedge of elements to check adequate support, instead of the three adjacent elements in the underneath row. Also, the critical angle can be chosen arbitrarily by changing the shape of the wedge. However, both the existing methods consider some set of elements underneath the considered element. In this way the build direction is implicitly assumed a priori. This makes these methods less suitable for the consideration of orientation. The orientation is an important aspect to be taken into account, as was seen in the methods to reduce the need for support structures.

An improved method for overhang constraints should improve the shortcomings of the current methods. Thereby, allowing for a continuously adjustable overhang angle, resulting in crisp and fully supported designs and, above all, be easily adjustable for different build directions such that the orientation can be readily considered. To include the build direction, the overhang restriction formulation should not be orientation dependent. The gradient of the density field could be a useful property to be used

in such a formulation. This property is intrinsic to the density field and therefore generally applicable. The idea of using gradient information of the density field to formulate an overhang constraint was hinted in [28] as ” the continuous nature of topology optimisation ”. However, in [28] it was opted for a more pragmatic approach using the discrete nature of topology optimisation. In principle this approach should function very well but suffers from the explained shortcomings.

In this research the suitability of the gradient of the density field will be considered for use in an overhang restriction method that also considers the build direction. The question that will be answered in this research is:

> *How can the gradient of the density field be applied in a constraint on overhang for density based topology optimisation and is this approach suitable for optimisation of the build direction?*

The overhang constraint should also be applicable for optimisation problems in 3 dimensions. The concept of the density gradient based constraint is easily extended 3 dimensional problems. However, to limit the scope of this research only 2 dimensional cases will be considered in this report.

4

Overhang constraint based on density gradient

A suitable overhang constraint based on the gradient of the density field will be derived in this chapter. It will be demonstrated that the constraint is usable for the identification of overhang and thus suitable for use in topology optimisation. This chapter starts with a discussion on methods that can be used to obtain the gradient of the density field.

4.1. Density of the gradient field

The overhang constraint is a geometric restriction on the topology. All boundaries between the material domain and void should be oriented such that they have an angle with respect to the base plate of at least the critical angle, typically $45°$, for the design to be self-supporting. In order to formulate such a constraint a property of the geometry must be used that could identify both this boundary and the orientation. For this, the density of the gradient field seems particularly suited. Indeed, the length of this gradient is a measure that indicates whether a boundary is present and the orientation of the gradient can directly be applied to find its orientation. In Figure 4.1 a typical density field resulting from a density based topology optimisation is displayed. In the blue encircled detail the gradient of the density field is shown, how the gradient is obtained is the subject of the next section. It can be seen that the gradients at the boundary are the biggest. Furthermore, the direction of the gradient is perpendicular to this boundary. By linking it to a known reference vector, red arrow, the relative angle of the boundary is identified. But, before the gradient of the density field can be used in a overhang constraint formulation, the gradient should be defined.

In density based topology optimisation the density field is discretised and the density in each element is typically constant. As such, the density field is no longer a continuous field. However, in order to find a gradient the density distribution is assumed to be continuous, such that a gradient exists. The gradient of the density field could now be approximated by taking the difference in density of adjacent pixels and dividing this by the distance between them. This should be done for the horizontal and vertical direction to obtain the horizontal and vertical component of the gradient respectively. It should be taken in mind that the diagonally neighbouring elements also provide support. These elements should also have a contribution in the components of the gradient. This is similar as calculating the gradient with a finite difference approach. In this research a commonly used density based topology optimisation Matlab code will be used [3]. This algorithm uses a mesh of square 4-node elements for the discretisation of the density field. For now the method should be as simple and straightforward as possible. Therefore, taking advantage of this highly regular mesh is justified. The mesh of square quadrilaterals resembles the pixels in a digital image, with the density as an equivalent for the pixel intensity. Computer vision and digital processing tools frequently use the gradient to extract information from images or improve their quality by for instance edge enhancement. In digital image processing the gradient of the pixel intensity is obtained by means of special kernels that are convolved with the image. Many different kernels have been suggested in literature, but effectively every kernel calculates the first derivative

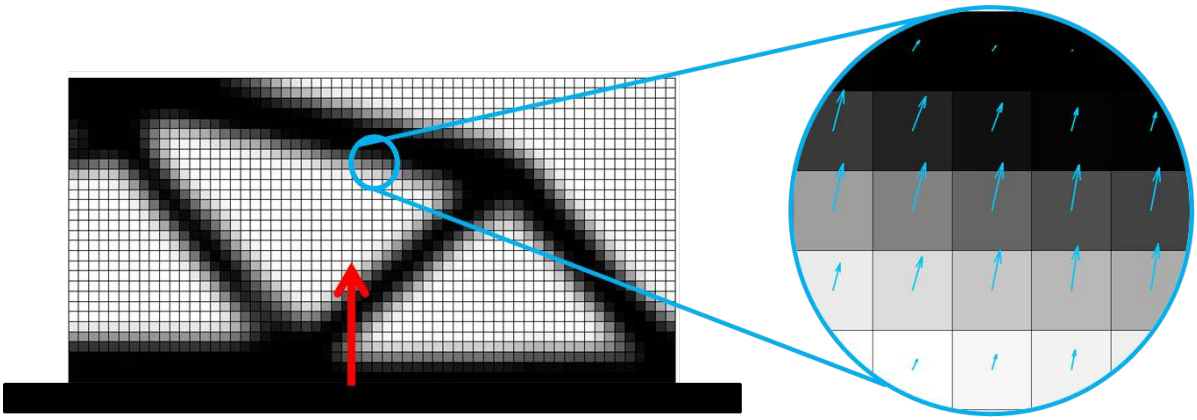

Figure 4.1: Hypothetical optimised structure on the base plate of a SLM machine. The red arrow indicates the build direction. The detail shows a part of the density field with approximated gradients of the density field. The gradients point in the direction of increasing density and indicate where boundaries of the structure lie and what the orientation of the boundary is.

of the pixel intensity. One kernel is used for the horizontal component of the gradient. The vertical component of the gradient is obtained from a kernel which is a rotated version of the horizontal kernel. The gradient for a density field obtained this way is given by Equation (4.1):

$$\nabla \mathbf{x} = \begin{bmatrix} \mathbf{K}_x \star \mathbf{x} \\ \mathbf{K}_y \star \mathbf{x} \end{bmatrix}. \tag{4.1}$$

Where, $\nabla \mathbf{x}$ is the gradient of the density field and $\mathbf{K}_{\{\cdot\}} \star \mathbf{x}$ is the convolution of the gradient operator and the density field. A different way to look at the convolution is to consider it as a high pass filter operation. This can be seen by noting that tonal details of an image are regions of similar intensity (low spatial frequency) and will result in a low or zero output. Conversely, edges (high spatial frequency) will give a large output. Important properties of a gradient kernel are their size and the ratio between the numeric values. Some of the first and most basic gradient kernels are the Robert cross, Prewitt and Sobel Kernels [7].

4.1.1. Roberts Cross operator

The Roberts cross filter uses a small 2×2 kernel, as shown in Equation (4.2):

$$\mathbf{K_x} = \begin{bmatrix} 1 & 0 \\ 0 & -1 \end{bmatrix}, \qquad \mathbf{K_y} = \begin{bmatrix} 0 & -1 \\ 1 & 0 \end{bmatrix}. \tag{4.2}$$

One issue immediately arises when this kernel is applied for overhang detection. This pair of kernels lacks precise information on the direction of the gradient. Usually, in digital image processing the magnitude of the gradient is more important than its direction. However, the direction of the gradient for overhang detection is crucial. A simple modification as in Equation (4.3) to the original Roberts cross kernel resolves the problem:

$$\mathbf{K_x} = \begin{bmatrix} -1 & 1 \\ -1 & 1 \end{bmatrix}, \qquad \mathbf{K_y} = \begin{bmatrix} 1 & 1 \\ -1 & -1 \end{bmatrix}. \tag{4.3}$$

Due to the size of this kernel the density gradient is calculated at the nodes of the mesh, whereas the density is defined on the centre of each element.

4.1.2. Prewitt and Sobel operator

A different type of kernel is the Prewitt operator. It uses a pair of 3×3 kernels instead of the smaller 2×2 Roberts cross. The Prewitt kernels are given in Equation (4.4):

$$\mathbf{K_x} = \begin{bmatrix} -1 & 0 & 1 \\ -1 & 0 & 1 \\ -1 & 0 & 1 \end{bmatrix}, \qquad \mathbf{K_y} = \begin{bmatrix} 1 & 1 & 1 \\ 0 & 0 & 0 \\ -1 & -1 & -1 \end{bmatrix}. \tag{4.4}$$

The Prewitt kernel measures the difference in density between a pair of three elements spaced one element apart instead of adjacent elements. Conversely to the Roberts cross, this kernel calculates the direction of the gradient more correctly and needs no modification. However, the larger 3×3 kernel causes a blurring of the spatial information, which results in less accurate localized gradients. The blurring effect can be somewhat reduced by weighting the numerical values of the kernel based on distance from the centre. A 3×3 kernel that does this is the Sobel kernel, depicted in Equation (4.5):

$$\mathbf{K_x} = \begin{bmatrix} -1 & 0 & 1 \\ -2 & 0 & 2 \\ -1 & 0 & 1 \end{bmatrix}, \qquad \mathbf{K_y} = \begin{bmatrix} 1 & 2 & 1 \\ 0 & 0 & 0 \\ -1 & -2 & -1 \end{bmatrix}. \tag{4.5}$$

Unlike the Roberts cross, the Prewitt and Sobel kernels define the gradient at the centre element of the kernel. So, the gradient and the density are calculated at the same place. This additional advantage could be convenient in an implementation of a overhang constraint.

4.1.3. Other operators

In literature other gradient operators with better performance have been suggested. Larger gradient operators are known to be less sensitive to noise. These operators are usually extended versions of the earlier discussed Sobel kernel. The size can be made arbitrarily large. Often used sizes are 5×5 or 7×7. A larger kernel is effectively a smoothing filter operation prior to the gradient operation. Although this smoothing has a positive effect on noise, the blurring causes a wide response area, i.e. badly localized edges. Also, large kernels have the tendency to miss small details in an image. Small details can be removed by for instance a minimum feature size filter. In order to be sure that no detail of the density field is missed, the size of a density filter should be at least equal to the size of the gradient operator. In [27] a method for wide support operators is discussed to minimize these negative effects. The high computational requirements are reported to be a major disadvantage. Optimised consistent gradient operators are suggested in [2]. The performance of these operators is claimed to be superior. However, it is outside the scope of this research to find the best working gradient kernel. So, for reasons of simplicity the basic gradient operators will be used in this work. Depending on the formulation of the overhang restriction, the modified Roberts cross (Section 4.1.1) or the Sobel operator (Section 4.1.2) might be more suitable. Next, the gradient will be used in the formulation of the constraint

4.2. Formulation of the overhang constraint

To come to an overhang constraint formulation, let us first consider the properties of the gradient of the density field. The gradient has two characteristics, length and direction. The gradient points in the direction of increasing density. So, in a discrete design the direction of the gradient indicates where the structure exists and what its orientation is. The length says something about the abruptness of the variation in density. That is, a large gradient corresponds to a true boundary and an intermediate value of the length is a region where the structure has not yet clearly formed. Ideally, the end design has only true boundaries. In that case all gradients have to be either zero or maximal, solid or void or a boundary respectively. The density gradient needs to be compared to a reference vector in order to say something about its orientation. Since the angle relative to the base plate of the SLM machine needs to be controlled, the reference vector should be linked to the base plate. The build direction is the direction perpendicular to the base plate pointing upward. This direction is used as the reference direction. For clarification, looking back at Figure 4.1. The red arrow indicates the build direction of the part in the SLM machine. In the detail on the right the density field shows that the length of the gradient increases at a boundary and that the orientation of the gradient is perpendicular to this boundary. The gradients are computed with the 3×3 Sobel operator, hence the gradients are given at the centre of the elements. It is again verified that the density gradient contains everything required for an overhang constraint.

Preferably, the constraint is as simple as possible. A linear constraint would be very beneficial for an optimisation. So, as a first suggestion for a constraint, the inner-product of the gradient with the reference vector comes to mind. This inner-product will be positive if more material is placed on top of less material. Furthermore, the constraint values increase in value with the length of the gradient. This means that in regions of intermediate density, small gradients, the constraint is less strongly present and at true boundaries, large gradients, the constraint values increase. The inner-product should be

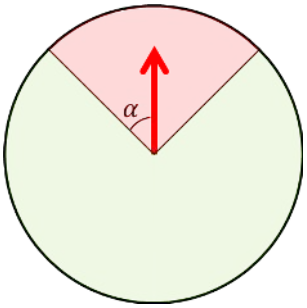

Figure 4.2: Circle with the red arrow as build direction, showing the allowed (green area) and not allowed (red area) angles of the density gradient with respect to the build direction for a critical angle α. Typically, the critical angle is equal to $45°$.

corrected for allowed overhang angles. Then, in a discrete design overhang will be correctly identified. However, the optimiser only has the tendency to place more material at the bottom but not to form structures under a certain allowed angle. Therefore, it is necessary to know the direction of the density gradient with respect to the reference direction. The angle that the gradient has with the build direction may not be within the crucial minimal overhang angle, for example $45°$. In Figure 4.2 the allowed gradient orientations are illustrated. The build direction is indicated bv the red arrow. If the density gradient is in the green part of the circle, then the corresponding elements is sufficiently supported and the constraint should be smaller or equal than zero. But, if the density gradient lies in the red part of the circle it should not be allowed by the overhang constraint.

The angle between the reference vector and the density gradient follows form their inner-product, see Equation (4.6):

$$\mathbf{n}^T \nabla \mathbf{x} = |\mathbf{n}||\nabla \mathbf{x}| \cos(\alpha), \tag{4.6}$$

where $\mathbf{x}$ are the densities of the elements, $\mathbf{n}$ is a unity vector pointing in the build direction and α is the critical overhang angle. Next, Equation (4.6) will be simplified and rewritten into the for optimisation standard negative null form, see Equation (4.7):

$$g(\mathbf{x}) = \frac{1}{\cos(\alpha)} \frac{\mathbf{n}^T \nabla \mathbf{x}}{|\nabla \mathbf{x}|} - 1 \leq 0. \tag{4.7}$$

The response function that is derived is negative for every angle between the build direction and the density gradient larger than α, positive for every angle smaller than α and zero if the overhang angle is just allowed.

4.3. Verification of the overhang constraint

In this section the overhang constraint given in Equation (4.7) will be inspected more closely. The constraint is calculated for an imaginary structure. This structure represents a beam consisting of four sections, each with a different angle with the horizontal base plate. Namely, a vertical section, a part with an angle of $45°$ to the base plate, a part with a flatter angle than $45°$ and a horizontal section, see Figure 4.3a. The constraint is calculated for an upward build direction and a crucial angle of $45°$. The modified Roberts cross kernel and the Sobel kernel are used for the determination of the gradient, see Figures 4.3b and 4.3c respectively. As can be seen, the overhang is detected with both kernels. For both kernels the vertical part of the test beam and the part with the $45°$ angle do not give a positive constraint value. The other two parts of the beam do. This is as expected. Furthermore, the Sobel kernel gives positive overhang values for a larger area around the boundary. This is also as expected, as was explained in Section 4.1.2. The constraint values for the elements on the edges of the design domain are not calculated. This is correct since the lowest elements can newer violate the overhang constraint and the upper elements do not have to support anything. The density field consist of 15×18 elements. So, the constraint fields consist of 14×17 and 13×16 values for the Roberts cross and Sobel kernel respectively.

Some remarks on the constraint calculations need to be made. The constraints are calculated on discrete designs. Actually, it is more complicated than this. During the optimisation intermediate density values will occur. In a non-discrete density distribution, it is no longer clearly defined where the

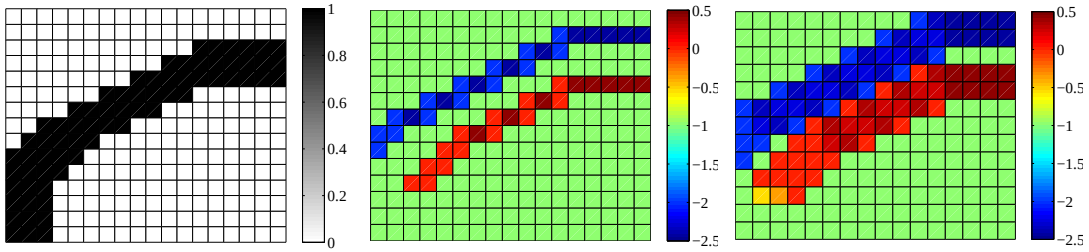

(a) (b) (c)

Figure 4.3: Structure with corresponding constraint values to verify the constraint function; a) density field of the test beam consisting of sections with different angles to the base plate. b) overhang constraint values obtained with the modified Roberts cross kernel showing correct constraint violations if the overhanging slope exceeds the critical angle of $45°$. c) overhang constraint values for Sobel kernel, also showing correctly indicated overhang. The response area of the Sobel operator is larger due to the increased size of the convolution kernel.

boundary lies. Because of the penalisation of intermediate densities the optimiser should form solid and void elements and a boundary. However, potentially the optimiser could misuse intermediate densities to find density configurations that satisfy the constraint.

The gradient kernels give an approximation to the density gradient. Since the density field is discretized, the real gradient is not available. The approximation of the gradient could lead under certain circumstances, even in discrete designs, to false positive or false negative outcomes. The configurations of the density field that are misinterpreted by the gradient operator are investigated and depicted in Figures 4.4 and 4.5 for the 2×2 and 3×3 kernels respectively. The figures show small sections of a hypothetical topology and the arrows indicate the density gradient. A gradient is calculated at the nodes in Figure 4.4 and at the elements in Figure 4.5. The configuration of Figure 4.4a has no overhang, since every element is supported by an element below. However, the gradient at middle node of the third row points upward and thus falsely indicates overhang. On the other hand, the configuration of Figure 4.4b clearly shows overhang of the centre element. But, all the density gradients have an angle of $45°$ with the build direction and are thus allowed. Also, the configurations shown in Figure 4.5 should not lead to a constraint violation because the middle element has sufficient support. However, the density gradient has in all four cases an angle of less than the crucial $45°$ with the vertical build direction, and thus the overhang constraint is violated. Summarizing, the density configuration shown by the Figures 4.4a and 4.5a to 4.5d give a false positive overhang constraint violation. The configuration in Figure 4.4b gives a false negative overhang constraint value.

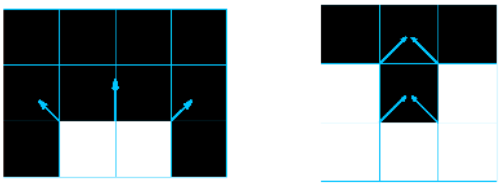

(a) (b)

Figure 4.4: Density configurations that are misinterpreted by the overhang constraint using the modified Roberts cross kernel; a) the centre node on the third row gives a false positive constraint value b) the middle nodes on the third row give false negative constraint values.

The gradient flaws depicted in Figures 4.4a, 4.5a and 4.5b play for example a role if two downward facing surfaces encounter in a wedge like structure. At the intersection of the two inclined surfaces one of the shown configuration will appear. Due to the difference in size of the gradient operators the optimiser will create wedges of different shape. In Figure 4.6 two such wedges are depicted. It is seen that the optimiser should place the symmetry axis of the wedge inside an element, Figure 4.6a, if a 2×2 gradient operator is used, but if a 3×3 gradient operator is used this symmetry axis should occur

(a) (b) (c) (d)

Figure 4.5: Density configurations that are misinterpreted by the overhang constraint using the Sobel or Prewitt kernel; a), b), c) and d) the constraint calculated for the centre element is gives a false positive constraint violation.

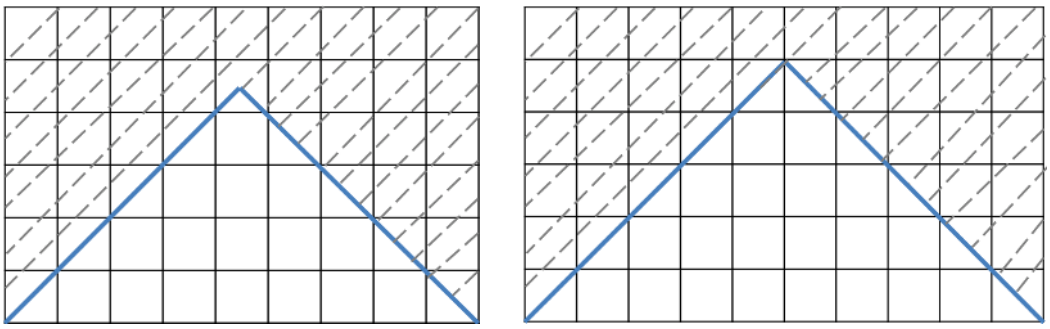

(a) (b)

Figure 4.6: Depending on the size of the gradient operator the optimiser should design wedges differently in order to obtain a feasible result. The marked area represent the material domain.; a) wegde for a 2×2 kernel, b) wegde for a 3×3 kernel.

at the boundary between two elements, Figure 4.6b, in order to satisfy the overhang constraint. So, by using one or the other shape for wedges, the optimiser can create overhang free designs despite the stencil flaws and no additional measures are required.

On the other hand, the flaws given by Figures 4.5c and 4.5d do need to be resolved. This is done in two ways. The simplest possibility is to slightly adjust the constraint, such that the faulty configurations are just zero, by subtracting a small number. This number is calculated as:

$$\kappa = \frac{1}{\cos(\alpha)} \frac{\mathbf{n}^T \nabla \mathbf{x}^*}{|\nabla \mathbf{x}^*|}, \tag{4.8}$$

where $\mathbf{x}^*$ is the configuration given by Figure 4.5c or Figure 4.5d. This method boils down to a small relaxation of the constraint and could therefore be misused by the optimiser in designs that are not completely discrete. Another possibility to prevent a constraint violation for the given density section is to adjust the Sobel kernel. A suitable alternative to the Sobel kernel is given in Equation (4.9):

$$\mathbf{K_x} = \begin{bmatrix} -2 & 0 & 2 \\ -0 & 0 & 0 \\ -3 & 0 & 3 \end{bmatrix}, \qquad \mathbf{K_y} = \begin{bmatrix} 1 & 2 & 1 \\ 0 & 0 & 0 \\ -1 & -2 & -1 \end{bmatrix}. \tag{4.9}$$

Finally, the gradient flaw of Figure 4.4a is not easily compensated for by changing the constraint or gradient operator. However, typically density filters are used in density based topology optimisation. The use of a density filter blurs these small features, and it should therefore not be a problem. Also, these density filters cause less clearly defined edges or 'soft' edges. It is difficult to predict how this will influence the behaviour of the optimisation.

Concluding, the method for obtaining the gradient of the density field has some undesirable effects. However, constraint violations will be correctly identified. In the case of false positive constraints violations the optimiser has workarounds to still find a feasible design. Therefore, the overhang formulation can be used in an overhang elimination method.

5

Research approach

This chapter treats the approach of this research. It starts with a brief mentioning of the framework for the implementation. Then, a discussion on verification of the methods and comparison measures follows. Also, test problems, that are used throughout this report, are introduced and explained.

5.1. Topology optimisation software

Topology optimisation software is already widely available. Most software uses the density based topology optimisation approach. Because the density based approach is the standard it will also be used in this research.

A density based topology optimisation program is the 88-line Matlab code [3]. Because this software is easily available, efficient and well documented, it is a suitable and popular framework to start from. The 88-line code solves a 2D compliance minimisation problem with a volume constraint in a rectangular design domain with a regular mesh of square, 4-node elements [3]. This code will be modified and extended to test and validate the density gradient based overhang restriction concepts.

In topology optimisation the well known method of moving asymptotes MMA is widely used. This method has been found very suitable for topology optimisation. However, it is not efficient in the case of many constraint functions. Therefore, also other optimisation methods are considered. Matlab comes with an extensive optimisation toolbox that will be used.

5.2. Verification

In this report different implementations of a density gradient based overhang elimination will be tested. In the end, we want te be able to say something on their performance. To this end, the criteria that are important for this research will be identified and listed. Based on these criteria, we will formulate performance measures in order to have objective data for a discussion and a comparison of the different implementations.

5.2.1. Criteria

The intention of the new method is to make topology optimised designs instantly ready for additive manufacturing. Manufacturability is therefore the most relevant criteria. The new constraint should prevent slopes beyond the critical build angle. So, above all the designs should be free from failing overhanging features. Furthermore, some general criteria that are important for all topology optimisations still hold. Numerical artefacts like checker boards and mesh dependency are still unwanted phenomena. Finally, fast and stable convergence, computational efficiency, and an easy implementation are desired. Below the criteria are listed in order of importance. The efficiency is regarded as the least important criteria of this list, because in this stadium of research the density gradient based method should first be found to be a working concept.

1. Manufacturable
2. Free of numerical artefacts

3. Fast and stable convergence
4. Easy implementation
5. Computationally efficient

5.2.2. Performance measures

The listed criteria will be used for the performance measures. Since the overhang restriction is the main goal of the new method, the end result will be checked to be overhang free. A discrete design is also important regarding manufacturability. It is to be expected that the overhang free designs have to compromise on performance. The level of performance compromise should be as small as possible. The relative compliance is used as a measure for comparison.

The level of greyness gives also an indication for the convergence. The optimiser could get stuck in a greyish topology. Furthermore, The algorithm might want to take advantage of the relaxation of the density values and use intermediate densities to artificially remove overhanging features and satisfy the constraint. This is obviously an unwanted side effect of the relaxation. A measure to observe to what extend a design has converged to a discrete solution was introduced in [29]. In this paper it was used to compare different restriction schemes for black-and-white designs. Here it will be used for measuring the discreteness of the optimised topology. In Equation (5.1) the formula for the level of non-discreteness is given:

$$M_{nd} = \frac{\sum_{e=1}^{n} 4x_e(1-x_e)}{n} \times 100\%. \tag{5.1}$$

This measure gives 0% if the design is completely black-and-white. If the design is completely grey, $M_{nd} = 100\%$. Hence, a low value for this measure is desired.

Usually the convergence is used to check whether the optimisation can be terminated. The convergence of the objective also gives information on the difficulty for the optimiser to find design improvements. A slow and unstable convergence might indicate that the constraint is too stringent.

The occurrence of numerical artefacts will be checked by inspection and mentioned if applicable. The remaining criteria will be discussed based on observation and experience.

5.3. Test problems

The proposed methods for overhang restriction are tested with numerical examples. By testing novel methods by means of a numerical example can never completely assure that the method will function in all situations. Therefore, throughout this report two test cases will be used to reduce the risk that the method is suitable in only one particular scenario. This section introduces the different test problems that will return in the chapters to follow.

The MBB beam is a commonly used test case in topology optimisation and is therefore adopted in this report. The problem definition with boundary conditions and external loads is shown at the left of Figure 5.1. As a second test case, the bridge problem is used. This example is chosen because its optimal solution has a large overhang at the top of the structure. It might be difficult for the optimiser to find a feasible solution to this problem. The problem definition with boundary conditions and the external load is presented in Figure 5.1 at the right.

The optimal topology for the MBB beam and bridge without an overhang constraint is shown in Figures 5.2a and 5.2d respectively. Obviously, it is important for the test cases to have overhang in the optimal solution without an overhang constraint. Figure 5.2 also shows the constraint violations for both solutions, computed with as well the alternative Sobel operator as the Roberts cross. The overhang in both designs is clearly visible. Important to mention, in all examples the base plate is assumed to be at the bottom and the build direction is vertically upward, unless mentioned otherwise.

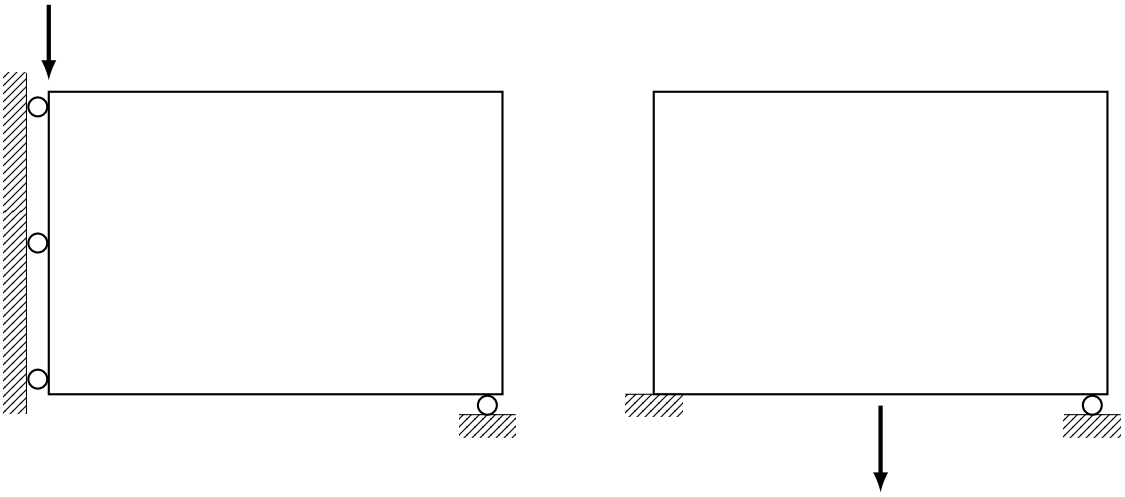

Figure 5.1: Schematic drawings of the test problems. The left figure shows the boundary conditions and loading for the MBB beam. The figure to the right gives the boundary conditions and applied load for the bridge problem.

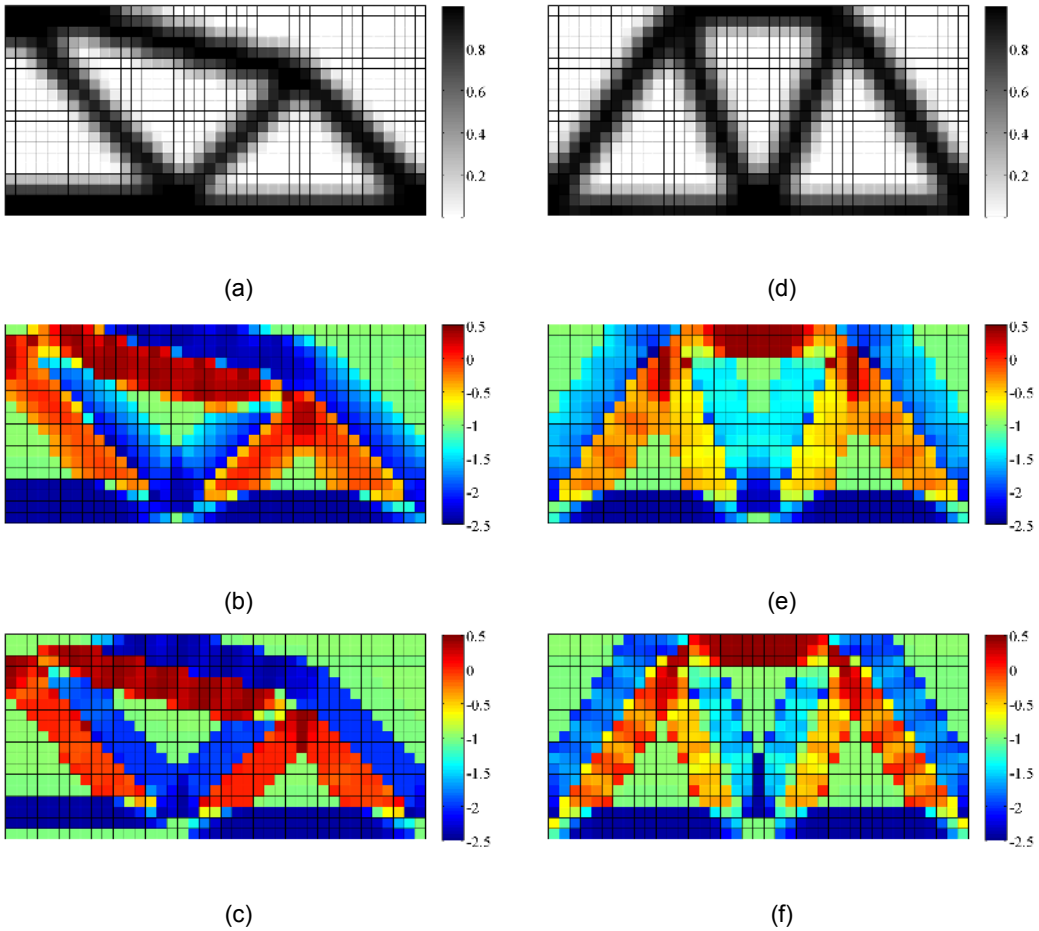

Figure 5.2: Optimal topology of the test problems without an overhang constraint and the corresponding constraint values computed for both the alternative Sobel gradient operator (middle row) and the Roberts cross operator (bottom row); a,b,c) mbb beam, the overhang at the upper beam is clearly seen. d,e,f) bridge, also in this case the upper horizontal beam is overhanging and will not be properly printed like this.

6

Direct constraint

The most straightforward implementation of the overhang constraint is as a direct constraint added to the existing topology optimisation formulation. In this chapter the direct overhang constraint is considered. In Section 6.1 the overhang constraint is formulated and the sensitivities are derived. Furthermore, additions to this simple implementation, that are expected to yield better results, are the subject of Sections 6.2 and 6.3. The different implementations are tested and compared. The test results are given in Section 6.4. In Sections 6.5 and 6.6 the results are compared and discussed.

6.1. Overhang constraint

The function that indicates overhang from a topology was derived in Chapter 4. Equation (6.1) gives the new optimisation problem:

$$\begin{aligned} \min_{\mathbf{x}} \quad & c(\mathbf{x}) \\ \text{s.t.:} \quad & V(\mathbf{x})/V_0 - 1 \leq 0 \\ & g_i(\mathbf{x}) = \frac{1}{\cos(\alpha)} \frac{\mathbf{n}^T \nabla \mathbf{x}_i}{|\nabla \mathbf{x}|_i} - 1 \leq 0 \\ & \mathbf{0} \leq \mathbf{x} \leq \mathbf{1}. \end{aligned} \tag{6.1}$$

Depending on whether the number of elements in the kernel of the gradient operator is even or uneven, the overhang constraint function defines a constraint at each element or node, with the exception of the outer elements or nodes. Consequently, the problem acquires a comparable number of constraints as it has design variables. Furthermore, the overhang constraints are clearly non-linear. So, the resulting optimisation problem has as many design variables as elements, lower and upper bounds on each design variable, one linear volume constraint and a number of non-linear overhang constraints comparable to the number of design variables. It is important that the optimisation method is suitable for such a problem. The general purpose optimisation algorithm of MatLab, *fmincon*, is designed for optimisation problems with many non-linear constraints. The default interior-point algorithm is used. More information on this algorithm can be found in the documentation of Matlab [21]. This is a gradient based optimisation algorithm, and thus the derivatives of the objective and constraint functions need to be provided to the solver. The derivation of the gradient of the objective and volume constraint will not be repeated here, but can be found in [3]. The derivation of the overhang constraints sensitivity is given next.

Sensitivities

In order to find the derivative of the overhang constraint equations with respect to the design variables $\mathbf{x}$, it is convenient to group the scalar product of the density gradient with the reference vector and the length of the gradient, as in Equation (6.1), and find the derivatives for them separately. Then, by the chain rule for differentiation it follows that:

$$\frac{dg}{dx} = \frac{\partial g}{\partial \mathbf{n}^T \nabla \mathbf{x}} \frac{d\mathbf{n}^T \nabla \mathbf{x}}{dx} + \frac{\partial g}{\partial |\nabla \mathbf{x}|} \frac{d|\nabla \mathbf{x}|}{dx}. \tag{6.2}$$

The partial derivatives of the constraint to the scalar product and the gradient length are easily found, see Equations (6.3) and (6.4):

$$\frac{\partial g}{\partial \mathbf{n}^T \nabla \mathbf{x}} = \frac{1}{\cos(\alpha)} \frac{1}{|\nabla \mathbf{x}|}, \tag{6.3}$$

$$\frac{\partial g}{\partial |\nabla \mathbf{x}|} = -\frac{1}{\cos(\alpha)} \frac{\mathbf{n}^T \nabla \mathbf{x}}{|\nabla \mathbf{x}|^2}. \tag{6.4}$$

For the scalar product and the length of the gradient the characteristic structure of the matrix of derivatives can be used to easily and efficiently compute the derivatives. Due to the shape of the gradient operator the design variables that are involved for a certain constraint are known in advance. This can be used to build the structure for a sparse matrix of derivatives before the optimisation starts. The computation of the density gradient is a purely linear operation. The derivatives of the two components of the density gradient with respect to $\mathbf{x}$ are simply the components of the corresponding gradient operator, K_x or K_y, at the appropriate position:

$$\frac{d(G_x)_e}{dx_i} = (K_x)_i \qquad i \in \Omega_e \tag{6.5}$$

$$\frac{d(G_y)_e}{dx_i} = (K_y)_i \qquad i \in \Omega_e, \tag{6.6}$$

where G_x and G_y are the x and y component of the density gradient and K_x and K_y are the gradient operator for that component, see also the computation of the density gradient in Section 4.1. Ω_e is the region of the design domain that influences the density gradient. Also, the scalar product is a linear operation. So, its derivatives are constants:

$$\frac{d\mathbf{n}^T \nabla \mathbf{x}}{dx} = n_x \cdot \frac{dG_x}{d\mathbf{x}} + n_y \cdot \frac{dG_y}{d\mathbf{x}}, \tag{6.7}$$

with n_x and n_y the horizontal and vertical component of the reference vector. The length of the gradient is non-linear in $\mathbf{x}$, and its derivatives are given by:

$$\frac{d|\nabla \mathbf{x}|}{dx} = \frac{\mathbf{G}_x \cdot \frac{d\mathbf{G}_x}{d\mathbf{x}} + \mathbf{G}_y \cdot \frac{d\mathbf{G}_y}{d\mathbf{x}}}{|\nabla \mathbf{x}|}. \tag{6.8}$$

6.2. Grey relaxation

At the start of a topology optimisation, the geometry of the structure is not defined. In the first stage the density field of intermediate densities slowly transforms into a structure. During this transformation it is difficult to point out what the boundary between void and solid is. The original constraint given by Equation (6.1) is very strict. A constraint is violated if at any moment any element has a gradient angle exceeding the maximum overhang angle. So, also during this initial stage of the optimisation process when a clear structure has not yet been formed. This way, the formulation of the constraint might obstruct the optimisation to converge to an optimal solution and get prematurely stuck at some local optima. To avoid this, constraint relaxation can be used. Constraint relaxation works by changing the original problem to a problem with less strict constraints, such that the optimiser is allowed to find a solution. Then, the constraint is gradually tightened, up to the point when the original problem is reimposed.

The initial stage of the optimisation process is characterised by regions of many elements with intermediate densities. To allow structures to be formed out of these areas, the optimiser should not be hindered by the overhang constraint. To achieve this, the original constraint formulation of Equation (6.1) is extended. The idea of this extension is to reduce the strictness of the constraints for low density elements. The relaxation of regions of elements that have not yet evolved to a well defined structure, involves the switching off of the constraint for elements with a density below a specified threshold. This is done by multiplying the constraint with the element density mapped by a continuous from of the shifted step function. The new constraint is given in Equation (6.9), the term inside square brackets is the continuous approximation of the shifted step function:

$$g(x) = \left[\frac{1}{1 + e^{-k(x-\delta)}}\right] \frac{1}{\cos(\alpha)} \frac{n^T \nabla x}{|\nabla x|} - 1. \tag{6.9}$$

k and δ are tuning parameters which determine the steepness of the approximated step function and the threshold between solid and void respectively. For elements with densities well beneath the threshold δ the constraint is always satisfied, irrespective of the density gradient. In Figure 6.1a the shifted step function is plotted for different values of parameter δ. Without a continuation scheme the optimiser could misuse relaxation by placing grey elements at difficult locations. A continuation scheme should slowly reduce the threshold parameter δ to ensure no overhang in the final optimal design.

The addition ensures no violation of the constraint for elements of intermediate density. This should prevent the optimisation process from getting hindered by the constraint in the beginning of the optimisation process. Regions that have not yet formed clear solid and void areas are not constrained and thus are free to form the optimal structure. The constraint will suppress overhang for elements that have attained a density above the threshold δ. The extension of the original constraint should give the optimiser the freedom to evolve into an optimal structure free from overhang.

Sensitivities

The extra product in the constraint formulation should be accounted for in the sensitivity analysis. Now that the constraint is explicitly depending on $\mathbf{x}$ the chain rule for differentiation gives:

$$\frac{dg}{dx} = \frac{\partial g}{\partial \mathbf{x}} + \frac{\partial g}{\partial \mathbf{n}^T \nabla \mathbf{x}} \frac{d\mathbf{n}^T \nabla \mathbf{x}}{dx} + \frac{\partial g}{\partial |\nabla \mathbf{x}|} \frac{d|\nabla \mathbf{x}|}{dx}, \tag{6.10}$$

where the extra term is computed as:

$$\frac{\partial g}{\partial \mathbf{x}} = \left[\frac{k \cdot e^{-k(x-\delta)}}{\left(1 + e^{-k(x-\delta)}\right)^2} \right] \frac{1}{\cos(\alpha)} \frac{\mathbf{n}^T \nabla \mathbf{x}}{|\nabla \mathbf{x}|}. \tag{6.11}$$

The partial derivatives of the constraint with respect to the scalar product of the density gradient with the build direction and the magnitude of the gradient change accordingly:

$$\frac{\partial g}{\partial \mathbf{n}^T \nabla \mathbf{x}} = \left[\frac{1}{1 + e^{-k(x-\delta)}} \right] \frac{1}{\cos(\alpha)} \frac{1}{|\nabla \mathbf{x}|}, \tag{6.12}$$

$$\frac{\partial g}{\partial |\nabla \mathbf{x}|} = -\left[\frac{1}{1 + e^{-k(x-\delta)}} \right] \frac{1}{\cos(\alpha)} \frac{\mathbf{n}^T \nabla \mathbf{x}}{|\nabla \mathbf{x}|^2}. \tag{6.13}$$

6.3. Crisp boundaries

Instead of relaxing the grey elements, a different approach to address the problem of not yet fully crystallised structures is to make the entire design discrete at every iteration, so that the boundaries of the structure are well defined and the overhang is readily identified. Again the shifted step function in its continuous form will be used. Filtering the density field by this function results in a more discrete design. The filtered density field is given by Equation (6.14).

$$\bar{x} = \frac{1}{1 + e^{-k(x-\delta)}} \tag{6.14}$$

Again, k and δ are parameters that determine the steepness of the approximated step function and the threshold between solid and void. The shifted step function is preferred over the heaviside function commonly used in topology optimisation for obtaining black-and-white structures [15], because the shifted step function better conserves the volume of the structure. Just as with the heaviside function, a continuation scheme has to be used to guide the optimiser to a feasible and optimal solution. As continuation scheme the steepness parameter k will be increased during the optimisation. In fact, this projection function is better known as the logistic function. Figure 6.1b show this function for different values of k. The continuation scheme initially makes the design less clear, because the range of the new densities $\bar{x}$ is smaller. Over the course of the optimisation the transition between solid and void becomes sharper. The optimiser should decide whether a specific element is actually necessary and if it can exist. The method should suppress the tendency of the optimiser to use grey elements to satisfy the overhang constraint. An additional advantage for this method is the discreteness of the final design.

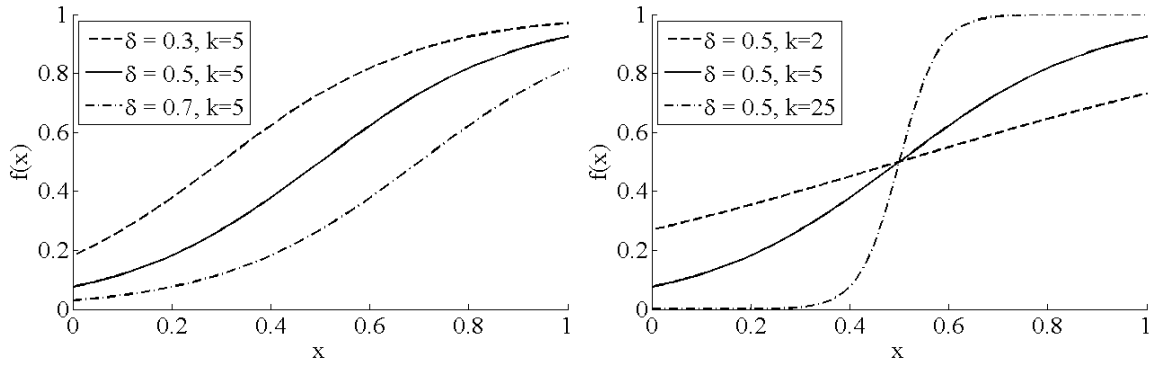

(a) (b)

Figure 6.1: Graphs showing the logistic function used for the relaxation method; a) for different values of δ, b) for different values of k.

Sensitivities

Again the sensitivities should be recalculated due to the filtering operation. The derivatives of the overhang constraint are now calculated with the filtered density field. The sensitivity of the design variables to the filtered density field is given in Equation (6.15):

$$\frac{d\bar{x}}{dx} = \frac{k \cdot e^{-k(x-\delta)}}{\left(1 + e^{-k(x-\delta)}\right)^2}. \tag{6.15}$$

Once more, the chain rule for differentiation leads to the total derivative:

$$\frac{dg}{dx} = \frac{\partial g}{\partial \bar{x}} \frac{d\bar{x}}{dx}. \tag{6.16}$$

6.4. Results of the direct constraint methods

The previously described methods will be tested on numerical examples. The standard test cases are used for this purpose, the MBB beam and the bridge, see Section 5.3. A mesh of 40 elements in the horizontal direction and 20 elements in the vertical directions are used. As is the case for all topology optimisations, a relatively large number of parameters is present. To make the comparison between the different methods as fair as possible these parameters are kept the same for all problems, unless mentioned otherwise. The used values for the parameters are given in Table 7.1. In the following sections the outcome of the methods is described and discussed. Figures showing the density field and corresponding field will be presented. In Section 5.2 we introduced performance measures for the comparison between methods: convergence, non-discreteness and feasibility. Also these items will be addressed in the discussion. In Appendix A the graphs of the convergence, non-discreteness and constraint violations can be found.

Table 6.1: Parameters used throughout the numerical examples presented in this chapter, unless stated otherwise.

# of elements	40×20
Volume fraction	40%
SIMP power	3
Density filter radius	2
Critical angle α	$45°$
Max nr. of iterations	600
δ and k	See corresponding sections, Sections 6.4.2 and 6.4.3

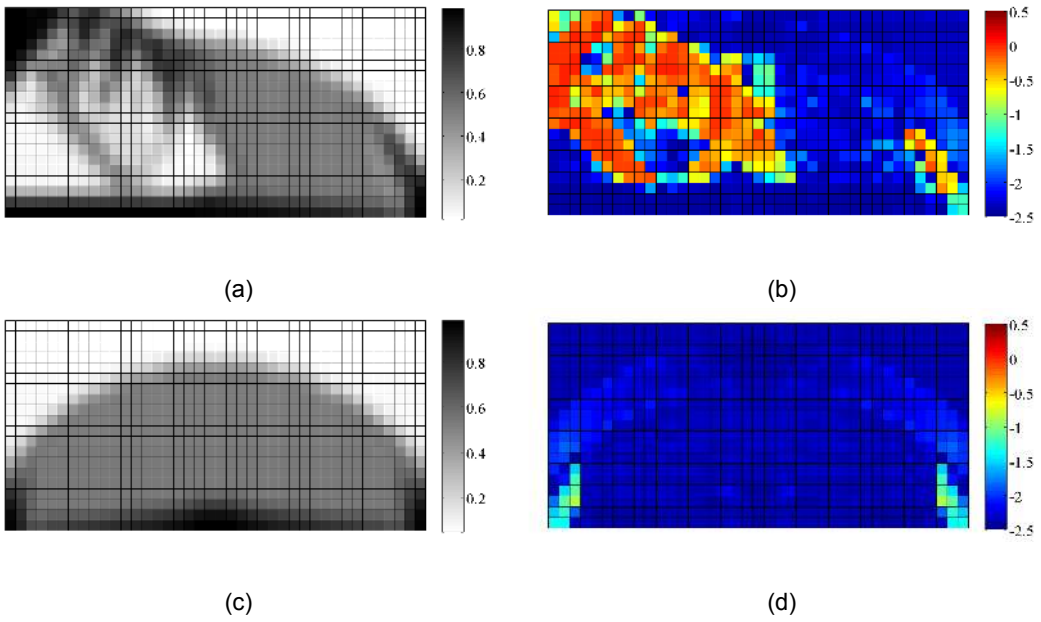

Figure 6.2: Optimal topology and the corresponding constraint values obtained by the overhang constraint and the modified Roberts cross gradient operator. It is seen that the final topologies did not attain a clear, recognizable structure; a,b) mbb beam; c,d) bridge.

6.4.1. Overhang constriant

The direct overhang constraint has been tested for both the Roberts cross gradient operator and the modified Sobel operator. The results of the MBB beam and bridge are shown in Figures 6.2 and 6.3, for the Roberts cross and Sobel operator respectively. The left column shows the obtained density fields and the right column the corresponding constraint values.

The most noticeable observation from the density fields are the large regions of intermediate densities. Fully dense elements have formed only at the bottom row, at the load and supports. Especially for the bridge problem, no clear structure, except for the outer contour, has been formed. At the left side of the MBB beam some vague resemblance of a structure can be identified. It seems that the overhang constraint hinders the optimiser to find a useful solution. Inspection of the constraint values verifies that all overhang constraints are satisfied. None of the overhang constraints are active in the bridge example. Active overhang constraints are present in the MBB beam, at the same areas where the structure did form.

The convergence starts very rapidly. After the first iteration a hiccup in the convergence is observed. This irregularity coincides with the sudden constraint violations in the beginning. The problems have difficulty converging. The optimisation is nearly always terminated because of exceeding the maximum number of iterations or because the change in design variables becomes too small. Before termination, the convergence is slow and the change in design variables very small. The non-discreteness of the problems does decrease during the optimisation, albeit very slowly. The final non-discreteness remains high, at roughly 70%.

6.4.2. Grey relaxation

The optimisation is run with relaxation of the overhang constraints at elements with a low density value. A proper choice for the tuning parameters that determines the steepness k and the threshold δ of the step function is not obvious. Also, the continuation scheme should be designed such that the tightening of the constraints is not too sudden, at the same time it should be fast enough to keep the duration of the optimisation reasonable. The initial choice for the threshold parameter is chosen large, $\delta = 0.8$, such that the overhang constraints are practically turned off. During the optimisation δ is decreased by a factor 2 until δ reaches zero. As last step the threshold parameter is set to -1 so that the original constraint is restored. The steepness parameter k is set to 5, a compromise between a smooth constraint function and a fairly good approximation of the step. In Figure 6.4 the obtained

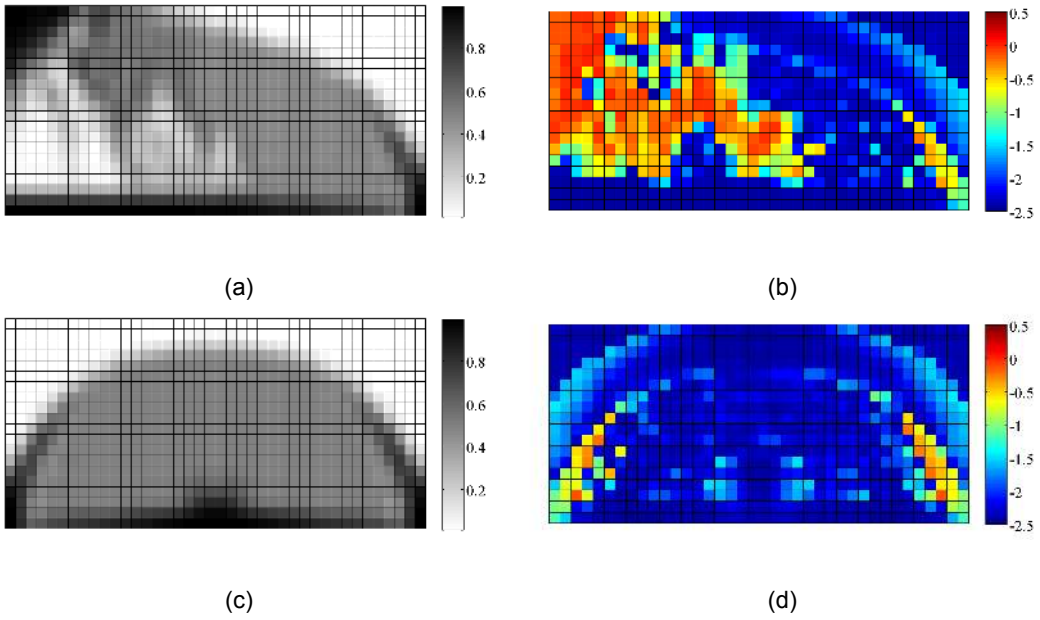

Figure 6.3: Optimal topology and the corresponding constraint values obtained by the overhang constraint and the alternative Sobel gradient operator. Also for this gradient operator, the optimiser did not succeed in finding a recognizable structure; a,b) mbb beam. c,d) bridge.

density fields for both test problems are given, together with the constraint values.

It is observed that the MBB beam did form a recognisable structure. The structure resembles much of the structure of the optimum MBB beam without overhang constraint. The difficult section at the top is partly rotated and partly supported by newly formed support structures. The support structures are not very clear and the density of the supporting elements reduces with height. Although possibly difficult to see from the constraint values plot in Figure 6.4b, all overhang constraints are satisfied. The large areas of light red, indicate that many of the overhang constraints are active. The convergence of the MBB beam is again fast in the beginning and slows down after about 200 iterations. Small peaks in the convergence due to the continuation scheme are visible. Also, the effect of the continuation scheme is clearly visible in the constraint history. After every step of the continuation scheme constraints are violated. The optimiser eliminates overhang to make the design feasible again. This is at the expense of the compliance. As soon as the design is free from overhang, the optimiser tries to improve the objective. The final non-discreteness is improved to 45%.

In contrast to the MBB beam, the bridge problem is again one large area of grey elements. The same was obtained without relaxation. Clearly, the relaxation did not have the desired effect in this case.

During optimisation after every step in the continuation scheme, overhang constraints are violated. The optimiser responds to this by changing the design in order to bring it back to the feasible domain. To do so, the optimiser reduces overhang by creating large regions of intermediate densities. After every continuation step the optimiser managed to adapt the topology of the MBB beam to comply with the stricter constraint. Apparently, the bridge is more difficult for the optimiser to make self-supporting. At some point, the optimiser was not able to bring the design back to a clear, black-and-white structure, hence the completely grey design. The issue might be resolved by making the steps of the continuation scheme more gradually. However, a suitable pace for the continuation scheme was not found. Slowing down the pace of the continuation scheme also increases the optimisation time. For even more difficult problems, this could lead to an unworkable prolonged computation times.

Making grey elements less favourable for the optimiser by increasing the penalisation power p, is also a possibility to force the solution to black-and-white designs. The results shown in Figures 6.4e and 6.4f, are obtained by the same continuation scheme, only the penalisation power was increased to $p = 5$. Now, a clearer structure for the bridge problem is found that also satisfies the overhang and volume constraint. The objective value is difficult to compare with the other problems because of the different penalisation power. The compliance of the new structure, calculated with $p = 5$, is actually

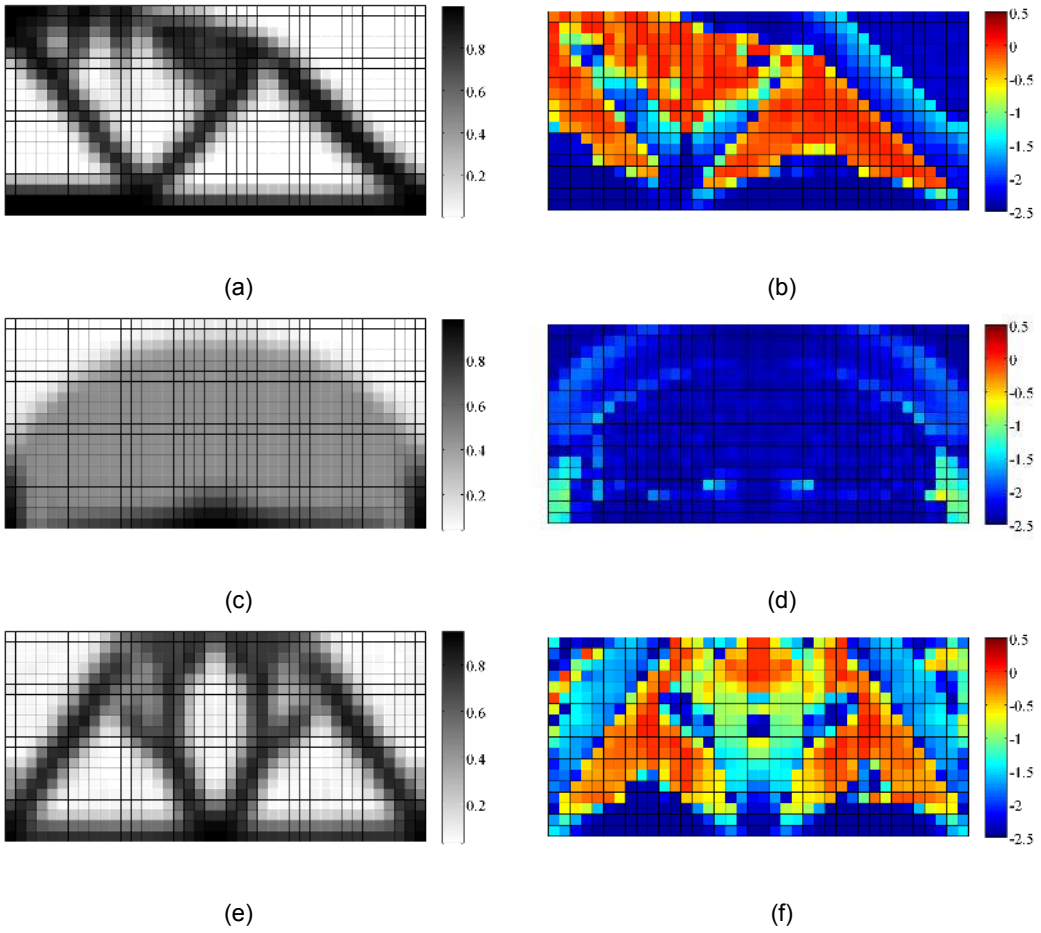

Figure 6.4: Optimal topology and the corresponding constraint values obtained by the grey relaxation method. The modified Sobel operator is used for computing the density gradient; a,b) density field of the MBB beam and the constraint values. Grey relaxation guided the optimiser to a feasible solution with a clear structure. The difficult top section is made self-supproting. The constraint value field shown many active constraints. c,d) density field and correspoinding constraint value field of the birdge problem. The relaxation of constraints at elements with intermediate densiteis did not have the desired effect, as the final desing shows no structure. e,f) density field and corresponding constraint values of the bridge problem. An increased penalisation of grey elements, $p = 5$ was necessary in order to obtain a clear and overhang free structure.

higher than the completely grey topology. If the compliance of the new structure is instead computed with $p = 3$, then the compliance is improved (reduced) by 24%.

6.4.3. Crisp boundaries

The crisp boundary method was named because the projection method it uses ensures clear black to white transitions. The results from the optimisation with the crisp boundary method are given in Figure 6.5. To acquire these results a continuation scheme was necessary, as explained in Section 6.3. The continuation scheme settings are again based on common sense. In contrast to the grey relaxation where constraints were tightened at every step in the continuation scheme, here the transition between solid and void becomes clearer at every step. Still, the same consideration needs to be made between optimisation time and strict black-and-white projection. A very sharp projection to a black-and-white design makes the optimisation problem even more non linear and correspondingly the sensitivity information is likely to change abruptly at every iteration. This will complicate the optimisation and a solution is not likely to be found. For this reason, the continuation starts with a small value for the steepness parameter for the black-and-white projection $k = 1$, and this parameter is increased by a factor 2 until a final value of $k = 32$. The threshold parameter δ is set halfway the allowed density range, $\delta = 0.5$, in order to better conserve the volume.

The most distinctive feature from the result, Figure 6.5, are the sharp transitions between solid and

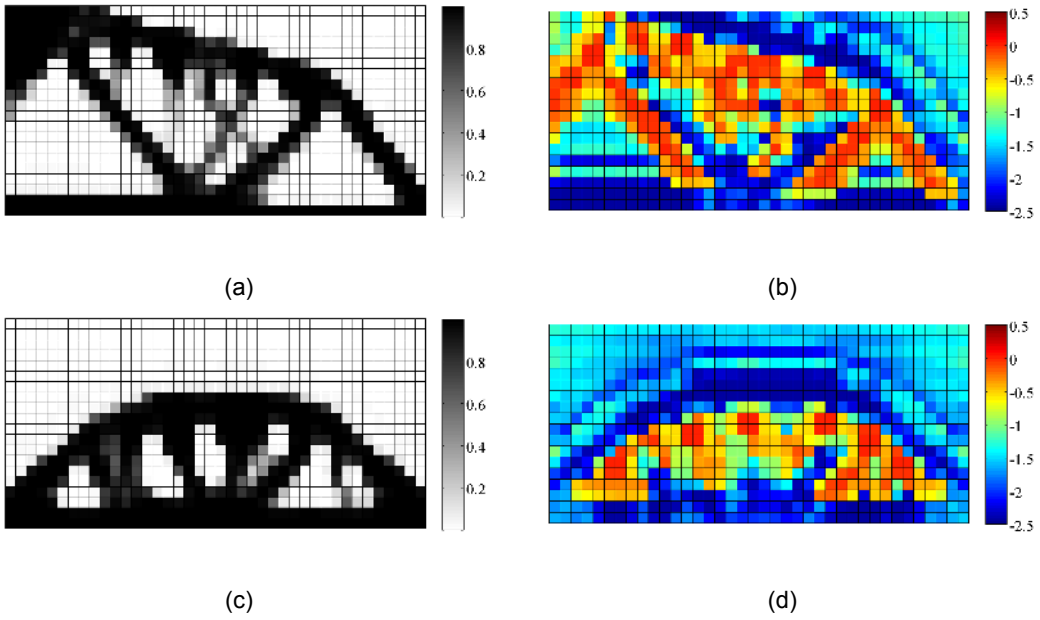

Figure 6.5: Optimal topology and the corresponding constraint values obtained by the crisp boundaries method. The modified Sobel operator is used for computing the density gradient; a,b) density field of the MBB beam and the constraint values. The final structure is free from overhang. The design has many similarities to the optimum without overhang constraint. To support the horizontal beam, support structures have formed. c,d) density field and correspoinding constraint value field of the birdge problem. The obtained topology is indeed overhang free. The design does not look similar to the optimum without overhang constraint. The height of the bridge, which is important for the stiffness, is reduced signicantly.

void. Not all the grey elements are removed. The elements with active constraints still have values of intermediate densities. Their density is close to half-density, and this is were the transition in the projection scheme occurs. An even stricter projection will get rid of these intermediate densities, but it is doubtful if the optimiser will converge if the problem becomes near discrete.

In Figures 6.5a and 6.5b the results of the first test case, the MBB beam, are shown. From the constraint values it is verified that the structure is clearly self-supporting. However, in the supports structures intermediate densities arise. The structure looks similar to the optimum without overhang constraint. At the left side, the structure has a 45° angle that makes the difficult horizontal beam shorter. The optimiser had no issues finding a minimum, the optimisation was terminated because the solution was near an optimum within the set tolerance. This example converged in 519 iterations, this includes all the continuation steps. The convergence was quite irregular due to the continuation. At continuation constraints are often briefly violated. Both the volume constraint and the overhang constraint are responsible for this. The continuation scheme is clearly visible from the graph of the non-discreteness progress. After every step in the continuation scheme the non-discreteness makes a sharp drop. The final value of the non-discreteness is expected to be much lower than for the other methods. The final non-discreteness is with 15.6% actually rather high. This is seen by the relatively large amount of intermediate densities used for the supports.

The same set up and continuation scheme is used for the bridge example. The results are depicted in Figures 6.5c and 6.5d. Also for this example, the method gave a design that complies with the constraints. However, the structure only uses a fraction of the height of the design domain. This might indicate that the optimiser had difficulty finding a feasible solution. After all, the height greatly influences the compliance but requires more support material. The performance of this structure is therefore expected to be bad. The convergence, constraint violations and non-discreteness progress shows similar behaviour as was the case for the MBB beam, with spikes after the steps in the continuation scheme.

6.4.4. Starting point

The main issue with the current optimisation is to evolve from grey regions to a clear structure. A grey region occurs immediately from the beginning because the initial configuration is an uniform distributed

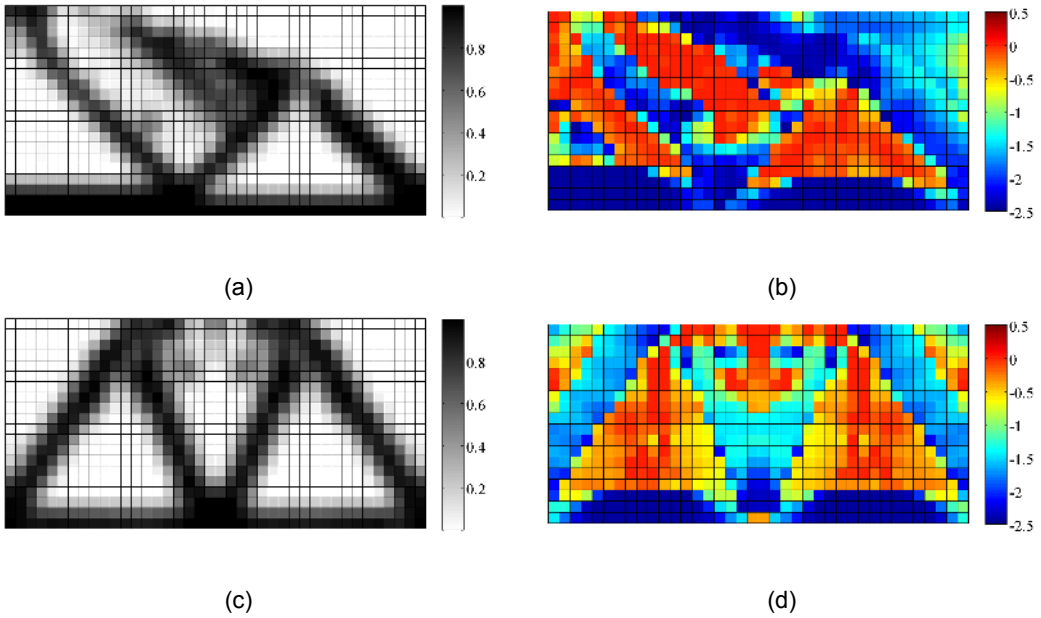

Figure 6.6: Optimal topology and the corresponding constraint values obtained from the overhang constraint started from the optimal solution without overhang constraint. a,b) density field of the MBB beam and the constraint values. The final structure is free from overhang. The design is changed relative to the optimum by a rotation of the overhanging top beam. The compliance of the structure is large because the beam is not properly connected at the top. c,d) density field and correspoinding constraint value field of the birdge problem. The obtained topology is overhang-free. Also for this example, material is removed were initially overhang exsisted such that the structure is practically cut in half.

density equal to the allowed volume fraction. The relaxation methods could evolve from this uniform field, but the direct constraint was not able to attain a clear structure.

An alternative approach to overcome the uniform intermediate density field at the start of the optimisation is to use a different starting point. This initial configuration should feature a clear structure with no areas of many grey elements. The optimiser will change the design to comply to the overhang constraint. The design will only be changed at the locations where constraint violations are present. As initial configuration the optimal solution without overhang constraint is used.

In Figure 6.6 the results of this initial point are shown. The density fields, Figures 6.6a and 6.6c, slow a quite crisp structure. Only the areas with initially overhang have some grey elements. From the constraint values, Figures 6.6b and 6.6d, it is verified that the final designs are indeed feasible. The structure for the MBB is changed by tilting the top beam to 45°. The bridge is made self-supporting by placing material underneath the horizontal top beam. Also, material is removed from overhanging areas. So much, that the structure is practically cut in half. This will have a large negative effect on the compliance.

From the graphs of the optimisation history it is seen that the maximum constraint violations reduces at the expense of the compliance and the discreteness. The objective of the MBB beam could be restored somewhat after the design became feasible. The optimisation of the bridge stopped immediately upon feasibility because the step size became to small.

6.5. Comparison

For a comparison between the methods Table 6.2 shows the total number of iterations, the compliance as percentage of the compliance of the optimal structure without overhang constraint, whether or not the design is feasible and the level of greyness.

The number of iterations is for all test cases really high. An optimisation without the overhang constraint takes typically around 100 iterations. Especially the methods that involve a continuation scheme require many iterations and thus a lot of time. As expected, the overhang constraint causes an impaired objective. The results of the overhang constraint did not yield a well defined structure. The compliance is about two times as high and the discreteness is relatively poor. The same holds for the bridge example with grey relaxation. The impact of the constraint on the compliance of the other test

Table 6.2: Performance measures of the final designs obtained with the different constraint formulations

Test case		Iterations	Compliance	Feasible	Non-discreteness
Overhang	MBB beam (Sobel)	600	191%	Yes	69.8%
constraint	MBB beam (Roberts)	487	173%	Yes	64.3%
	Bridge (Sobel)	600	174%	Yes	69.5%
	Bridge (Roberts)	600	188%	Yes	70.6%
Grey	MBB beam	1374	124%	Yes	40.9%
Relaxation	Bridge	1132	206%	Yes	78.4%
	Bridge (p=5)	1323	157%	Yes	63.6%
Crisp	MBB beam	519	110%	Yes	15.6%
boundaries	Bridge	1128	108%	Yes	10.6%
Initial	MBB beam	1710	804%	Yes	40.8%
point	Bridge	279	293%	Yes	43.0%

cases is still significant. The objective comes reasonably close to the objective of the solution without constraint. The compliance of the examples that used the benchmark solution as initial configuration is extremely bad. This was expected from their density field, the structure was cut in half in order to satisfy the overhang constraint.

All test cases resulted in feasible solutions. The discreteness is very bad for the simple constraint solutions. The other methods have non-discreteness values that is about 10% higher than the benchmark. The discreteness of the crisp boundary method is comparable to the benchmark problem. It is noticed that that high non-discreteness corresponds to high compliance.

6.6. Discussion

It proved difficult to find solution without excessively many elements of intermediate density with the direct constraint. The many local constraints obstruct the optimiser to form a structure out of a uniform grey density field. The relaxation methods helped to some extent to ease the initial problem, allowing the optimiser to find useful solutions. However, mainly the grey relaxation technique had issues upon continuation. At every step of the continuation scheme constraints are suddenly violated. To make the design feasible, grey regions are formed and the optimiser might get stuck in these areas similarly to the case without relaxation. Smoothing the transitions of the continuation scheme could help because the design would be made feasible with smaller changes. However, this cannot be applied indefinitely, as it would increase the duration of the optimisation to unacceptable levels.

Furthermore, it was shown that using an increased penalty power for the stiffness penalisation of grey elements could lead to improved solutions, because intermediate densities are discouraged more strongly. However, a real risk of increasing the penalisation power is the increased non-linearity. The changed optimisation problem will move faster to a black-and-white configuration, and it is less favourable to evolve from a certain configuration to another. So, the optimiser might get stuck in a configuration and this could lead to less optimal designs. For the MBB beam example, an increase of the penalisation power resulted in a worse design. So, it is not predictable what choice for the penalisation power will give the best result. Using it to improve the outcome of the optimisation is for this reason not recommendable.

The crisp boundary method does not suffer from greyish topologies due to the projection to a discrete density field. However, this method has the tendency to get locked in a configuration. When the continuation scheme has progressed to the point that it makes a sharp transition between solid and void, the final shape of the structure should have been already formed. The supports were found to be greyish and should become black in the final design. To make the supports solid, more volume is necessary. But, the volume constraint is already active. The structure cannot be adjusted, because the final shape was already formed. This conflict will probably result in infeasible designs if the discreteness is strongly enforced by the step function.

Starting the optimisation from the optimal solution without overhang constraint also resulted in clearer structures. The question comes to mind, why the continuation scheme does not work but an abrupt start of the simple constraint from an unfeasible domain does. Indeed, the first few steps of the

relaxed problem should result in structures that are similar to the solution without constraint. This can be explained by the effect of the grey relaxation method. This extension to the overhang constraint makes the relaxed constraint explicitly dependent on the element density, thereby giving the optimiser the incentive to decrease the density of elements that violate the constraint, because elements with a density lower than the threshold are never violating the constraint. After a step in the continuation scheme many constraints are abruptly violated. Hence, the emergence of the large areas of intermediate densities after a step in the continuation scheme. After the transition to a field consisting mainly of grey elements, the optimiser cannot get back to a clear structure, similarly to the situation without relaxation. The start from a clear structure made the resulting topology less grey. However, it was found that the objective became much worse. The overhang constraint removed too much material causing the structure to be practically disconnected. The optimiser was not able to restore this after the design became feasible. This behaviour is partly due to the optimisation method that first makes the design feasible, and partly because the constraint does not allow the optimiser to restore the topology after the design is feasible.

7

Constraint aggregation

In the previous chapter the overhang constraint was implemented as a direct local constraint. The resulting optimisation problem was characterized by many design variables and a comparable amount of non-linear response functions. This type of optimisation problems are difficult to handle. The popular and frequently used optimisation algorithm for topology optimisation MMA is for instance not suitable in the case of many constraint functions. However, by means of constraint aggregation all the individual local constraints can be lumped together into one global constraint. In this manner the optimisation problem can be made more suitable for other algorithms such as MMA. This chapter examines constraint aggregation as an alternative for the individual overhang constraints. The effect of aggregation is tested on the test cases and the results are discussed. But first, a suitable aggregation method is explored.

7.1. Aggregation functions

The reasoning of constraint aggregation is as follows: when of a set constraints g_i the largest constraint $g_j \leq 0$, then it follows that all $g_i \leq 0$. In other words, a feasible design is obtained if the maximum constraint value is satisfied. However, by just using the constraint that attains the maximum value at a particular iteration, no sensitivity information of the other, not maximal, constraints is acquired. The direction of the optimiser is only determined by the largest constraint violation and the objective function, this usually results in a constraint violation of another constraint in the next iteration and a feasible solution is not likely to be found [20]. Better would be to use a continuous approximation of the max-operator. From literature it is found that both the p-norm and the Kreisselmeier-Steinhauser function are commonly used [6, 20].

7.1.1. KS function

The Kreisselmeier-Steinhauser function produces a conservative estimate of the maximum, i.e. the maximum value is overestimated. It uses the exponential function to exaggerate the largest value in a set, such that only this value is significant upon summation. Then, by means of the inverse operation, the natural logarithm, the approximated maximum is obtained. The KS-function is given in Equation (7.1):

$$max_{KS}(x) = \lim_{KS \to \infty} \frac{1}{KS} \ln \left(\sum_{i=1}^{n} e^{KS x_i} \right). \tag{7.1}$$

Where KS is the aggregation parameter that can be tuned to reduce the error of the approximation. In Figure 7.1 the KS-function is applied to find the maximum of two functions for different values or the aggregation parameter. It is seen that the approximation is worst when the two functions are equal. At that instance, the error is calculated by Equation (7.2):

$$\varepsilon_{KS} = \frac{1}{KS} \ln (n). \tag{7.2}$$

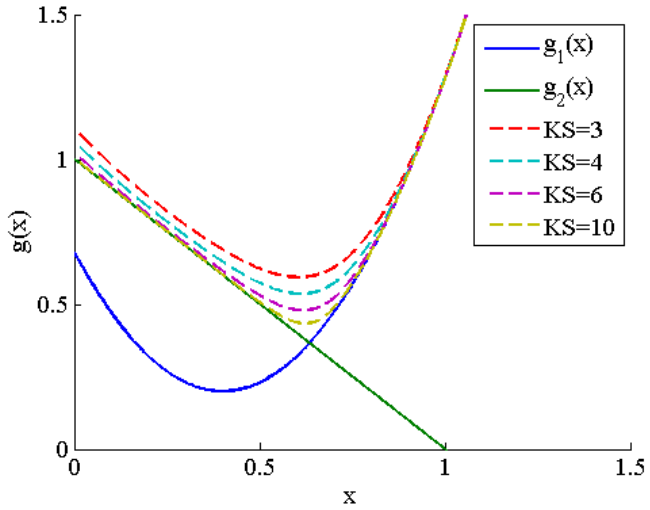

Figure 7.1: Two function, $g_1(x)$ and $g_2(x)$, and their approximated maximum by the KS-function for different values of the aggregation parameter KS.

From both Equation (7.2) and Figure 7.1 it is readily seen that by increasing KS the error is reduced. However, a too large value for KS leads to numerical difficulties. Martins and Poon [20] recommend to use $KS = 50$ as a reasonable value for the aggregation parameter. One numerical difficulty is caused by computing the exponential of large numbers. An alternative formulation of the KS-function to reduce the numerical overflow is given by eq. (7.3):

$$max_{KS}(x) = x_{max} + \frac{1}{KS} \ln\left(\sum_{i=1}^{n} e^{KS(x_i - x_{max})}\right). \tag{7.3}$$

Due to the improved numerical behaviour, this alternative formulation is usually applied instead of the original KS-function.

7.1.2. P-norm

The P-norm is also often used for constraint aggregation. It uses powers instead of exponentials to exaggerate the largest value in the set. If the power $P = \inf$ the P-norm corresponds to the max-operator, see the formula of the max-norm in Equation (7.4):

$$max_P(x) = \lim_{P\to\infty} \sqrt[P]{\sum_{i=1}^{n} x_i^P}. \tag{7.4}$$

Like KS, P is the aggregation parameter and should be chosen sufficiently large to predict the maximum accurately enough. The larger P, the better the approximation. The difficulty is the numerical problems associated with using too large P, in literature $P = 4$ is reported to be a good choice [6]. Similarity to the KS-function, also the max-norm gives an overestimation and the maximum error occurs when all x_i are equal. The error of the P-norm is dependent on the maximum value in the set. The maximum error, in the case all values in the set are equal, is calculated as in Equation (7.5):

$$\varepsilon_P = x_{max}\left(\sqrt[P]{n} - 1\right). \tag{7.5}$$

It should be noted that the max-norm is only valid if all numbers in the set are non-negative. Since the overhang constraint does attain negative values a shift of the constraint values would be necessary.

7.1.3. Comparsion

An attempt has been made to make a comparison between the two aggregation methods, in order to decide what method is better applicable for the overhang constraint. It is deduced that the error

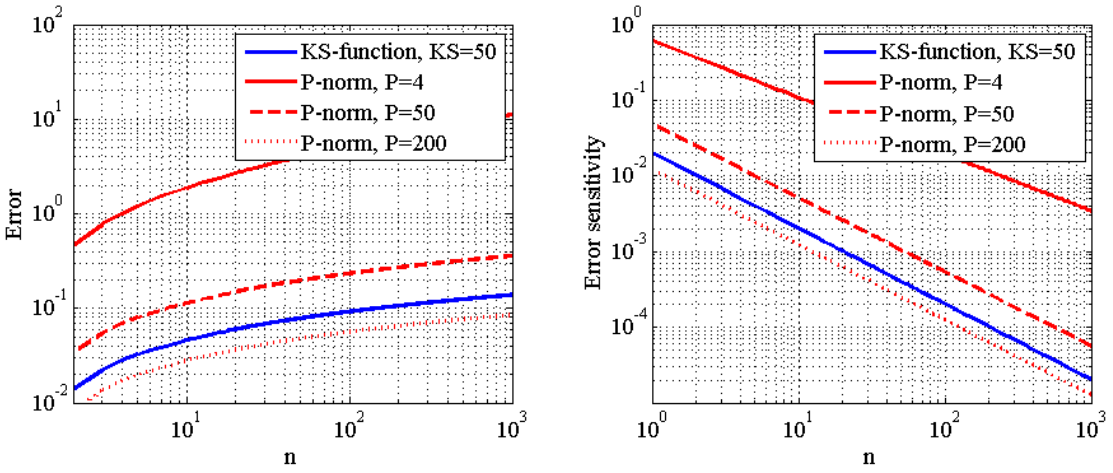

(a) (b)

Figure 7.2: The graphs show the aggregation error (a) and error sensitivity (b) as function of the number of (near) maximum constraints. For the solid blue and red lines, the in literature recommended values for the aggregation parametes are adopted. For these values, a preferable behavior of the KS-function is seen. The red dashed and dotted lines show the P-norm for increased values of P. It is noted that the error can be arbitrarily tuned.

of the approximation is determined by the aggregation parameter and the number of equal or close values in the set of overhang constraints. The aggregation parameters can be chosen as one pleases. However, one should be aware of the possible numerical instabilities when the aggregation parameter is chosen too large. The constraint values that play a role in the error are mainly the values that are close or equal to the maximum value in the set, for a feasible design these are the active constraints. The number of active constraints will increase with the total amount of constraints. Thus, the mesh size affects the accuracy of the aggregation. For the max-norm, the error is furthermore determined by the maximum value in the set. The maximal constraint value in the most favourable case, when the design is feasible, equals zero. However, as was mentioned, the constraint values needs shifting to the non-negative numbers. It can be expected that the most negative value in the set is equal to the lowest possible constraint value, i.e. when the gradient points opposite to the build direction. So, the shifting amounts: $\frac{1}{cos(\alpha)} + 1$. Which, for a critical angle of $45°$, is 2.41.

The error for a variable number of equal maximum constraint values for both the KS-function and the max-norm aggregation is plotted in Figure 7.2a. The aggregation parameter values found in literature are adopted. For the maximum value in the set x_{max}, see Equation (7.4), the lowest possible constraint value is used. For these settings, it is seen that the KS-function performs better than the max-norm. Off course, increasing the aggregation parameter of the max-norm can change the picture completely. We have less control over the number of values in the set that are equal or close to the maximum value. It was explained that the error of the aggregation methods increase with the number of active constraints. To have a better comparison, the sensitivity of the error on the number of active constraints will be considered. The sensitivity of the error for both aggregation functions are given in by Equation (7.6):

$$\frac{\partial \varepsilon_{KS}}{\partial n} = \frac{1}{KS}\frac{1}{n}, \tag{7.6}$$

$$\frac{\partial \varepsilon_{P}}{\partial n} = x_{max}\frac{1}{P}\frac{1}{n^{1-1/P}}. \tag{7.7}$$

For illustration, the sensitivities of the error are plotted in Figure 7.2b. Since P is a positive and finite number, the power of n in the denominator is always larger for the KS-function than for the P-norm. It can be concluded that, all else being equal, the error of the KS-function increases less rapidly for an increasing number of active constraints.

Both aggregations methods are used in literature, for example in problems with many stress constraints. It is hard to argue why one method is better suited for the overhang constraint than the other. By choosing different values for KS or P the error can be tuned as one wishes. In this discussion only

Table 7.1: Parameters used throughout the numerical examples presented in this chapter, unless stated otherwise.

# of elements	40×20
Volume fraction	40%
SIMP power	3
Density filter radius	2
Aggregation parameter	50
Critical angle α	$45°$
Max nr. of iterations	1000

the values for KS respectively P are considered that were found in literature, and this does not necessarily mean that the comparison is completely fair. However, this research has not as goal to find the better aggregation algorithm but merely to investigate the effect of aggregation on the overhang constraint. Nevertheless, the KS-function will be used for the aggregation because it performs better with the aggregation parameter settings recommended in literature and for larger problems with more active constraints.

7.2. Implementation of constraint aggregation

The implementation of constraint aggregation is very straightforward. After all local constraints have been computed they are plugged into the alternative formulation of the KS-function, Equation (7.3). The sensitivities of the aggregated constraint are calculated from the local constraint sensitivities via Equation (7.8):

$$\frac{dg_{max}(\mathbf{x})}{dx_j} = \frac{\sum_{i=1}^{n} e^{KS \cdot g_i(\mathbf{x})} \frac{dg_i(\mathbf{x})}{dx_j}}{\sum_{i=1}^{n} e^{KS \cdot g_i(\mathbf{x})}}. \tag{7.8}$$

What we are left with is a considerably less demanding optimisation problem, as it has only two constraints. Optimisation algorithms that were not suitable for the formulation with individual constraints can be applied to the aggregated formulation. The method of moving asymptotes (MMA) [32], is known to perform well on topology optimisation problems. This algorithm will be applied for testing the aggregated constraint formulation. The overhang constraint formulation in its standard form is used for the implementation because it does not require any continuation and the results will be better interpretable, since less confounding factors are involved.

7.3. Constraint aggregation results

Numerical examples are run to test the aggregated overhang constraint. Again, to produce comparable results, the various variables and tuning parameters are kept the same for every example. In Table 7.1 the used setting are summarized. For the aggregation parameter KS, the in literature recommended value is adopted. However, tests are also performed for an increased value. Furthermore, the effect of starting the optimisation from the optimum without overhang constraint is investigated. In Figures 7.3 and 7.4 the results are shown for the MBB beam and the bridge problem respectively. For these figures the Roberts cross operator was used to compute the gradient of the density field. The results obtained with the Sobel operator are essentially the same, and are therefore omitted. The left column shows the optimal density field, and the right column the corresponding overhang constraint values. The first set of images are the results for the constraint aggregation with the tuning parameters as in Table 7.1. Then, the second set of images shows the results when the aggregation parameters is increased, $KS = 100$. The last set of figures are obtained from the optimisation started from the optimum with overhang. In the following these results will be elaborated on. The discussion includes the performance measures, these can be found in Appendix B.

7.3.1. Aggregation with standard settings

By inspection of the density field and the corresponding constraint values it is seen that the optimiser succeeded in finding designs that feature no overhang below the critical angle for both the MBB beam, Figures 7.3a and 7.3b, as well as the bridge, Figures 7.4a and 7.4b. At least, according to the overhang constraint formulation. In fact, the aggregated overhang constraint for the bridge problem is not com-

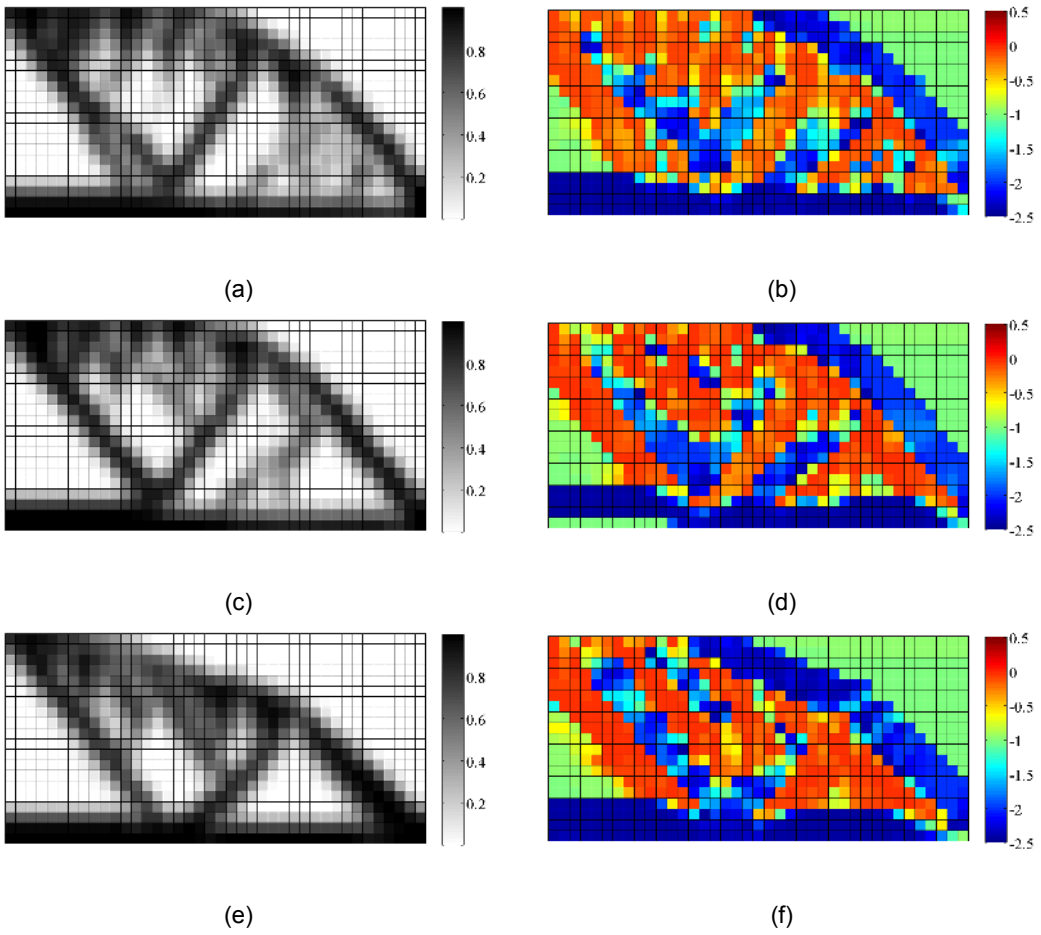

Figure 7.3: The left column shows the density field of the MBB beam and the right column the corresponding constraint values. The density gradient is computed with the Roberts cross operator. a,b) Optimisation settings as mentioned in Table 7.1 are used. The aggregation parameter follows from recommendations in literature. Final topology is overhang-free. c,d) Increased aggregation parameter $KS = 100$ has no significant effect on the topology. Some of the grey regions disappeared. e,f) Optimisation started from the optimal design without overhang constraint gives a result close to the starting point and accordingly a better performance. However, the aggregated constraint was not satisfied.

pletely satisfied. Due to the overestimation of the maximum constraint value the aggregated constraint can be violated, while the design is actually already feasible. In both designs it is noted that extra material is placed underneath members that significantly add to the stiffness. This supporting material is not fully dense. Also, areas are seen where intermediate dense elements remain that have not much use. This might indicates a troublesome convergence. The objective value hardly improves after about 300 iterations. The non-discreteness improves rapidly for the first fifty iterations, from there it reduces gradually to a value of about 50%. From the constraint progress the overestimation of the KS-function is clearly visible. Furthermore, constraints are suddenly violated throughout the whole optimisation. Exceeding the maximum number of iterations was the reason to terminate the optimisation.

7.3.2. Increased aggregation parameter

The aggregation parameter used, $KS = 50$, followed from the in literature recommended value. The same examples are repeated for $KS = 100$ to see the effect of the aggregation parameter and accordingly the accurateness of the maximum approximation. The outcome is presented in Figures 7.3c and 7.3d for the MBB beam and in Figures 7.4c and 7.4d for the bridge. While the increase in aggregation parameter has no immediate effect on the topology of the MBB beam, the bridge is structurally different from the former result, note the massive vertical beam in the middle. For both the MBB beam and the bridge some of the areas of intermediate densities have disappeared, resulting in an improved discreteness for the MBB beam. The discreteness of the bridge did not improve because new grey

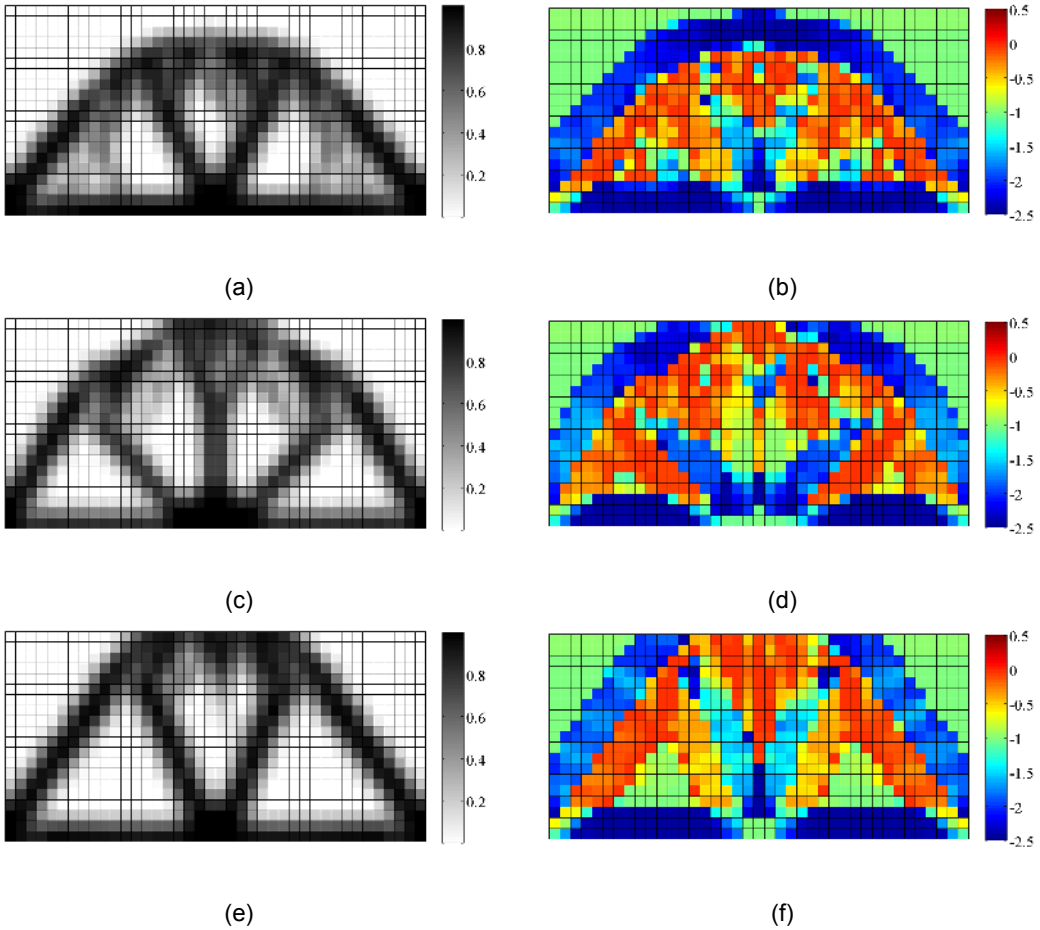

Figure 7.4: The left column shows the density field of the bridge and the right column the corresponding constraint values. The density gradient is computed with the Roberts cross operator. a,b) Optimisation settings as mentioned in Table 7.1 are used. The aggregation parameter follows from recommendations in literature. Final topology is overhang-free. c,d) Increased aggregation parameter $KS = 100$ results in a structurally different design. e,f) Optimisation started from the optimal design without overhang constraint gives a result close to the starting point and accordingly a better performance. However, the aggregated constraint was not satisfied.

elements formed. Despite the different structure for the bridge, the stiffness did not increase. The objective of the MBB beam was found to be lower. The aggregated constraint did not become feasible for both problems, although the original constraints are satisfied. Again, the optimisation terminated because of reaching the iteration limit. The progress of the convergence, constraint and non-discreteness is not notably changed due to the increased aggregation parameter. Not surprisingly, the discrepancy between the actual maximum constraint and the aggregated constraint reduced.

7.3.3. Diferent initial design

The starting point of the optimisation is set to the optimal solution without overhang constraint. The resulting topologies remain very close to this starting position, see Figures 7.3e and 7.3f and Figures 7.4e and 7.4f for the optimised MBB and bridge respectively. Only at initially overhanging areas, design changes have occurred. In comparison with the solution for the initial uniform density distribution, the final topologies feature less intermediate densities and have a higher stiffness. It is found that this starting point leads more often to solutions that do not satisfy the aggregated constraint. Nevertheless, the original constraint is usually still satisfied.

7.4. Discussion of constraint aggregation

It was shown that the constraint aggregation results in overhang free topologies. The density field evolves better to a clearly defined structure then was the case with local constraints. This comes from the fact that the aggregated constraint focusses mainly on the largest violated constraint, the rest of the density field will mainly be adjusted to improve the compliance. This effect becomes more pronounced if the maximum is more accurately determined, that is if a higher value for the aggregation parameter KS is used. This is confirmed by the numerical examples. A higher KS value resulted in even clearer defined structure of the MBB beam. On the other hand, in the case of the bridge, the higher KS parameter caused the optimiser to end up in a different, local minimum. Starting the optimisation from the optimal design, so without overhang constraint, can resolve the issue of a local minimum. It was verified that those designs remain close to the optimal design. Design changes occurred only at those locations where the critical overhang angle was violated. This agrees with the absence of regions with intermediate densities, as was observed in the other test cases.

Probably, the main issues with aggregation of the overhang constraint is the reason that forms the basis of the error in the approximation of the maximum. It was explained that the approximation becomes worse if many values in the set are equal or close to the maximum value in the set. As long as one or more of the local constraints are violated, this will not be of any concern. First of all, the aggregated constraint will correctly disqualify the design as infeasible. Secondly, only few constraints will be violated and thus the approximation will be reasonably accurate. However, as soon the design becomes in the feasible domain of the original constraints, problems are likely to occur. The aggregation is always overestimating the largest constraint value. With other words, the feasible domain is inevitably reduced more than strictly necessary, resulting in designs with lower performance. This effect is enhanced even more for feasible designs. It can be expected that, in a feasible design, a significant amount of downward facing slopes just comply to the 45° overhang constraint. Those active constraints corresponds to the maximum constraint value in the set. So, the approximation is worst for feasible designs. Consequently, the designs needs to be further adjusted at expense of the performance.

The issue of many active constraints and the therefore bad aggregation is also reported for topology optimisation with a maximal stress constraint. In literature methods are developed to improve the accurateness of the aggregation. [20] and [24] describe a scheme to automatically adjust the aggregation parameter. Other methods separate the local constraints into blocks and use one aggregated constraint per block [23]. It is also possible to group the constraints in such a way that the difference between the constraint values is maximal and thus the error as small as possible. These methods are reported to have positive results and could be applied in the same way for the overhang constraint.

8

Overhang and orientation

So far, we have discussed methods to eliminate overhang from topology optimised designs during the optimisation. These methods assumed a fixed build direction before the optimisation started. However, very often it is possible to choose the orientation of a part in the build chamber of the SLM machine to reduce the overhang. This already happens in practice to reduce the amount of needed sacrificial support material. A cleverly chosen orientation could simplify to elimination of overhang from designs. Lets for example consider the MBB beam, see Figure 8.1, it is noticed that the overhang is significantly reduced by printing the optimised MBB beam from the side instead of from the bottom. Consequently, the MBB beam could be made self-supporting with less modifications to the design. Also, judging from Figure 8.1, the design modification will be less radical. This will result in better performing structures, as the final design will be closer to the optimum without overhang constraint. A true optimisation of manufacturable structures should also considerer the build orientation.

In literature attempts have been made to determine the optimal orientation of a part in the build chamber of the SLM machine in order to minimize the needed amount of sacrificial support material [31]. The used approach was to repeatedly calculate the amount of overhang for a number of orientations, for instance every 5°. This approach minimises overhang after the design phase. Obviously, in combination with an overhang elimination method this would not work, because the design is overhang-free for the assumed build direction. So, the orientation should somehow be considered during the optimisation. This was one of the reasons to use the density gradient in the overhang formulation, as it is designed to also be applicable for a variable build direction.

In this chapter attempts are made to take the build direction into account during the optimisation. First, difficulties of the orientation in an optimisation are considered. Then, a suitable approach is described and numerical examples are performed to test this approach.

8.1. Approach

A straightforward approach to include the build direction in the optimisation problem is to make it one of the design variables. With the additional design variable $\mathbf{n}$, the optimisation problem would look something as in Equation (8.1):

$$\begin{aligned} \min_{\mathbf{x},\mathbf{n}} \quad & c(\mathbf{x}) \\ \text{s.t.:} \quad & V(\mathbf{x})/V_0 - 1 \leq 0 \\ & OH(\mathbf{x},\mathbf{n}) \leq 0 \\ & \mathbf{0} \leq \mathbf{x} \leq \mathbf{1} \\ & |\mathbf{n}| = 1. \end{aligned} \tag{8.1}$$

The sensitivities with respect to the build direction tell the optimiser to change the orientation in order to improve the overhang constraint. The sensitivity analysis will not be troublesome to perform, since the problem is linear in the build direction. However, on forehand certain difficulties can be pointed out.

In the case of an unsupported surface parallel to the base plate, a rotation clockwise has the same effect as a rotation counter clockwise. This means that the sensitivity of the build direction is zero.

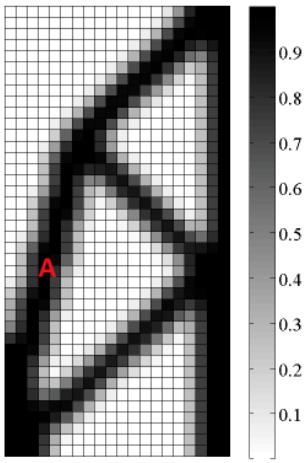

Figure 8.1: The optimal MBB beam is rotated $90°$ counter clockwise to have a favourable build direction regarding overhang. The large ovehanging member, indicated by the red A, forms in this configuration no problem since it stands vertical. The diagonal beams might still needs some small adjustments. However, this is far easier corrected for. The final manufacturable design needs less modifications and will stay closer to the optimum, and therefore will have a better performance.

So, the optimiser has no preference for one particular rotation and will not change the build direction. In Figure 8.2 this is shown for an imaginary structure. Although the structure has overhang with the orientation shown in Figure 8.2a and not with the orientation shown in Figure 8.2b, the optimiser will not change the build direction from scenario of Figure 8.2a because the sensitivity is zero.

In addition, as was seen from the example at the beginning of this chapter, the overhang can strongly change with orientations. With other words, the overhang is a very non-linear function of the build direction. The optimiser will search for a better orientation in the proximity of the current orientation and will gradually change the orientation in the direction pointed out by the sensitivities. However, a favourable build direction is often found by a large rotation and its likely that the structure has to pass a worse orientation to get there. Due to this non linearity, the optimiser is likely to get stuck in a local minimum. This makes the end result also very dependent on the initial build direction. Again this is visualized with an imaginary structure, see Figure 8.3. In Figure 8.3a the structure has some overhang. An orientation without overhang is obtained by a rotations $90°$ counter clockwise, shown in Figure 8.3c. In order to reach that orientation from the situation in Figure 8.3a, the structure first has to pass orientations that are worse in sense of overhang and the optimiser will not reach the optimum.

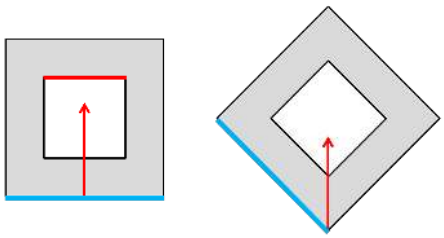

(a) (b)

Figure 8.2: The structure shown in orientation *(a)* has overhang, as marked by the red line. The build direction is given by the red arrow and the blue line serves as a reference line. A $45°$ rotation of this structure would eliminate all overhang, see *(b)*. However, a rotaion clockwise and counter clockwise are equivalent in terms of overhang and an optimiser would not obtain a move direction from gradient information to improve the desing. So, the structure will not rotate to the favourable orientation.

In this chapter a different approach will be used. Instead of letting the build orientation vary continuously during the optimisation a fixed set of orientations will be considered throughout the optimisation. A measure of the total amount of overhang will indicate what the preferable build direction for the current design is. The total overhang for a specific build orientation will be a function of the local overhang corresponding to that orientation $g(\mathbf{x}, \mathbf{n}_i)$. The local overhang is simply calculated as before with the

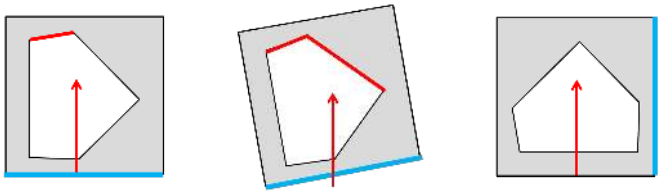

(a) (b) (c)

Figure 8.3: The structure shown in configuration *(a)* has overhang, as indicated by the red line. The build direction is depicted by the red arrow and the blue line serves as reference line. The same structure but rotated as in configuration *(c)* will eliminate all overhang. However, to attain this orientation the build direction should pass orientations that are less favourable in terms of overhang, see configuration *(b)*. Therefore, configuration *(c)* will not be reached and the optimiser is stuck in a local minimum.

overhang constraint function, see Chapter 4. Then, the minimum of these total overhang measures is determined. During the optimisation the design is updated to improve the stiffness and eliminate overhang for the orientation that corresponds to the minimum total overhang. The flow chart in Figure 8.4 shows schematically the described process for overhang elimination including orientation. The compliance and volume are not mentioned in the flowchart but, off course, are still part of the optimisation. The measure for total overhang and the restriction method will be addressed next.

The measure for total overhang should address some aspects. First of all it should increase when more constraints are violated. Also, since larger constraint violation are more difficult to repair, the measure should increase for larger violations. On the other hand, a smaller constraint value than zero should not be more beneficial than a constraint that is just satisfied. Otherwise, the optimiser will have the tendency to increase the slope of overhanging surfaces as much as possible. A simple sum of all local overhang constraints is therefore not suitable. A mapping of the local constraints with the ramp function before adding them resolves this issue. To keep the problem differentiable not the true ramp function but a continuous approximation is more appropriate. The continuous ramp function is given by Equation (8.2):

$$g_{ramp}(x) = \frac{1}{R}\ln\left(1 + e^{(R\cdot x)}\right), \tag{8.2}$$

R is a tuning parameter that controls how accurate the approximation is, a larger R gives a better approximation. Since it is an approximation, this function will never return a zero but a small positive value. As a consequence the total overhang measure will always be positive, even if all constraints are satisfied. Therefore, this measure is not suited in a constraint based restriction method, because the constraint would never be satisfied. An alternative is to add the total overhang to the objective function as a penalty term. The downside being that the constraint is not enforced strictly anymore. Overhang will not be removed if this will have a larger negative effect on the compliance.

In summary, the measure for the total overhang of a design for all k build directions is the sum of all m constraints after that they have been mapped with the continuous ramp function, see Equation (8.3):

$$OH_j^{tot} = \sum_{i=1}^{m} \frac{1}{R} ln\left(1 + e^{R\left(\frac{1}{\cos(\alpha)}\frac{\mathbf{n}_j^T \nabla \mathbf{x}_i}{|\nabla \mathbf{x}|_i} - 1\right)}\right) \qquad j = 1, 2, \ldots, k. \tag{8.3}$$

Then, the minimum of this set of total overhang values is calculated with a similar function as the P-norm, discussed in Section 7.1. This approximated min-operator uses the inverse of the input of the P-norm and is shown in Equation (8.4). Where, P is again a tuning parameter that can be increased to improve the approximation of the true minimum. Also here the reason to choose for a continuous form is to conserve the differentiability:

$$g_{min}(x) = \frac{1}{\sqrt[P]{\sum_{i=1}^{n} \frac{1}{x_i^P}}}. \tag{8.4}$$

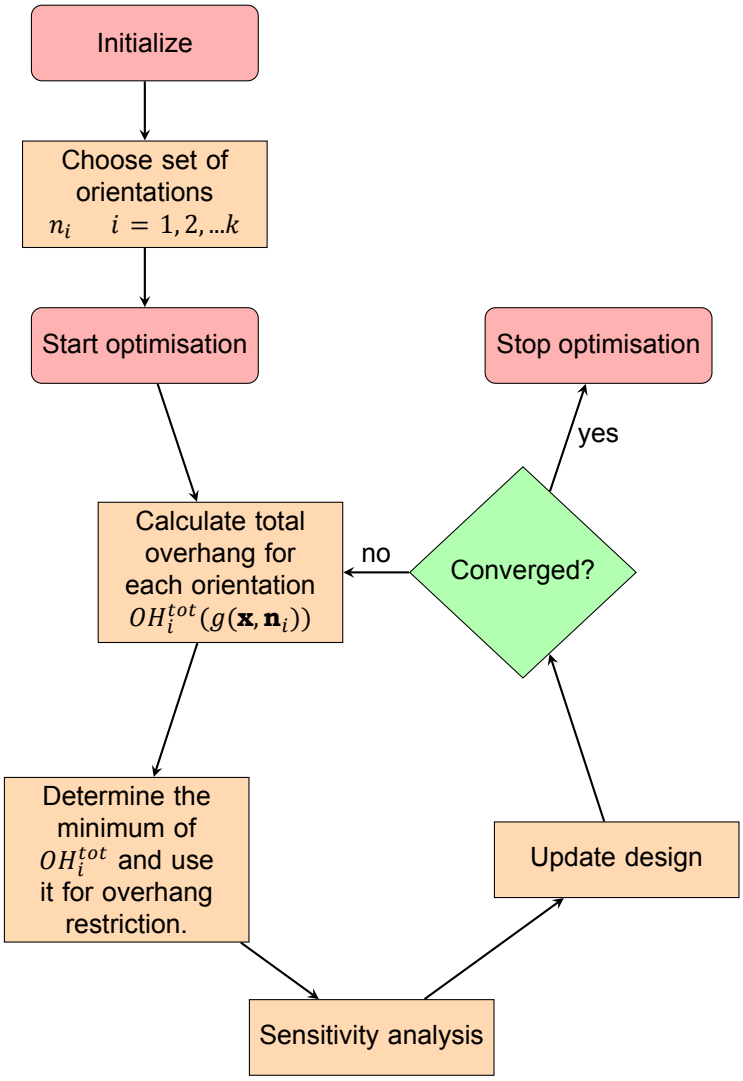

Figure 8.4: Flow chart showing the general method for an overhang restriction method that also considers the build orientation. The compliance and volume are not mentioned in the flowchart but, off course, are still part of the optimisation.

To recapitulate the above, in Equation (8.5) the new full optimisation problem is stated. An additional advantages of this method is the elimination of the many local constraints, because the local constraints are, so to speak, aggregated by Equation (8.3):

$$\begin{aligned} \min_{\mathbf{x}} \quad & c(\mathbf{x}) + \Omega \cdot g_{min}\left(OH_i^{tot}\right) \\ \text{s.t.:} \quad & V(\mathbf{x})/V_0 - 1 \leq 0 \\ & \mathbf{0} \leq \mathbf{x} \leq \mathbf{1}. \end{aligned} \tag{8.5}$$

In Equation (8.5), Ω is a factor in order to correct for the units of the compliance. Furthermore, Ω could be used to scale the cost of overhang in respect to the compliance. As was mentioned previously, the overhang constraint is not enforced strictly and the optimiser can choose to retain overhang if this is more beneficial for the stiffness. By choosing a proper scaling the cost of overhang can be made arbitrary high, such that a completely self-supporting final design is obtained.

The derivative of the new function is easily found with systematically applying the chain rule for differentiation. The derivatives of the newly used functions g_{ramp} and g_{min} are given by Equations (8.6) and (8.7) respectively:

$$\frac{\partial g_{ramp}}{\partial x} = \frac{e^{R \cdot x}}{1 + e^{R \cdot x}}, \tag{8.6}$$

$$\frac{\partial g_{min}}{\partial x_s} = \frac{1}{x_s^{1+p}\left(\sum_{r=1}^{m} \frac{1}{x_r^p}\right)^{1+1/p}}. \tag{8.7}$$

So far, two gradient operators are used, the 2×2 Roberts cross and the 3×3 Sobel operator. For reasons discussed in Chapter 4, both operators had to be modified for a proper functioning. The modified Sobel operator lost its rotational symmetry after the modifications. This property did not have much relevance because the reference vector remained constant. In fact, the modification to the density gradient operator was effective because the rotational symmetry was removed and a fixed build direction assumed. However, the build direction can no longer be assumed a priori and the rotational symmetry of the operator becomes an issue. Therefore, the modified Sobel operator can not be used for this approach.

It is also important to mention that this approach does not consider a shift to the base plate, i.e. the possibility that the material domain of a design does not necessarily has to be at the boundary of the design domain. So, for certain optimisation problems the situation could occur that a perfectly printable design is regarded overhanging.

8.2. Results

For the numerical examples the standard test problems are used once more. In Table 8.1 the used parameter settings for these examples are given. The first test considers four different build direction, namely: north, west, south and east. These directions should be seen from the original orientation, as was used in the previous chapters. The same test are performed with the diagonal directions added to the set of considered build orientations. So, a total of eight build orientations are considered. To see what the effect of a diagonal build direction on the topology is, the last tests only consider the diagonal directions. In Appendix C data on the performance measures is available.

Table 8.1: Parameters used throughout the numerical examples presented in this chapter, unless stated otherwise.

# of elements	40×20
Volume fraction	40%
SIMP power	5
Density filter radius	2
Critical angle α	45°
Max nr. of iterations	1000
Cost scaling Ω	1
Ramp parameter R	5
Minimum parameter P	4

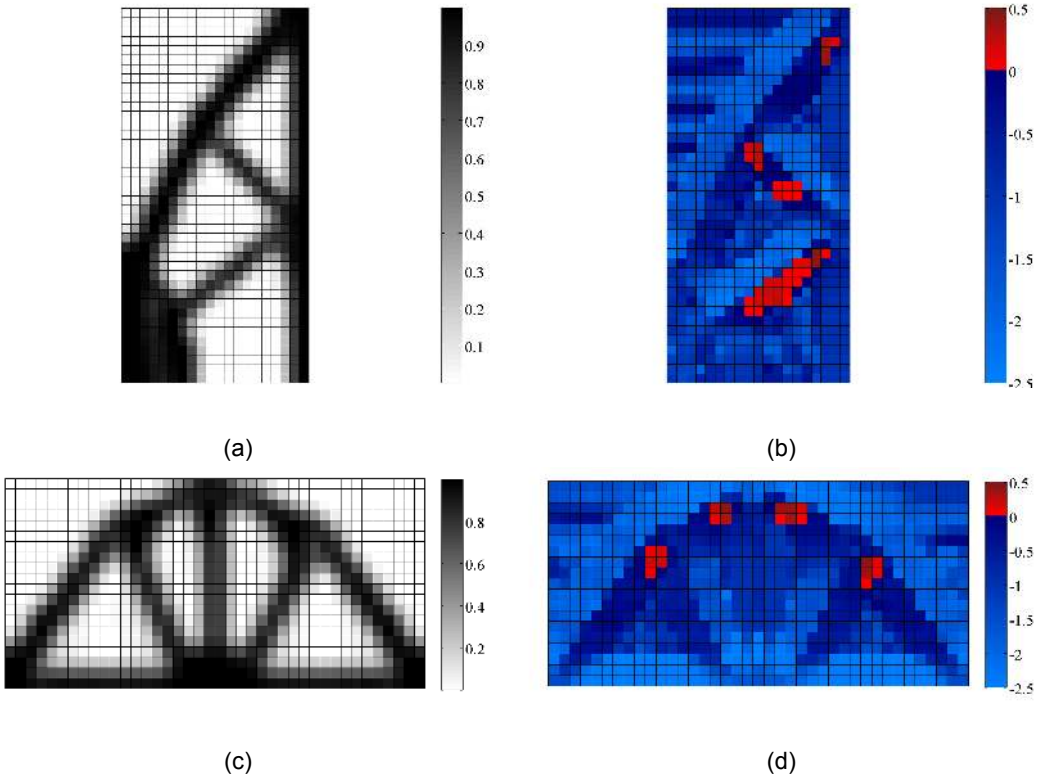

Figure 8.5: Results of the topology optimisation including overhang constraint with variable orientation. The four directions perpendicualr to the edges of the design domain are considered as build directions.The figures are rotated such that the bottom of the figure corresponds with the base plate of the SLM machine. a,b) Density field and corresponding constraint values of the MBB beam. c,d) Density field and constraint values of the bridge.

8.2.1. Four directions

The results are shown in Figure 8.5. Figures 8.5a and 8.5c present the topology of the optimised MBB beam and bridge respectively. The figures are rotated accordingly with the found optimal build orientation. It is seen that for the MBB beam the most favourable build direction is to the east. The corresponding design is practically the same as the original design without overhang constraint, except for the larger block of material at the lower left corner where the structure rests on the base plate. The orientation for the bridge did not change. It is still build in the original north direction. The top beam is made self-supporting by placing a large supporting beam at the middle.

In Figures 8.5b and 8.5d the corresponding constraint values are shown. The colour scaling is adjusted to make it easier to spot constraint violations. For both test cases it is seen that the final topologies do not fully satisfy the overhang constraint. Apparently, the cost of constraint violations did not outweigh the performance loss by design modifications. The scaling factor Ω should be increased to find fully self-supporting designs. In Appendix D the effect of scaling is shown. During the optimisation Ω is increased by a factor 10. It is found that the bridge problem returned completely feasible. The MBB beam still retained some overhang, albeit much less. This is explained by the higher compliance value of the MBB beam. An even further scaling of the overhang measure is expected to yield also for this design fully self-supporting solutions.

In Appendix C the convergence, non-discreteness and total overhang history is captured in graphs. The optimisation for the MBB beam stopped after 140 iterations because the change in objective function reached the tolerance. The optimiser sticks to the east direction from the beginning. The overhang measure for the west direction is very close to the east direction. The bridge did not converge and the optimisation was terminated because the limit of iterations was exceeded. The convergence is initially fast but does hardly change after about 150 iterations. The optimiser cleary opts for the north build direction during the whole optimisation.

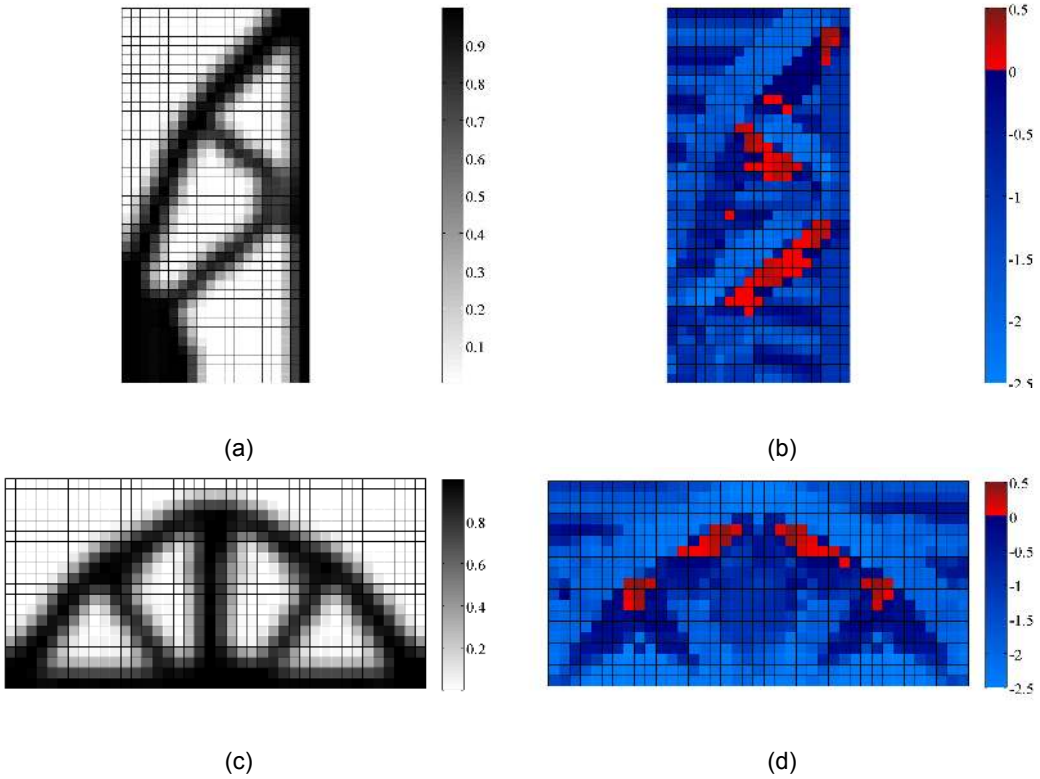

Figure 8.6: Results of the topology optimisation including overhang constraint with variable orientation. Eigth build directions are considered. The four directions perpendicualr to the edges of the design domain together with the diagonal directions.The figures are rotated such that the bottom of the figure corresponds with the base plate of the SLM machine. a,b) Density field and corresponding constraint values of the MBB beam. c,d) Density field and constraint values of the bridge.

8.2.2. Eight directions

In Figure 8.6 the results of the same problems are shown, but now with four more directions in the set of considered build orientations. The design of the MBB beam did hardly change compared to the previous test, Figure 8.6a. Also the bridge structure remains more or less the same except that it is somewhat lower, Figure 8.6c. Looking at the constraint values in Figures 8.6b and 8.6d, it is seen that again constraints remain violated.

The course of the optimisation for the MBB beam is very much the same as previously. Again, the optimiser sticks to the east build direction. The addition of the other possible build directions has almost no effect. The optimisation of the bridge ended after 90 iterations because the objective function did not decrease sufficiently. However, the compliance and discreteness significantly improved compared to the previous test case. Again, the optimal build direction is north. At the start of the optimisation the east and west direction are shortly in favour.

8.2.3. Diagonal directions

The diagonal directions are considered without the north, west, south and east directions to investigate the effect of these direction. The density fields and constraint values are given in Figure 8.7. The topologies are cleary adjusted to the new build direction. The build direction for the MBB beam is north-west. The opposite south-west direction is the second most favourable build direction. This is easily seen from the density field. The middle beam is for these direction the only real overhanging member. The optimiser rotated this beam such that it is less overhanging, but did not rotate it completely to satisfy the overhang constraint.

The optimiser choose the north-east direction as the build direction for the bridge. After 25 iteration, the optimiser sticks with the north-east direction and changes the design to accordingly. It is seen that the design of the bridge is not longer symmetric. Constraint violations are still present at the corners of the wedges.

The convergence was more difficult for these examples. Both cases terminated the optimisation

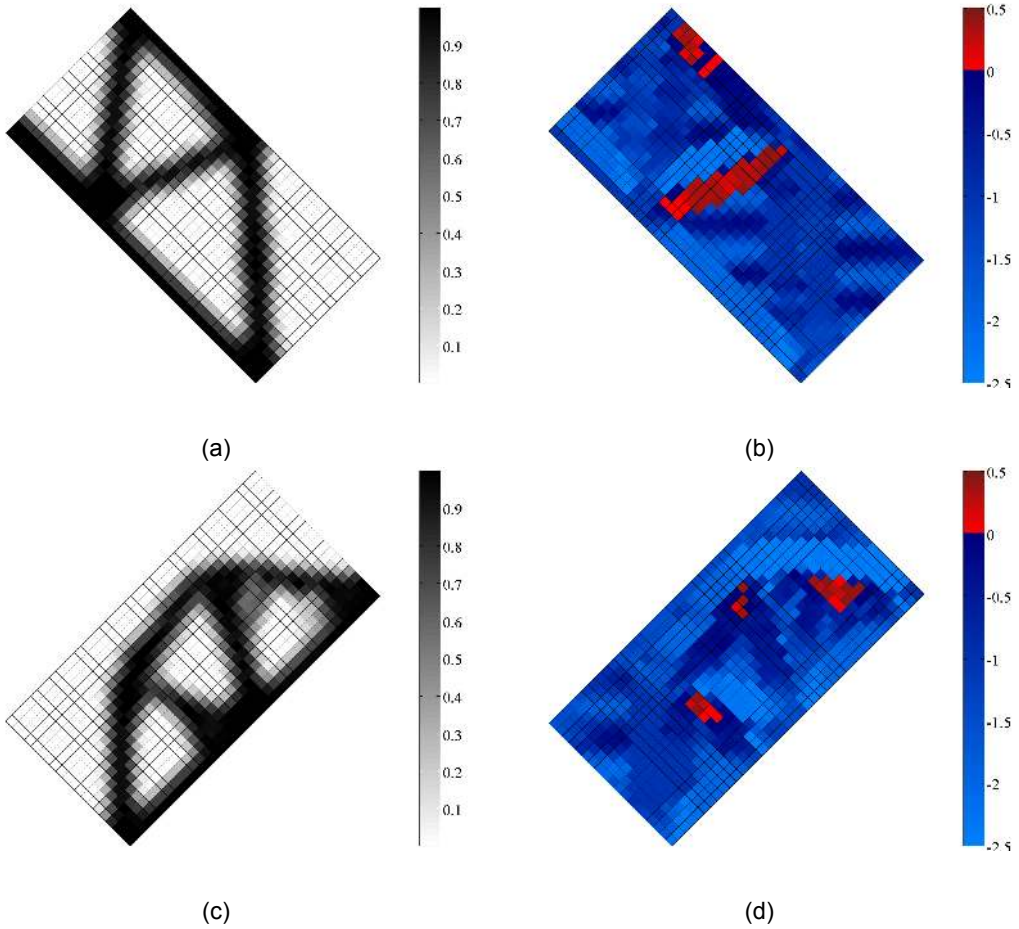

Figure 8.7: Results of the topology optimisation including overhang constraint with variable orientation. Only the four diagonal directions are used as possible build direction.The figures are rotated such that the bottom of the figure corresponds with the base plate of the SLM machine. a,b) Density field and corresponding constraint values of the MBB beam. c,d) Density field and constraint values of the the bridge.

due to exceeding the iteration limit. Although the final compliance and discreteness are slightly better than in the previous examples, the measure for total overhang remained higher.

8.3. Comparison

In Table 8.2 the number of iterations, compliance and non-discreteness measures are listed for the numerical examples. It is seen that the number of iterations are reasonable for those cases that converged for an other reason than exceeding the maximum number of iterations. The objective is given as percentage of the optimal solution without overhang constraint. It is noticed that the compliance is in general fairly close to the compliance of the benchmark. Also the final non-discreteness of the test cases attained values that are normal for a topology optimisation with density filtering.

8.4. Discussion

The major advantage of the local overhang constraint is the usability in a relatively cheap optimisation that also regards a variable orientation. An arbitrary number of orientations can be considered. Although the computational effort increases with the number of orientations, the only thing that needs to be calculated separately for every orientation is the scalar product of the density gradient and the build direction together with the applicable sensitivities. The structural analysis and the gradient field can be reused. So, only a relatively small fraction of the computations needs to be repeated for every orientation and the major part of the computational cost remains the same. The approach has some similarities with a multistart optimisation, as both methods concern some set of different orientations.

Table 8.2: Performance measures of the final designs from the numercial examples that considered a different set of build orientaitons.

Test case		Iterations	Compliance	Non-discreteness
4 Directions	MBB beam	140	109%	31.3%
	Bridge	1000	130%	41.3%
8 Directions	MBB beam	299	111%	31.4%
	Bridge	91	114%	36.0%
Diagonal directions	MBB beam	1000	104%	29.8%
	Bridge	1000	114%	32.9%

However, the here presented approach is much cheaper. A multistart performs a complete optimisation for every orientation. Here all orientations are considered during one optimisation. Thus, the more orientations are considered the more beneficial this method is. Especially for a 3D problem this implies huge savings in terms of computing time.

A possible danger of this method is to get stuck for a certain configuration. The optimiser assumes the at that moment most favourable build direction. The design changes will improve the objective as well as the constraint for that build direction. So, the current build direction has an advantage over the other build directions. Only if the objective is strongly improved by changes to the design unfavourable for the current build direction, the optimiser will switch orientation. A proper scaling between the overhang constraint and the objective is therefore crucial.

Another aspect that should be taken into account is the weak enforcement of the overhang constraint. It was seen from the numerical examples that the overhang constraint was not completely satisfied. The penalty on the overhang did not compensate the resulting loss in stiffness. The effect of a simple increase of the scaling factor Ω was shown to result in fully satisfied constraints. However, a proper balance between compliance and overhang is required. For this, a problem dependent scaling is necessary. Furthermore, a variable scaling is expected to yield the best results. At the start of the optimisation the objective should have the priority. At the end of the process the overhang constraint should prevail in order to ensure overhang-free designs.

The test case with only the diagonal direction had more troubles converging. It was seen that especially the overhang measure remained high. The simple approximation of the density gradient is the cause for this. The square convolution kernels disadvantage the diagonal direction. For the diagonal directions, the optimiser has no possibility to make a properly supported wedge without applying elements of intermediate density. The orthogonal directions (north, west, south, east) are, with this approximation of the density filter, easier satisfied and will therefore in general be preferred over another direction. A true rotationally symmetric density gradient approximation should be used in order to optimise for any build orientation.

9 Discussion

The overhang elimination methods based on the density gradient have been applied in numerical tests. Some methods gave better results than others, but a flawless functioning algorithm was not found. In this chapter some general issues encountered during the tests will be discussed.

9.1. Grey supports

In the results of the numerical examples it was seen that in some cases support material was formed, e.g. Figures 6.4a and 6.5a. However, it was noticed that the density of the supporting elements reduced in the vertical direction. This unwanted effect is due to a weakness in the formulation of the overhang constraint. The constraint was designed to allow all density gradients with an angle of 45 degrees or more with respect to the build direction. Supporting members are typically placed vertically, that is parallel to the build direction. Consequently, the angle of the density gradient with the build direction would be 90 degrees and this means that the constraints are not active. In the situation when purely supporting members are indispensable, the constraint should be active, i.e. on the edge of feasible and infeasible. Otherwise, the optimiser is given too much freedom and will find ways to improve the design until it reaches the boundary of feasibility. Since the supporting members do not add to the stiffness, the optimiser will reduces material as long as the overhang constraint is inactive. The optimiser exploits this weakness in the constraint formulation to make supports more material economic. The final design features supporting members with an artificial angle of 45 degrees to the base plate by reducing the density of the lower elements. Because of this, long support structures seem to grow out of thin air. Such a characteristic support structure is shown in Figure 9.1a. The corresponding constraint values, Figure 9.1b, clearly show that the overhang constraint is indeed satisfied.

9.2. Constraint sensitivity

Besides the supports originating out of nothing, other issues related to the overhang constraint were observed. For one, designs did not evolve as close to a discrete solution as might have been expected. The intermediate densities at the boundaries of the structure are explained by the application of density filtering without a heaviside projection method. However, the benchmark problems without one of the overhang constraint methods resulted in much more discrete solutions than with an overhang constraint. In some of the examples grey areas remained that had no particular use. So, there are other mechanisms at work that prevent the optimiser to converge to a discrete solution. Furthermore, it was noticed that the convergence was troublesome. At some point during the optimisations the convergence became very slow, while a clear structure was not yet formed. These observed phenomena might indicate particularities in the sensitivity information of the overhang constraint. A detailed examination of the overhang constraint sensitivities will be performed to find the underlying reason.

Pure overhang

First, the scenario of a purely overhanging beam is investigated. This situation is presented in Figure 9.2a, together with the constraint values in Figure 9.2b. Clearly, overhang constraint violation

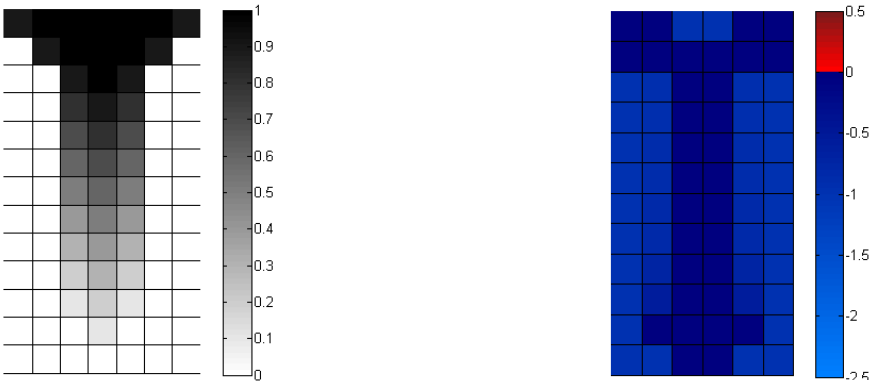

(a) (b)

Figure 9.1: This typical support structure, that becomes less dense to the bottom, was encountered in some of the numerical examples. The constraint allows this kind of support structures, as is seen from the left subfigure. Supports like these are formed because they require less material and the stiffness penalisation has no effect since support structures have in general a small contribution to the stiffness. a) Density field; b) Corresponding overhang constraint values.

is present. The sensitivity information of the overhang constraint should guide the optimiser to an overhang-free design. However, computation of the sensitivities reveal that they are in fact zero, see Figure 9.2c. This is seen by noting that in the case of pure overhang the density gradient points in the direction of the build direction. That is, at the violated constraints the gradient is parallel to the reference vector. Therefore, the in-product of the density gradient and the build direction is equal to the length of the density gradient:

$$\mathbf{n}^T \nabla \mathbf{x} = |\nabla \mathbf{x}|. \tag{9.1}$$

Consequently, their derivatives are equal as well. Also, compare Equations (6.7) and (6.8):

$$\frac{d\mathbf{n}^T \nabla \mathbf{x}}{dx} = \frac{d|\nabla \mathbf{x}|}{dx}. \tag{9.2}$$

Furthermore, from the constraint equation it follows that the derivative of the constraint to the in-product has a sign opposite to that of the derivative of the constraint with respect to the gradient length:

$$\frac{\partial g}{\partial \mathbf{n}^T \nabla \mathbf{x}} = -\frac{\partial g}{\partial |\nabla \mathbf{x}|}. \tag{9.3}$$

It can be concluded that the total derivative is zero:

$$\frac{dg}{dx} = \frac{\partial g}{\partial \mathbf{n}^T \nabla \mathbf{x}} \frac{d\mathbf{n}^T \nabla \mathbf{x}}{dx} + \frac{\partial g}{\partial |\nabla \mathbf{x}|} \frac{d|\nabla \mathbf{x}|}{dx} = \mathbf{0}. \tag{9.4}$$

In a realistic optimisation pure overhang is not very likely to occur. However, it shows a potential problem with the application of a gradient density. In real life, the phenomenon can cause relatively small sensitivities.

Tension beam

A more realistic scenario is investigated next. For this, a new test case is used. The problem comprises a horizontal force at the right upper corner of the design domain and supports at the left upper corner. In Figure 9.3 the schematic drawing of the problem is shown. This theoretical example is used because it is easy to interpret. The optimiser will build a solid beam at the top to carry the pulling force, hence tension beam. The overhang constraint will force the optimiser to produce supporting scaffolds underneath. The outcome of the optimisation is given in Figure 9.4a and the corresponding overhang constraint values in Figure 9.4b. The result clearly shows the denser top rows and the characteristic supports. As a side note, the beam at the bottom of the design domain is created to gain some stiffness from the support material.

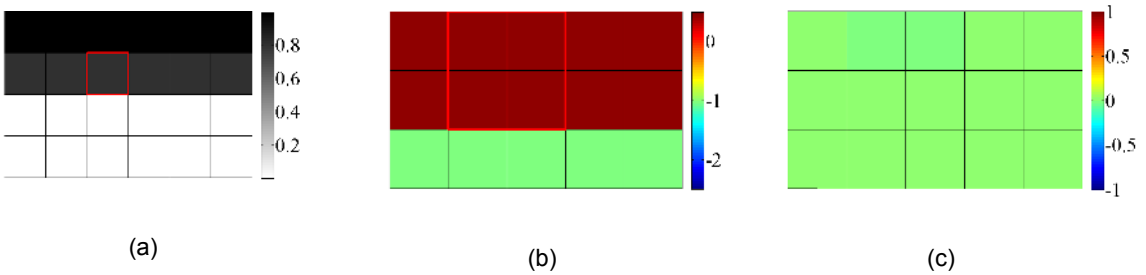

(a) (b) (c)

Figure 9.2: a) Density field of a pure horizontal overhanging beam. b) Corresponding overhang constraint values. The reddish colored constraints are larger than zero and thus violating the overhang constraint. c) Sensitivity information of the constraints with respect to the red outlined element in *a*, showing zero sensitivity.

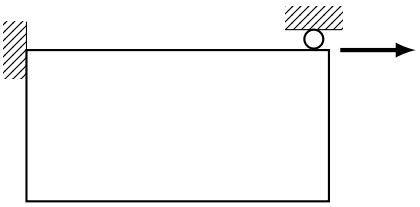

Figure 9.3: Schematic drawing of the tension beam problem indicating the design domain, support and applied force.

On closer inspection, it is observed that the top beam is not fully solid but has gaps in between. Also, grey areas remained that do not belong to the supporting scaffolds, see middle right part of the design domain. This behaviour can be explained by the sensitivity information. In Figure 9.4a, one element in each of the mentioned areas is red outlined. The influenced constraints are red outlined as well, see Figure 9.4b. Figures 9.4c and 9.4d show the corresponding overhang constraint sensitivities. It is important to notice that both negative and positive constraint sensitivities occur for the same element. This implies that an increase of the density of one of these elements will improve some constraints, but at the same time it will deteriorate others. The conflicting sensitivities in the grey areas will definitely complicate the optimisation and will slow down convergence, which was seen to be the reason for termination of the optimisation in many of the examples.

It is good to mention that for the aggregation this should be less of an issue. Indeed, with aggregation not all the constraints have to be strictly satisfied at all times. This is in correspondence with the results from Section 7.3, which were clearly improved as compared to the results from Section 6.4.1.

The underlying cause is the locality of the overhang constraints. The sensitivity information can not oversee the whole design domain but only in the proximity of the constraint. To build a support for an element that is far from a supporting surface, this can be the base plate or a different part of the structure, the optimiser should violate other constraints until the support reaches this surface. However, the optimiser cannot predict when and if this surface will come or where the nearest surface is located. This makes the convergence slow and gives rise to greyish topologies.

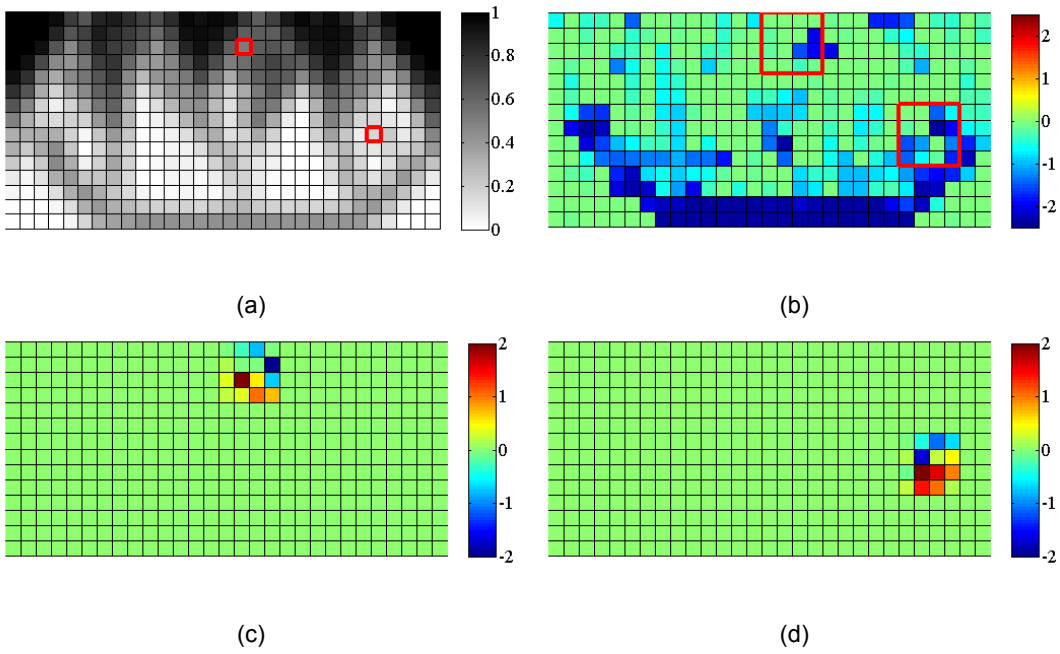

Figure 9.4: a) Density field of the tension beam showing the characteristic supports and grey areas. Two elements in the areas of interest are red outlined. b) The corresponding constraint values of the tension beam show no violations. The red outlined regions are the constraints that are influenced by the marked density element in subfigure a. c,d) Sensitivities of the constraints with respect to the respectively left and rigth marked element in subfigure a, showing conflicting sensitivity information.

10

Conclusion and Recommendations

10.1. Conclusion

The purpose of this research has been to investigate the possibility of using the gradient of the density field as the basis of an overhang restriction method in topology optimisation. This restriction method should serve the purpose of a manufacturing constraint for additive manufacturing processes. An overhang constraint that utilises the density gradient should allow for an arbitrary critical angle and a relatively easy inclusion of a variable build direction.

In this thesis an overhang identification that uses the gradient of the density field has been developed. This is applied in the formulation of a minimal compliance topology optimisation with overhang constraint. A density dependent relaxation method to loosen the overhang constraint in the initial stages of the optimisation is proposed as well as a filtering and thresholding procedure for crisp boundaries. Furthermore, aggregation of the overhang constraint to reduce the complexity of the optimisation problem is investigated. Finally, a novel method to include a variable build direction is proposed.

The implementation of the overhang formulation by means of many individual hard constraints in the topology optimisation problem does not yield useful results. It was found that the optimiser is likely to get stuck in areas with elements of intermediate density. A probable cause is the difficulty of optimisation problems with many design variables and a comparable amount of constraints. It was found that the sensitivities of the overhang constraints are conflicting. Furthermore, a weakness in the constraint formulation that allowed support structures reduce density with height has been identified.

Relaxation of the overhang constraint by means of neglecting the constraint for low density elements improved the results. However, upon continuation designs became infeasible and regions of intermediate density formed to restore the feasibility of the design. For some cases this led to the same problems as for the original overhang constraint, i.e. without relaxation. A carefully set up continuation scheme or an increased stiffness penalisation power is necessary to obtain a recognizable structure.

Filtering and thresholding of the design variables to a more discrete field helped to find clearer structures. However, the convergence to a full discrete solution remains problematic because the support structures remain grey and will disappear eventually due to the volume constraint. Also this method requires a continuation scheme.

Constraint aggregation was shown to reduce the complexity of the problem. This allowed the optimiser to find recognisable structures, and no continuation is required. It was found that the aggregation error is worst at the supreme moment when the design becomes feasible. Consequently, plain aggregation has the tendency to result in sub-optimal designs.

The density gradient based overhang constraint has also been used in a novel approach to include the build orientation into the optimisation. This approach considers a set of build directions at the same time and optimises the structure mainly according to the most promising orientation. This makes the method efficient because the structural analysis has to be performed only once and the additional computational cost of the constraint is remote. The numerical examples showed promising first results. Optimal structures and corresponding build direction were obtained that fully satisfied the original over-

hang constraint.

The overhang restriction based on the gradient of the density field was shown to have certain advantages over the existing methods, although challenges remain in developing a fully functioning algorithm that delivers optimal and manufacturable designs.

10.2. Recommendations

A flawless method to eliminate overhang from designs has not been found, although various approaches have shown promising results. More research is necessary to develop the density gradient approach further. Some aspects that need extra attention are listed below.

- The weakness in the overhang constraint concerning support structures growing out of thin air should be resolved. Possibly, this could be accomplished by composing a penalty term that captures the characteristic smooth transition from void to solid in the vertical direction.
- A more generally applicable method to find the density gradient should be developed. Currently, the simple approximation of the gradient with the convolution kernels is only applicable for regular meshes. Also, the applied gradient operators resulted in biased orthogonal build directions. A gradient that is obtained from a circular section of the mesh is expected to give better results.
- The constraint aggregation method can be improved by using an adaptive aggregation parameter or other methods to improve the aggregation at feasible designs, see also Section 7.4.
- Relaxing the problem by penalising overhang in the objective could be more suitable than a constraint approach. To overcome the weak enforcement of the constraints and make sure that the original constraints are satisfied, a continuation scheme that increases the cost of overhang with iteration number could be used in a penalty-based approach or the critical angle can be chosen slightly more strict.
- The measure for the total overhang in the variable orientation approach could be extended. For example by increasing the cost of overhang at a greater distance from the base plate. Because, in general, overhang far from the base plate requires more support material and thus has a larger impact on the objective.
- A proper scaling of the objective and overhang measure should be investigated in order to prevent getting stuck at one orientation and obtain a final structure that is overhang-free. The simple scaling used in Appendix D already showed that completely satisfying designs can be found by proper scaling. However, the scaling should be more robust, such that it finds feasible solutions for every design problem.
- For the variable build orientation, the base plate should be placed at the lowest boundary of the structure, material domain, for that orientation. Currently, the base plate is always at the boundary of the design domain. This could give erratic overhang measures. An improved version of the method should make shifts of the base plate possible.

A

Results direct constraint methods

A.1. Overhang constraint

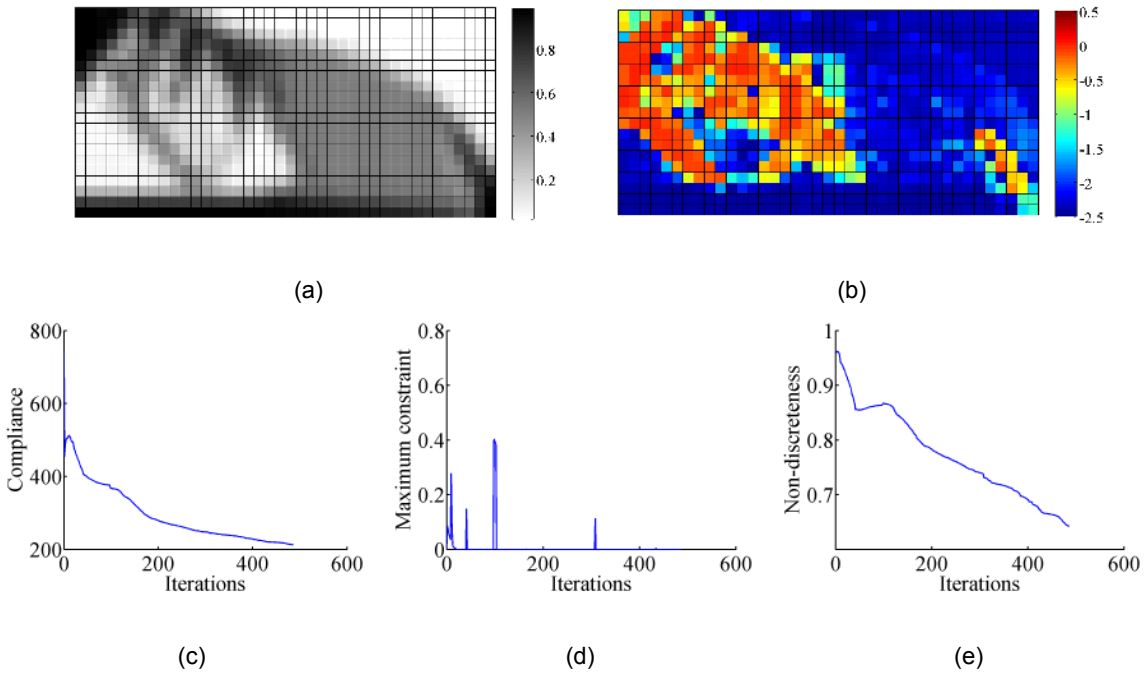

Figure A.1: Results of the overhang constraint in combination with the Roberts cross gradient kernel tested on the MBB beam. a) Density field; b) Constraint field; c) Convergence; d) Maximum overhang constraint value; e) Non-discreteness.

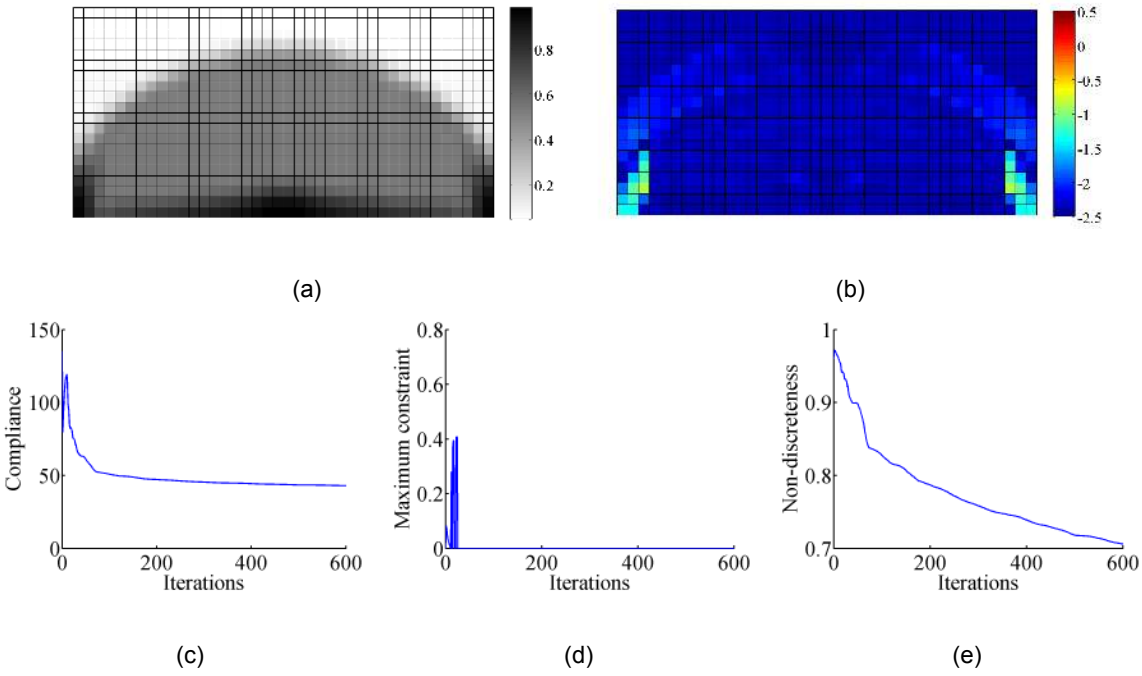

Figure A.2: Results of the overhang constraint in combination with the Roberts cross gradient kernel tested on the bridge. a) Density field; b) Constraint field; c) Convergence; d) Maximum overhang constraint value; e) Non-discreteness.

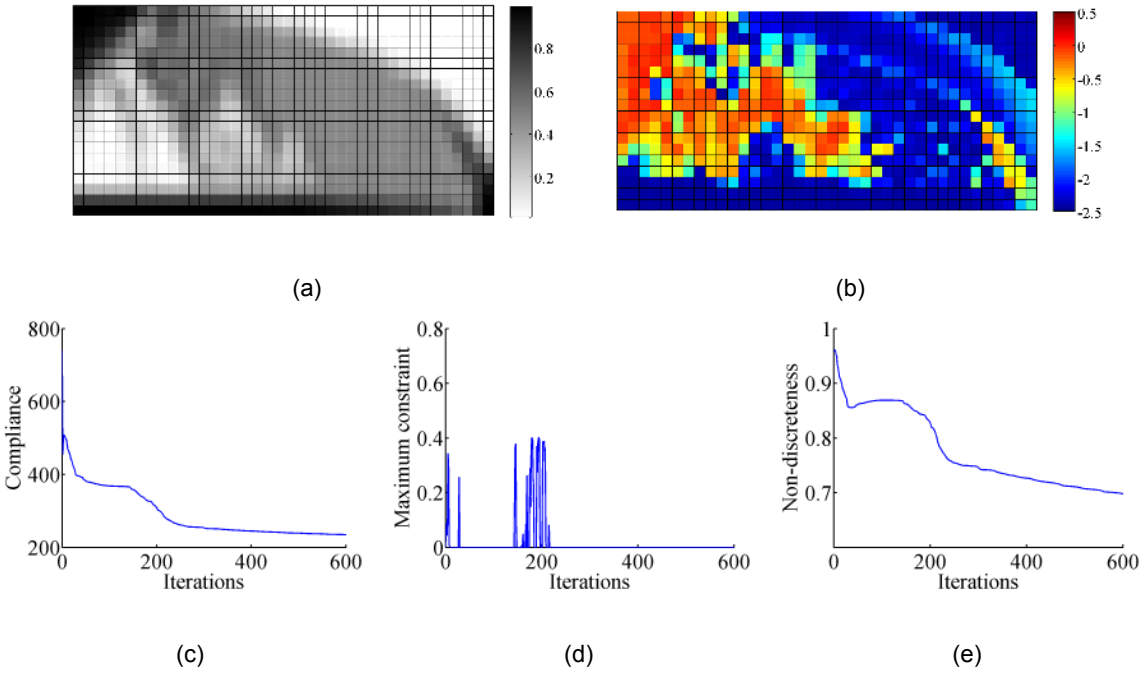

Figure A.3: Results of the overhang constraint in combination with the Sobel gradient kernel tested on the MBB beam. a) Density field; b) Constraint field; c) Convergence; d) Maximum overhang constraint value; e) Non-discreteness.

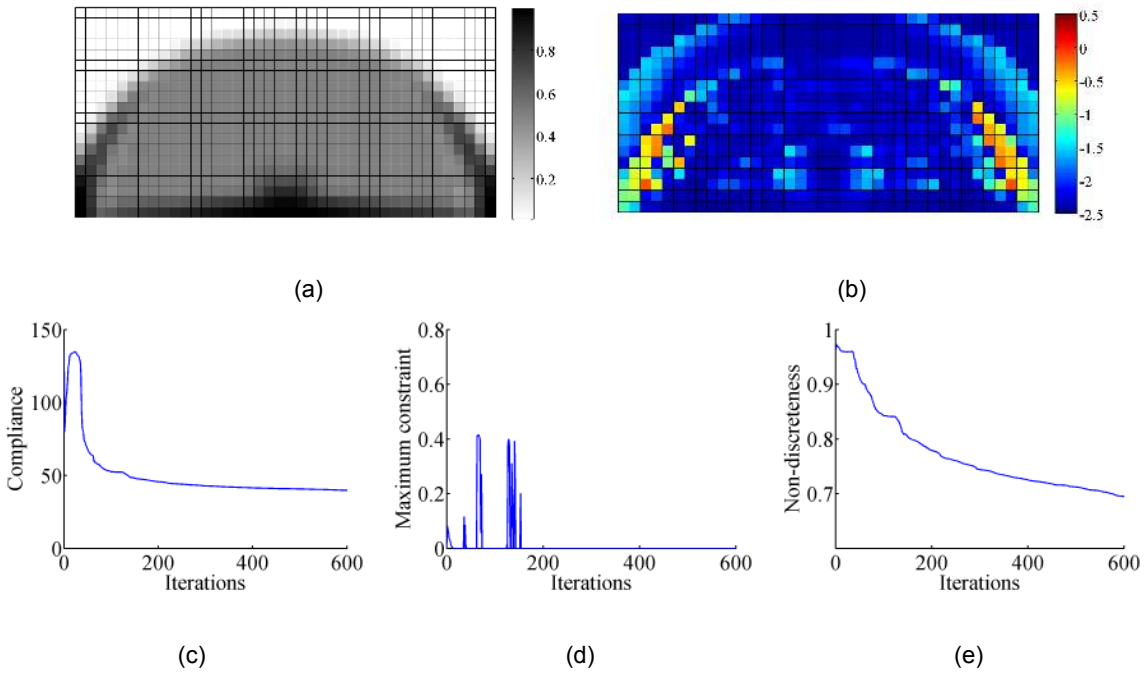

Figure A.4: Results of the overhang constraint in combination with the Sobel gradient kernel tested on the bridge. a) Density field; b) Constraint field; c) Convergence; d) Maximum overhang constraint value; e) Non-discreteness.

A.2. Grey relaxation

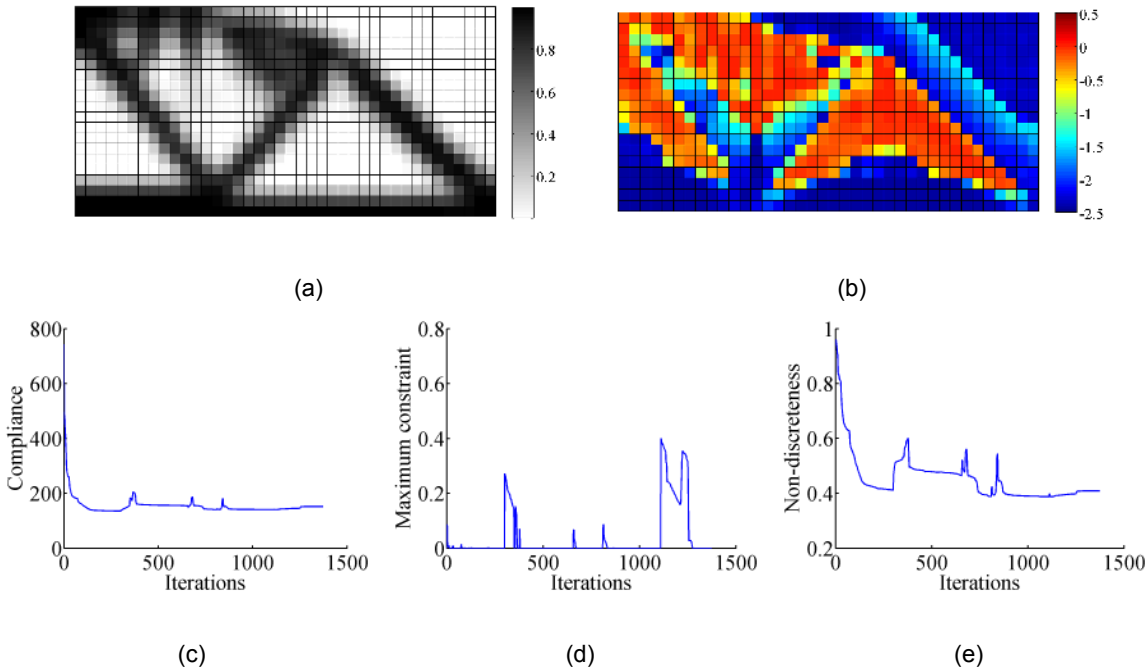

Figure A.5: Results of the overhang constraint with grey relaxation tested on the MBB beam. a) Density field; b) Constraint field; c) Convergence; d) Maximum overhang constraint value; e) Non-discreteness.

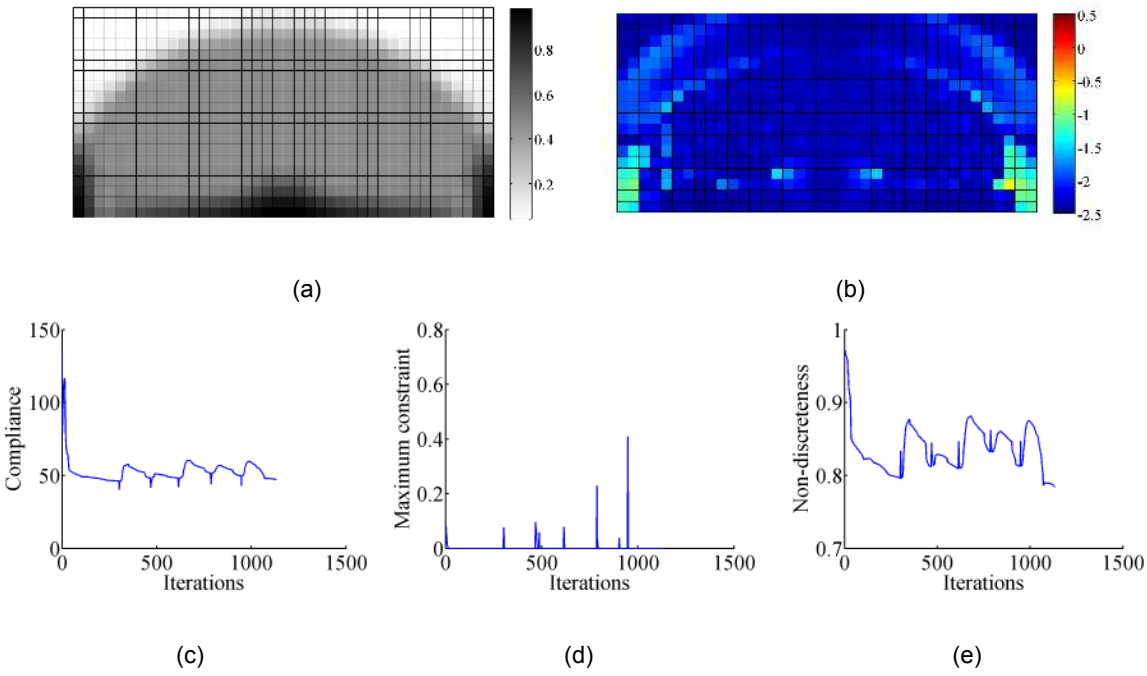

Figure A.6: Results of the overhang constraint with grey relaxation tested on the bridge. a) Density field; b) Constraint field; c) Convergence; d) Maximum overhang constraint value; e) Non-discreteness.

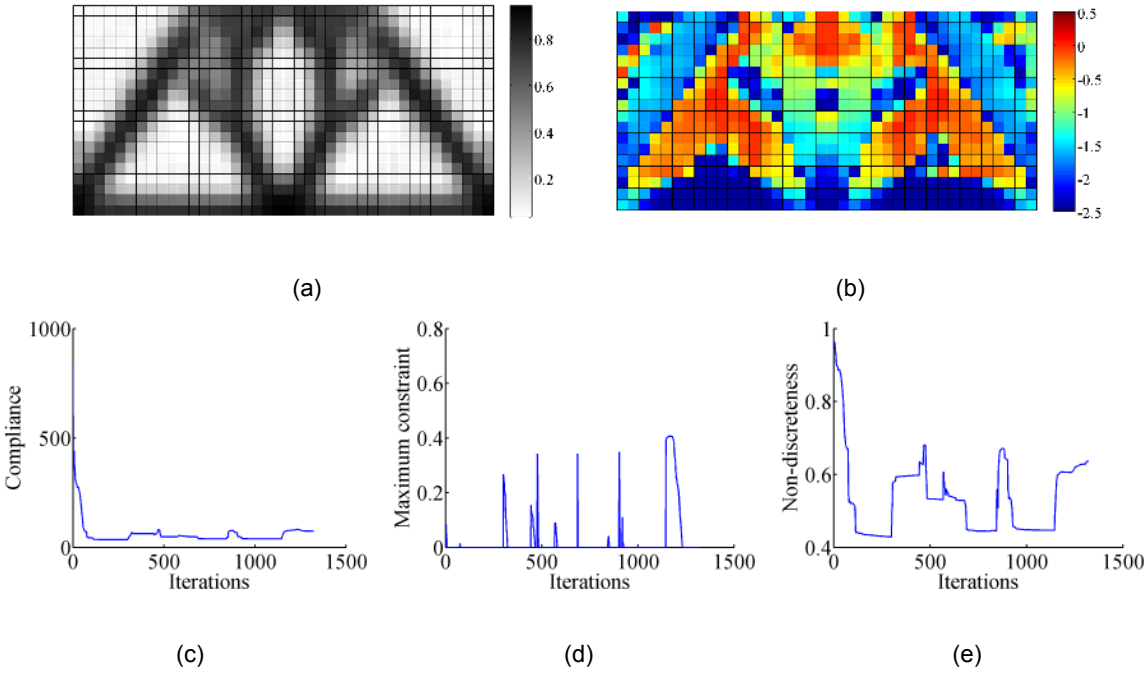

Figure A.7: Results of the overhang constraint with grey relaxation tested on the bridge with an increased grey penalisation factor. a) Density field; b) Constraint field; c) Convergence; d) Maximum overhang constraint value; e) Non-discreteness.

A.3. Crisp boundaries

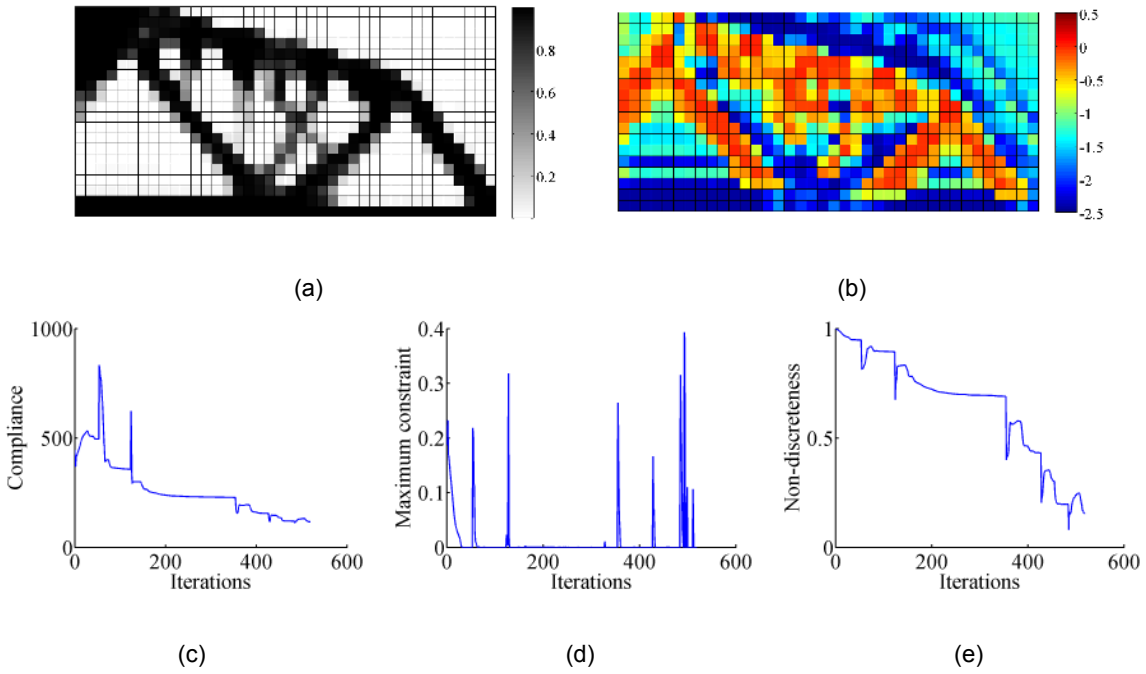

Figure A.8: Results of the overhang constraint with crisp boundary projection tested on the MBB beam. a) Density field; b) Constraint field; c) Convergence; d) Maximum overhang constraint value; e) Non-discreteness.

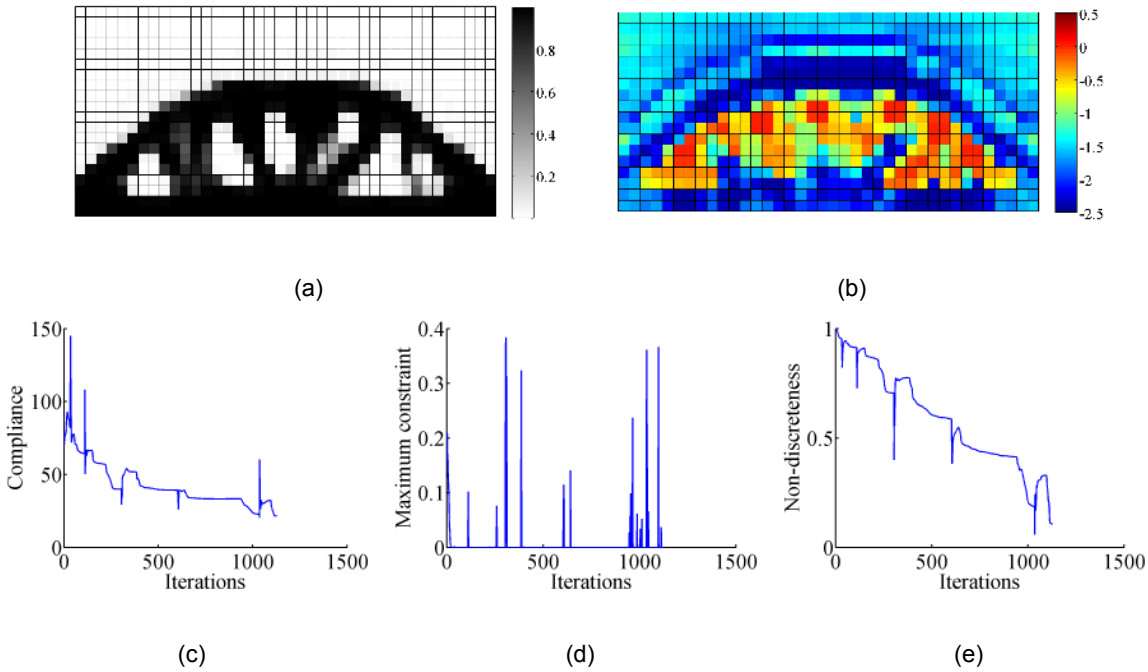

Figure A.9: Results of the overhang constraint with crisp boundary projection tested on the bridge. a) Density field; b) Constraint field; c) Convergence; d) Maximum overhang constraint value; e) Non-discreteness.

A.4. Starting point

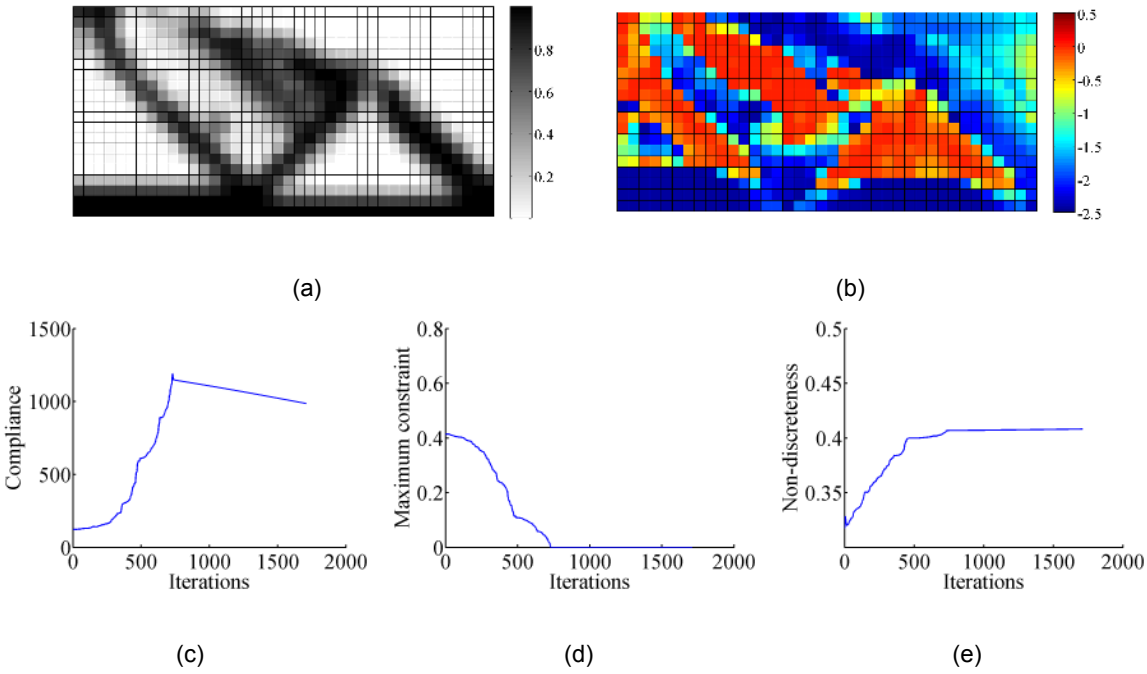

Figure A.10: Results of the overhang constraint started from the optimal design without constraint on the overhang tested on the MBB beam. a) Density field; b) Constraint field; c) Convergence; d) Maximum overhang constraint value; e) Non-discreteness.

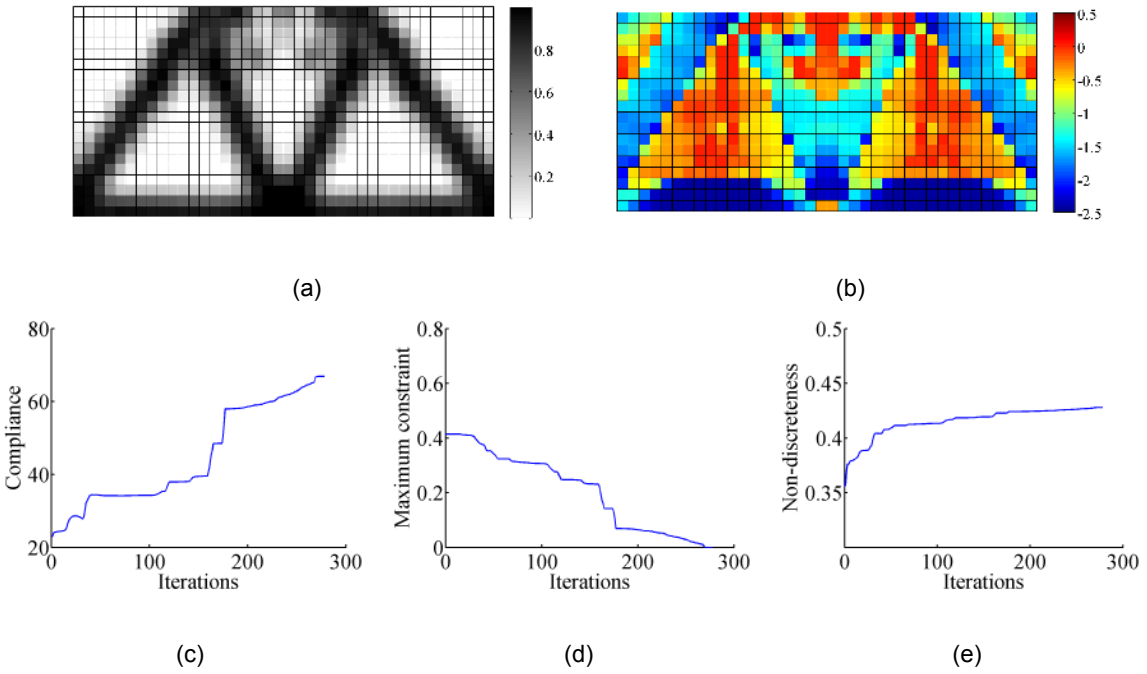

Figure A.11: Results of the overhang constraint started from the optimal design without a constraint on the overhang tested on the bridge. a) Density field; b) Constraint field; c) Convergence; d) Maximum overhang constraint value; e) Non-discreteness.

B

Results aggregated constraint method

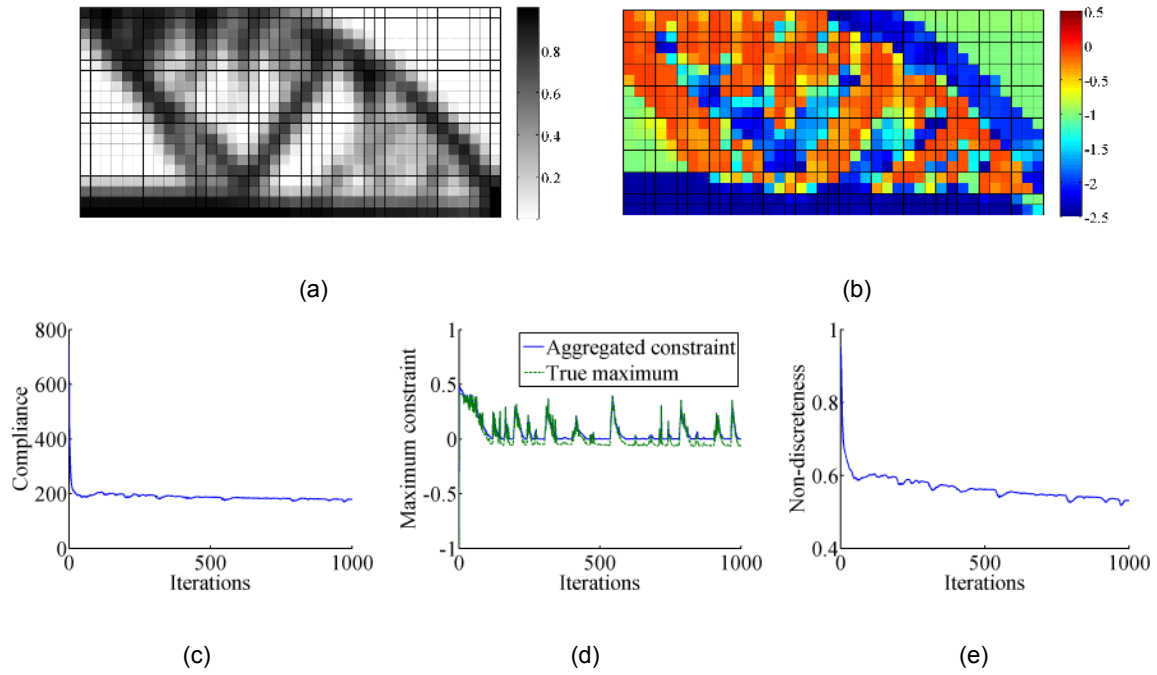

Figure B.1: Results of aggregated overhang constraint with in literature recommended aggregation parameter tested on the MBB beam. a) Density field; b) Constraint field; c) Convergence; d) Maximum overhang constraint value; e) Non-discreteness.

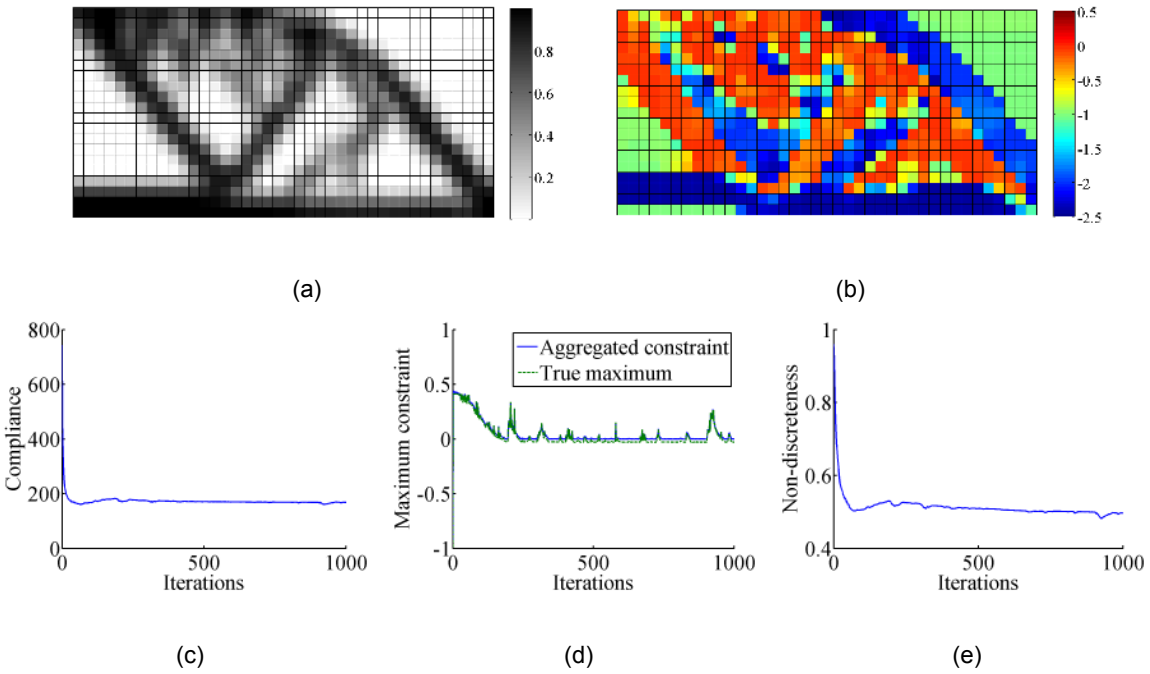

Figure B.2: Results of aggregated overhang constraint with increased aggregation parameter tested on the MBB beam. a) Density field; b) Constraint field; c) Convergence; d) Maximum overhang constraint value; e) Non-discreteness.

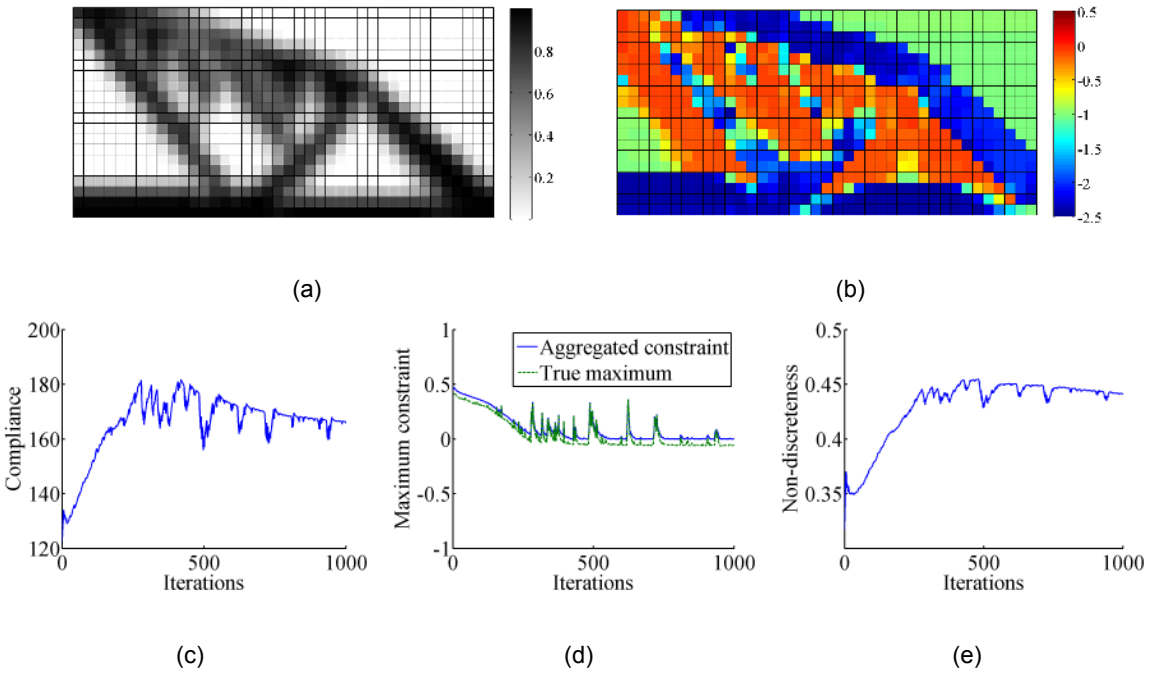

Figure B.3: Results of aggregated overhang constraint started from the optimal solution without overhang constraint tested on the MBB beam. a) Density field; b) Constraint field; c) Convergence; d) Maximum overhang constraint value; e) Non-discreteness.

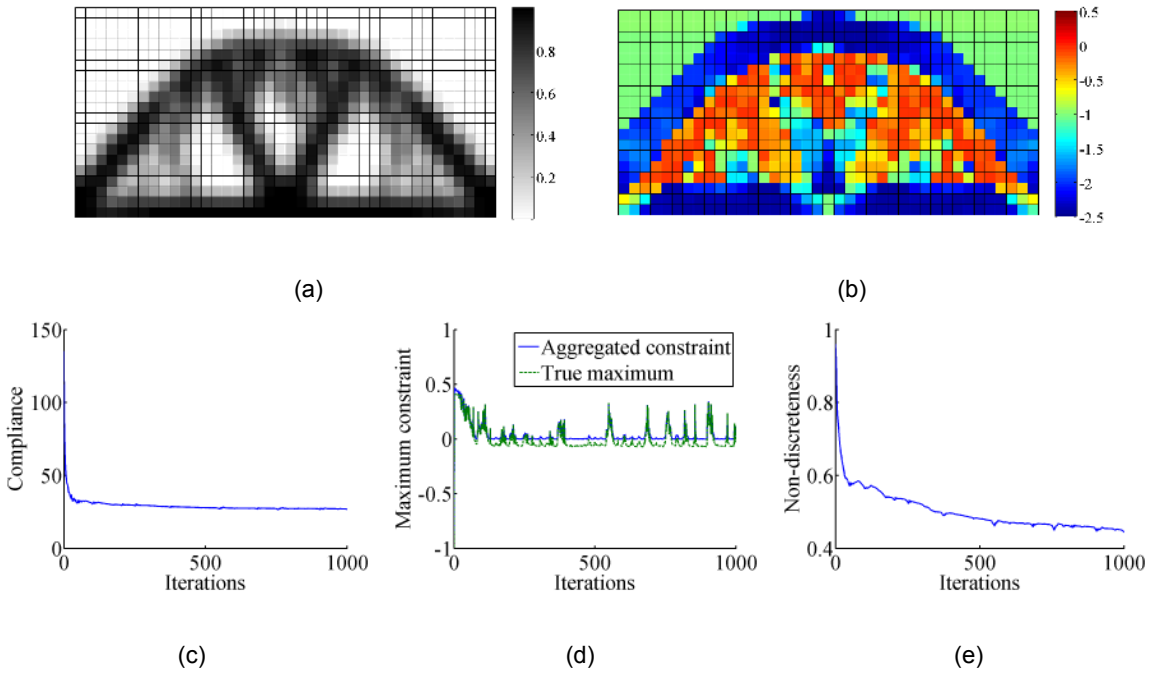

Figure B.4: Results of aggregated overhang constraint with in literature recommended aggregation parameter tested on the bridge problem. a) Density field; b) Constraint field; c) Convergence; d) Maximum overhang constraint value; e) Non-discreteness.

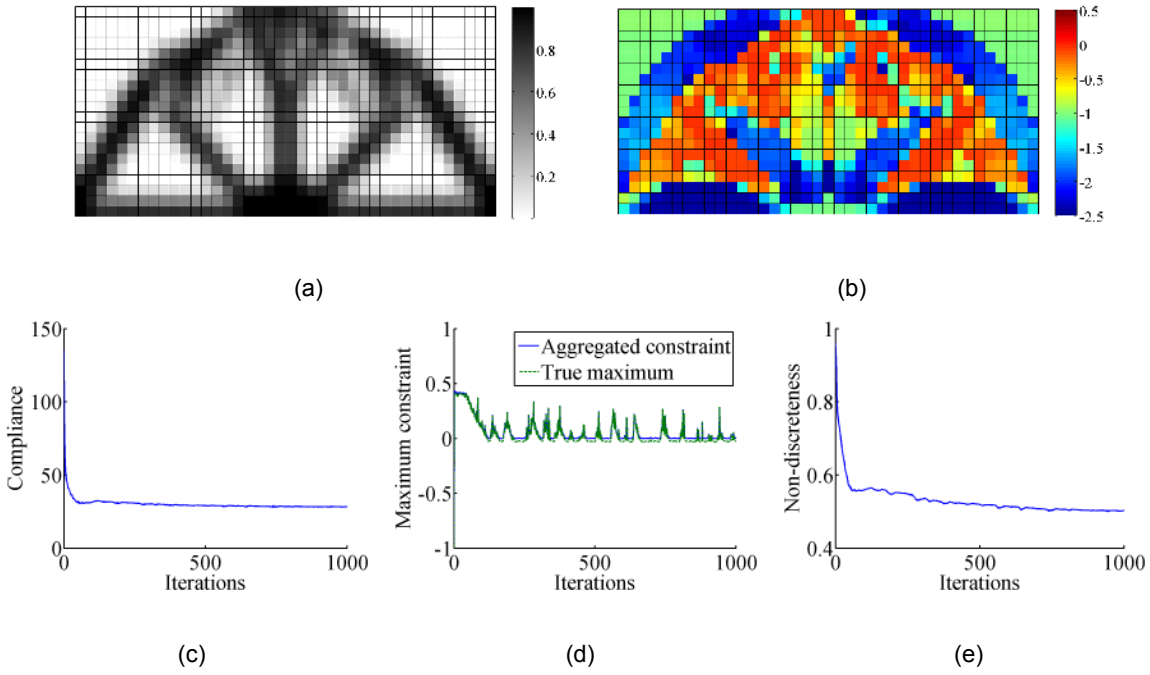

Figure B.5: Results of aggregated overhang constraint with increased aggregation parameter tested on the bridge problem. a) Density field; b) Constraint field; c) Convergence; d) Maximum overhang constraint value; e) Non-discreteness.

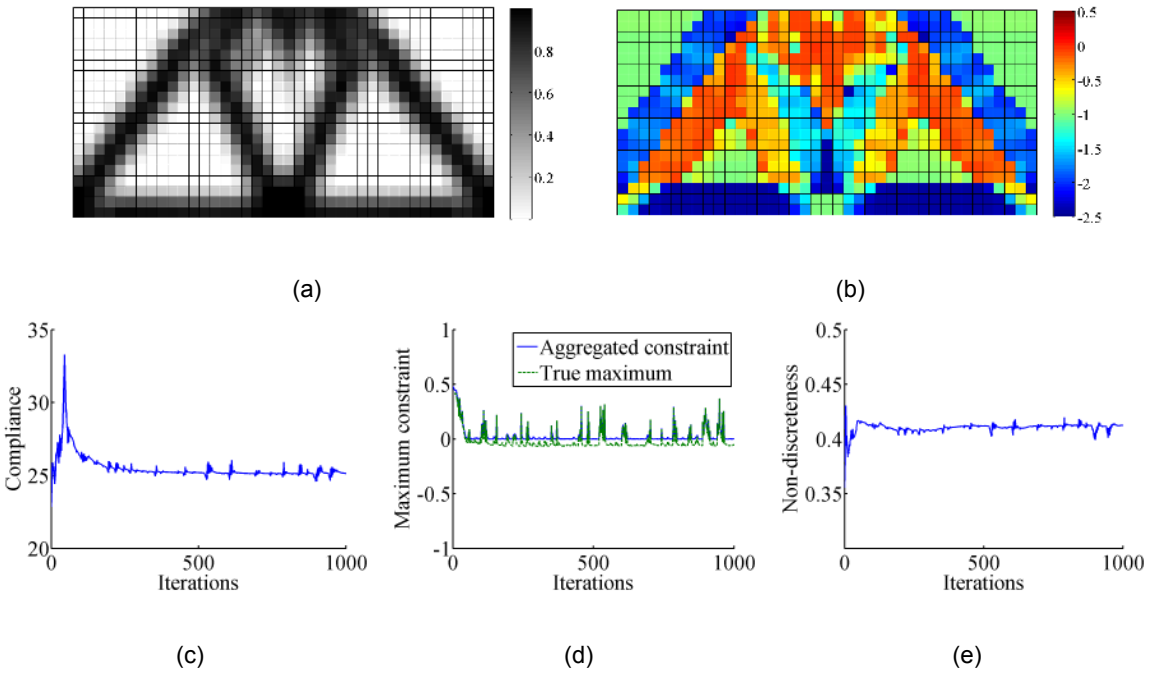

Figure B.6: Results of aggregated overhang constraint started from the optimal solution without overhang constraint tested on the bridge problem. a) Density field; b) Constraint field; c) Convergence; d) Maximum overhang constraint value; e) Non-discreteness.

C

Results overhang and orientation method

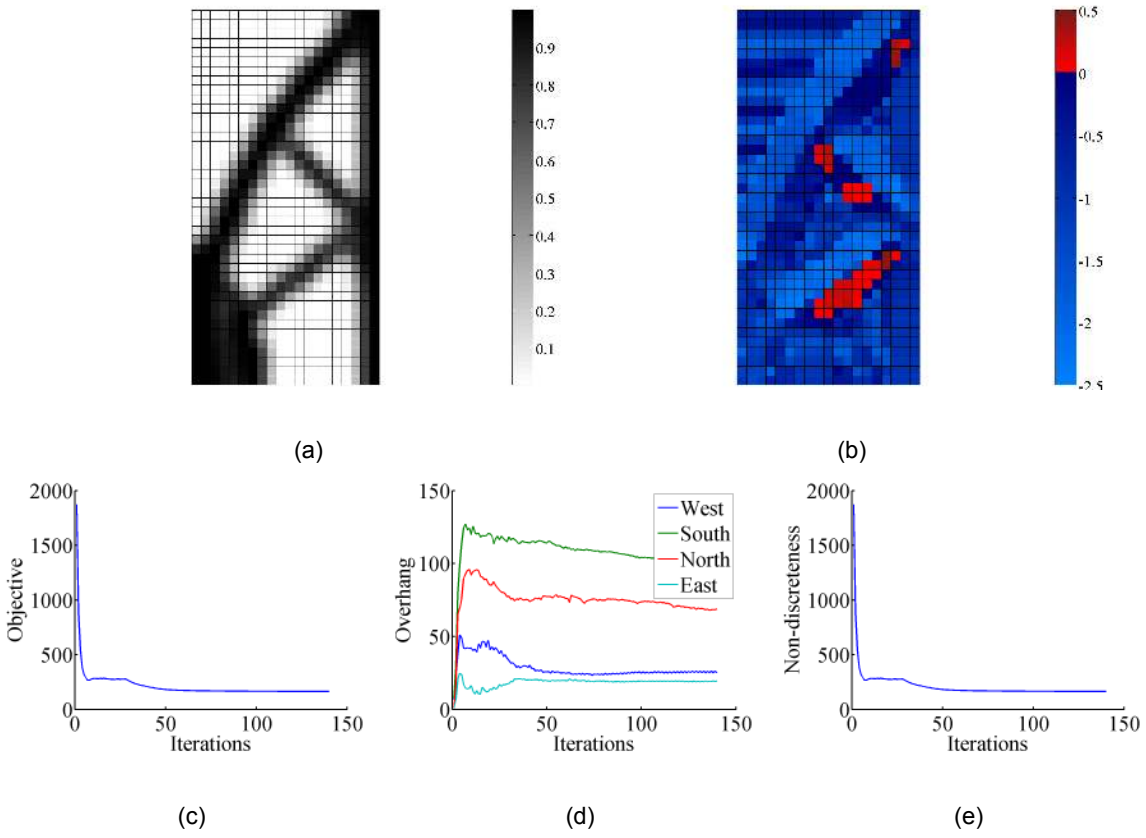

Figure C.1: Results of the overhang restriction including variable orientation with four different directions tested on the MBB beam. a) Density field; b) Constraint field; c) Convergence; d) Maximum overhang constraint value; e) Non-discreteness.

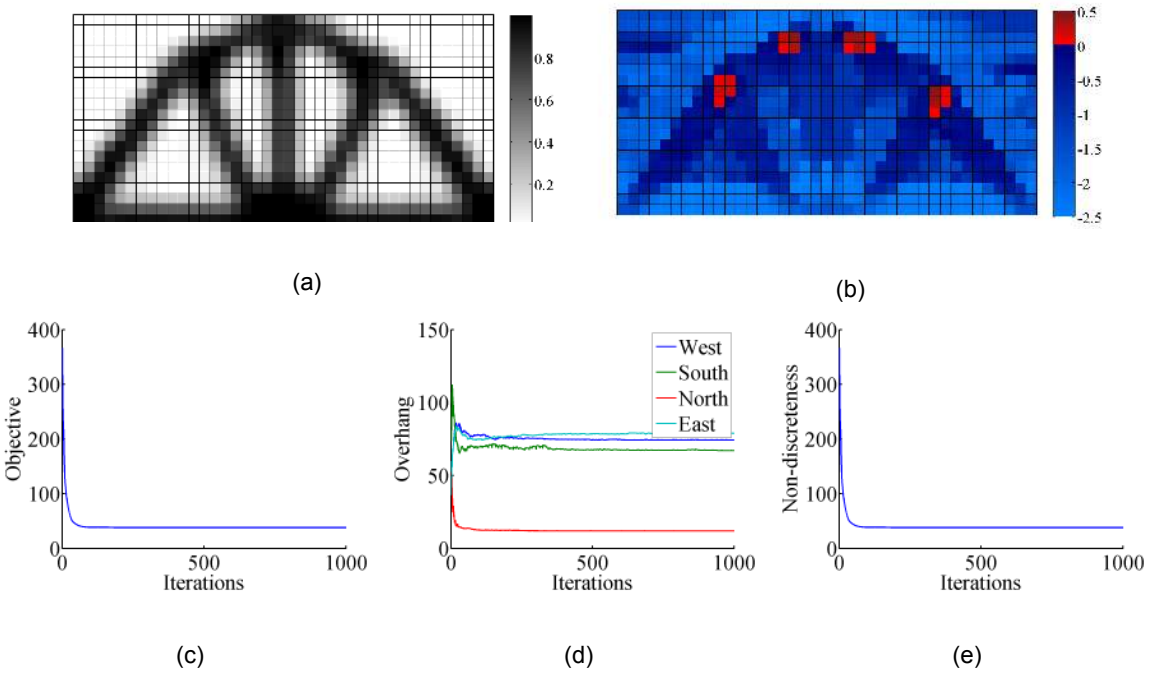

Figure C.2: Results of the overhang restriction including variable orientation with four different directions tested on the bridge problem. a) Density field; b) Constraint field; c) Convergence; d) Maximum overhang constraint value; e) Non-discreteness.

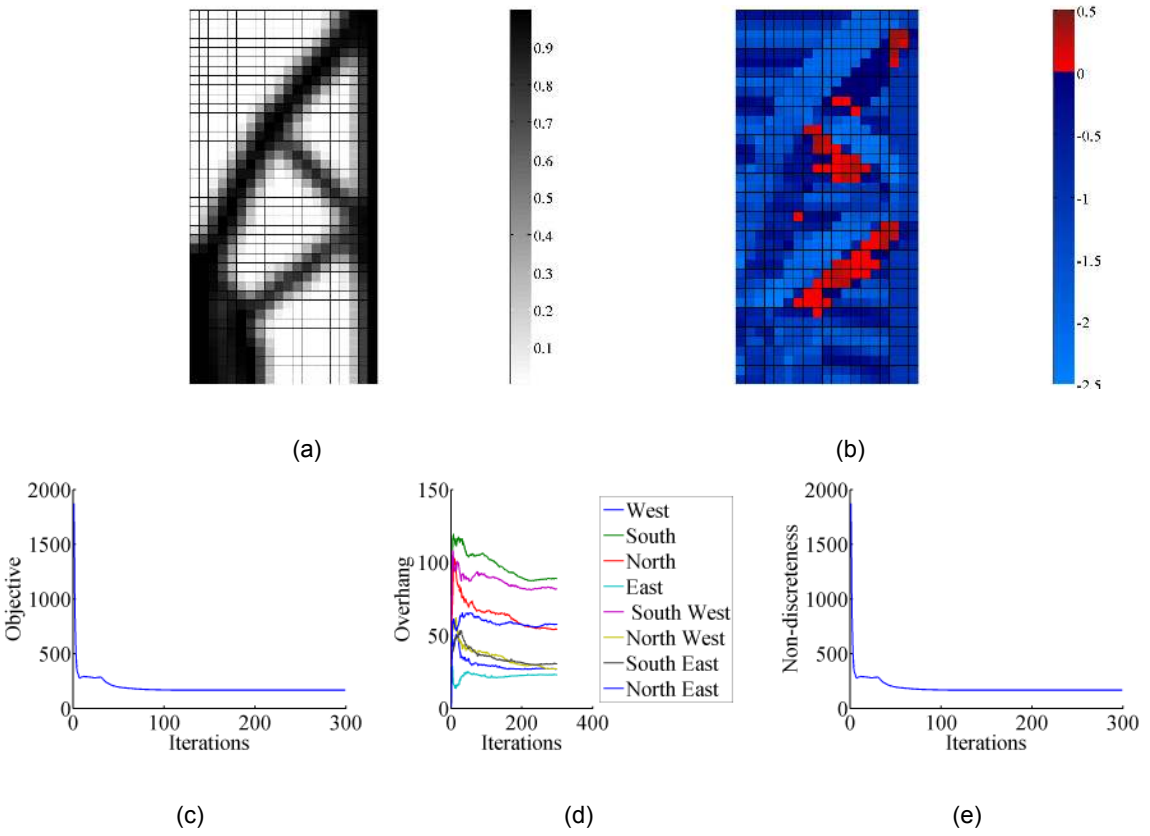

Figure C.3: Results of the overhang restriction including variable orientation with eight different directions tested on the MBB beam. a) Density field; b) Constraint field; c) Convergence; d) Maximum overhang constraint value; e) Non-discreteness.

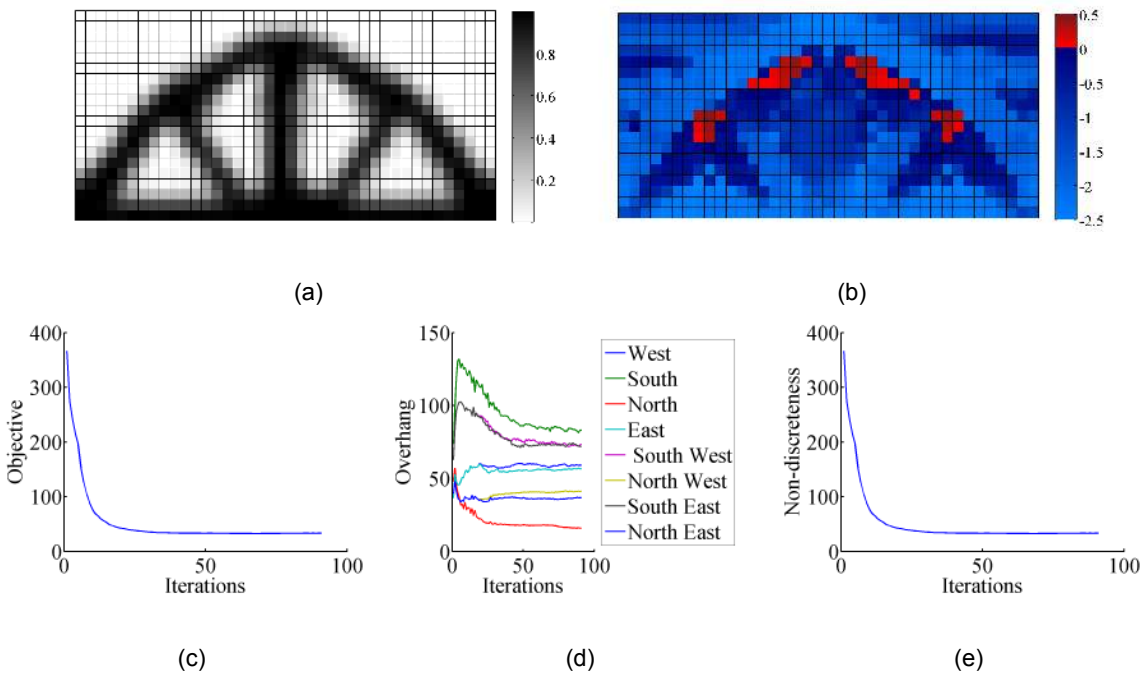

Figure C.4: Results of the overhang restriction including variable orientation with eight different directions tested on the bridge problem. a) Density field; b) Constraint field; c) Convergence; d) Maximum overhang constraint value; e) Non-discreteness.

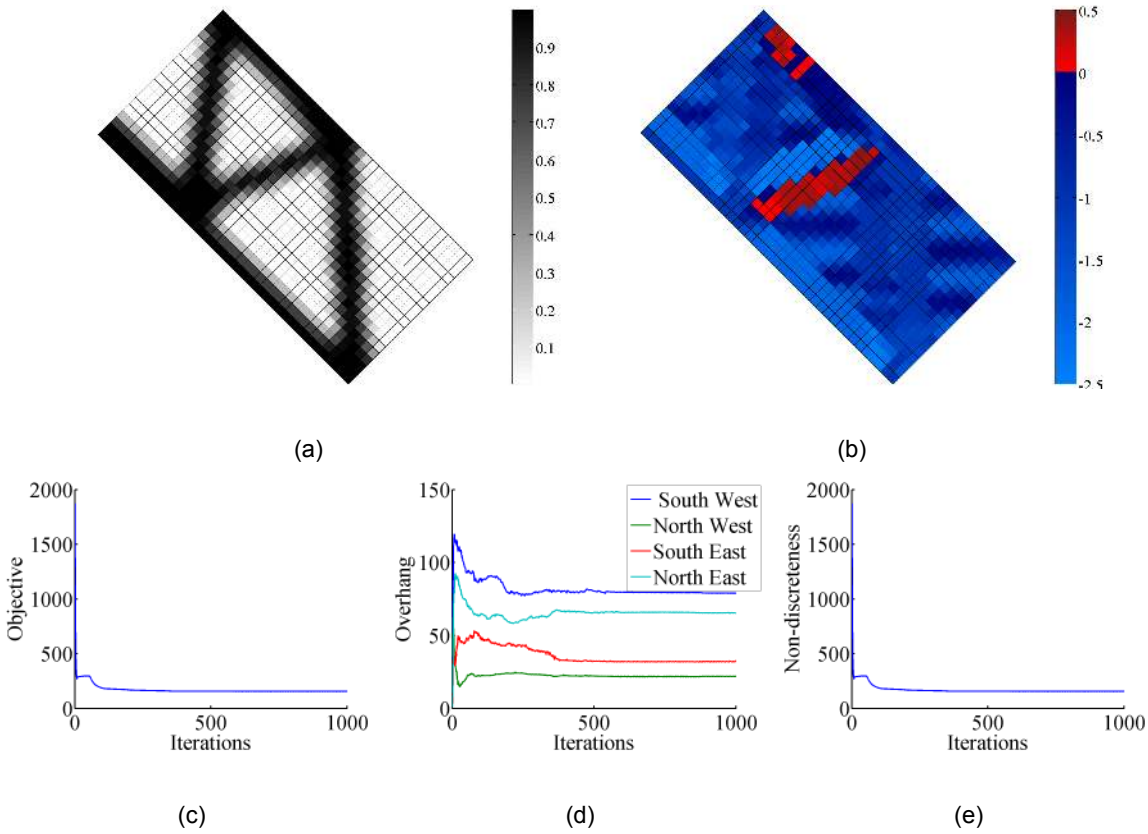

Figure C.5: Results of the overhang restriction including variable orientation with the four diagonal directions tested on the MBB beam. a) Density field; b) Constraint field; c) Convergence; d) Maximum overhang constraint value; e) Non-discreteness.

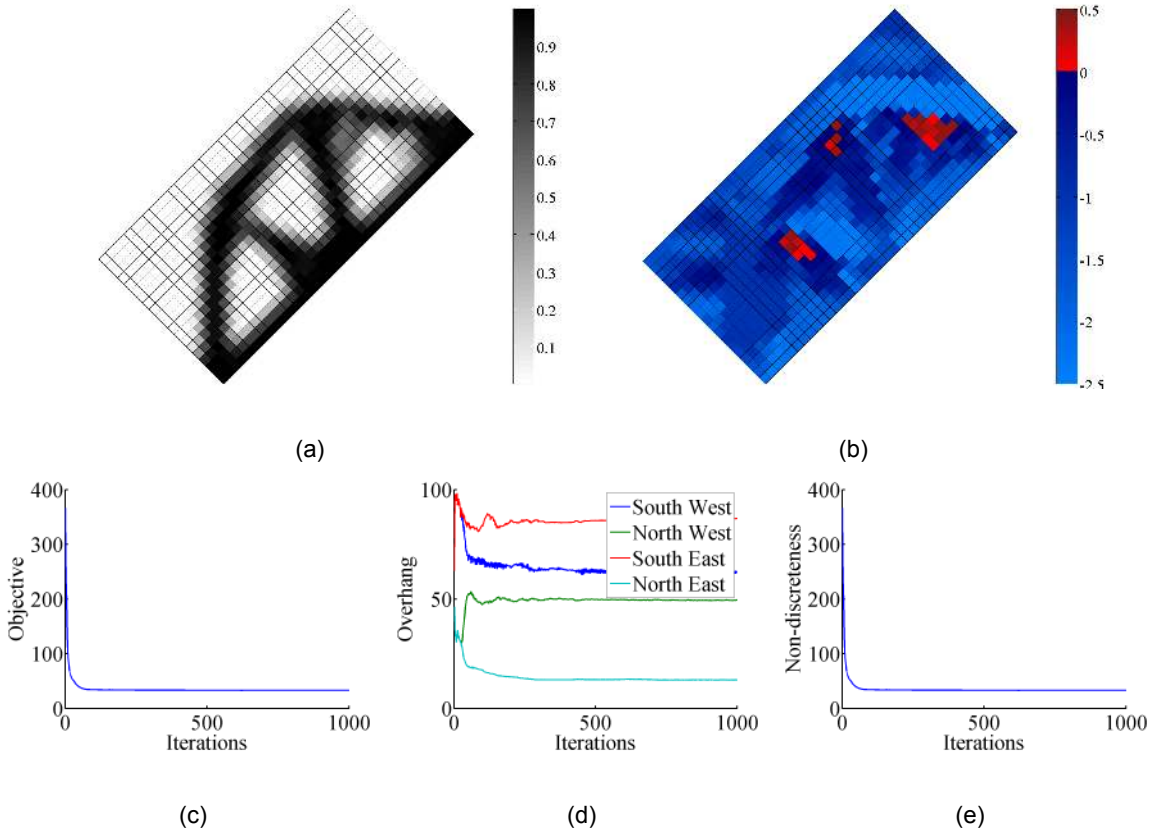

Figure C.6: Results of the overhang restriction including variable orientation with the four diagonal directions tested on the bridge problem. a) Density field; b) Constraint field; c) Convergence; d) Maximum overhang constraint value; e) Non-discreteness.

D

Results overhang and orientation method with scaled cost function

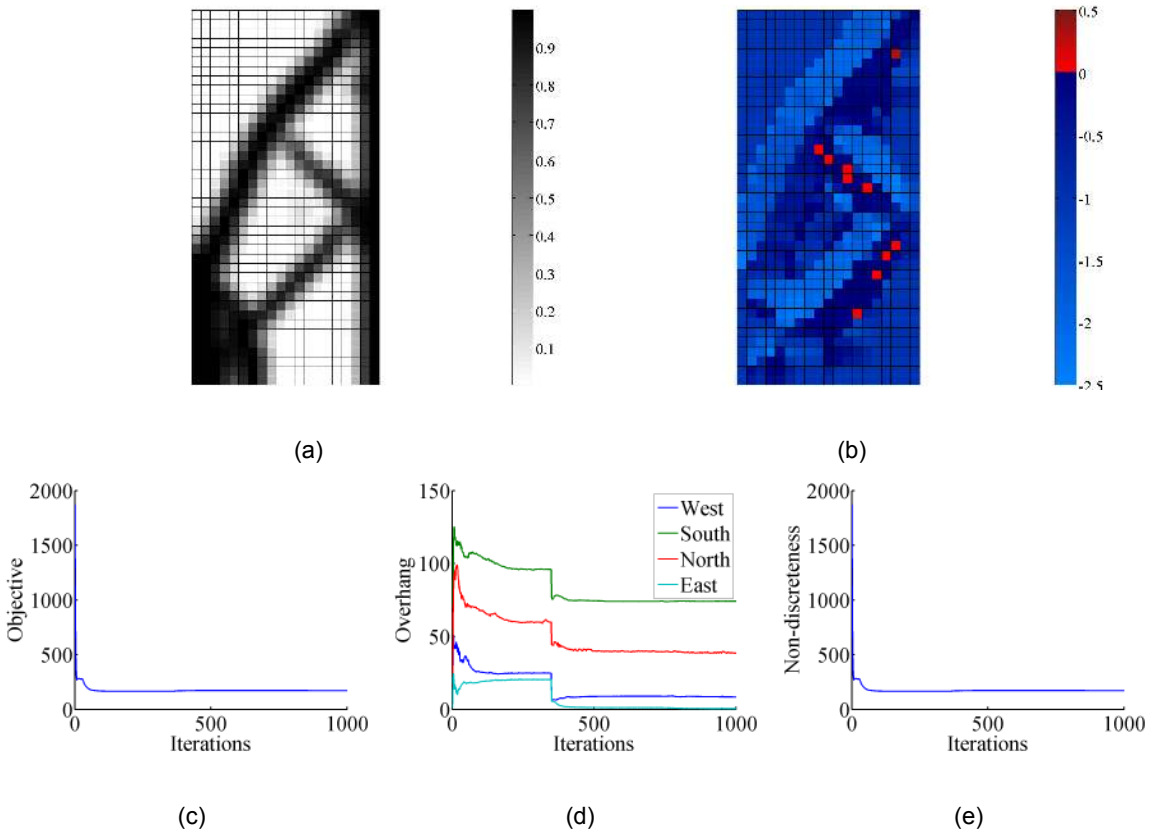

Figure D.1: Results of the overhang restriction including variable orientation with four different directions tested on the MBB beam. In this example the scaling factor for the cost of overhang is increased by a factor 10 during the optimisation after 350 iterations. This is clearly seen from the sudden drop in the overhang measures (subfigure d). The overhang in the final design is strongly reduced but still not completely eliminated. For this, an even higher scaling would be necessary. Important to mention, with a larger scaling factor the accurateness of the approximation of the ramp function becomes important. The ramp parameter is for this example increased to 100. a) Density field; b) Constraint field; c) Convergence; d) Maximum overhang constraint value; e) Non-discreteness.

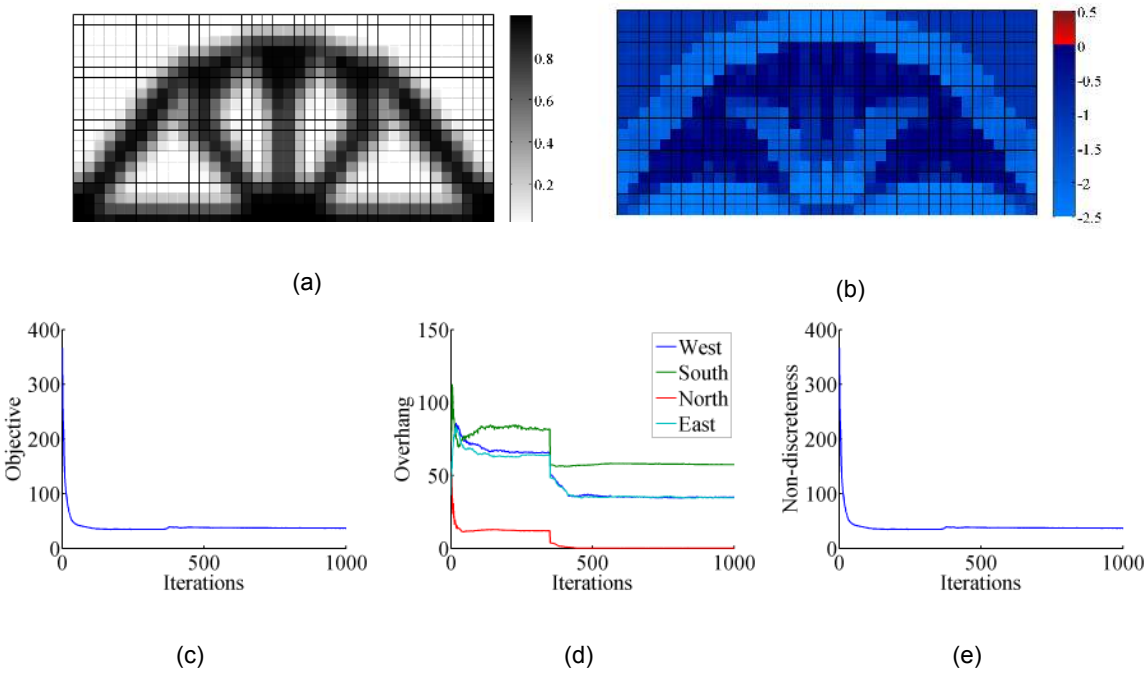

Figure D.2: Results of the overhang restriction including variable orientation with four different directions tested on the bridge problem. In this example the scaling factor for the cost of overhang is increased by a factor 10 during the optimisation after 350 iterations. This is clearly seen from the sudden drop in the overhang measures (subfigure d). The overhang in the final design is completely eliminated. Furthermore, it is seen that the objective increases slightly (subfigure c) after 350 iterations. Important to mention, with a larger scaling factor the accurateness of the approximation of the ramp function becomes important. The ramp parameter is for this example increased to 100. a) Density field; b) Constraint field; c) Convergence; d) Maximum overhang constraint value; e) Non-discreteness.

Bibliography

[1] Guido AO Adam and Detmar Zimmer. Design for additive manufacturing - element transitions and aggregated structures. *CIRP Journal of Manufacturing Science and Technology*, 7(1):20–28, 2014.

[2] Shigeru Ando. Consistent gradient operators. *Pattern Analysis and Machine Intelligence, IEEE Transactions on*, 22(3):252–265, 2000.

[3] Erik Andreassen, Anders Clausen, Mattias Schevenels, Boyan S Lazarov, and Ole Sigmund. Efficient topology optimization in matlab using 88 lines of code. *Structural and Multidisciplinary Optimization*, 43(1):1–16, 2011.

[4] Eleonora Atzeni and Alessandro Salmi. Economics of additive manufacturing for end-usable metal parts. *The International Journal of Advanced Manufacturing Technology*, 62(9-12):1147–1155, 2012.

[5] M Badrossamay and THC Childs. Further studies in selective laser melting of stainless and tool steel powders. *International Journal of Machine Tools and Manufacture*, 47(5):779–784, 2007.

[6] Martin Philip Bendsøe and Ole Sigmund. *Topology optimization: theory, methods and applications*. Springer, 2003.

[7] Roger Bourne. *Fundamentals of digital imaging in medicine*. Springer, 2010.

[8] D. Brackett, I. Ashcroft, and R. Hague. Topology optimization for aditive manufacturing. In *Proceedings of the 24th Solid Freeform Fabrication Symposium (SFF 11)*, 2011.

[9] F Calignano. Design optimization of supports for overhanging structures in aluminum and titanium alloys by selective laser melting. *Materials & Design*, 2014.

[10] Stijn Clijsters, Tom Craeghs, and Jean-Pierre Kruth. A priori process parameter adjustment for slm process optimization. *Innovative developments on virtual and physical prototyping*, pages 553–560, 2012.

[11] M Cloots, AB Spierings, and K Wegener. Assessing new support minimizing strategies for the additive manufacturing technology slm. In *Solid Freeform Fabrication Symposium (Austin, Texas, 2013), http://www. inspire. ethz. ch/irpd/publications/index_EN*, 2013.

[12] Anton Michiel Driessen. Topology optimisation for additive manufacturing. 2015.

[13] Andrew T Gaynor and James K Guest. Topology optimization for additive manufacturing: Considering maximum overhang constraint. AIAA/ISSMO Multidisciplinary Analysis and Optimization Conference, 2014.

[14] Ian Gibson, David W Rosen, Brent Stucker, et al. *Additive manufacturing technologies*. Springer, 2010.

[15] James K Guest, JH Prévost, and T Belytschko. Achieving minimum length scale in topology optimization using nodal design variables and projection functions. *International Journal for Numerical Methods in Engineering*, 61(2):238–254, 2004.

[16] Nannan Guo and Ming C Leu. Additive manufacturing: technology, applications and research needs. *Frontiers of Mechanical Engineering*, 8(3):215–243, 2013.

[17] Ahmed Hussein, Liang Hao, Chunze Yan, and Richard Everson. Finite element simulation of the temperature and stress fields in single layers built without-support in selective laser melting. *Materials & Design*, 52:638–647, 2013.

[18] Ahmed Hussein, Liang Hao, Chunze Yan, Richard Everson, and Philippe Young. Advanced lattice support structures for metal additive manufacturing. *Journal of Materials Processing Technology*, 213(7):1019–1026, 2013.

[19] Martin Leary, Luigi Merli, Federico Torti, Maciej Mazur, and Milan Brandt. Optimal topology for additive manufacture: A method for enabling additive manufacture of support-free optimal structures. *Materials & Design*, 63:678–690, 2014.

[20] JRRA Martins and Nicholas MK Poon. On structural optimization using constraint aggregation. In *VI World Congress on Structural and Multidisciplinary Optimization WCSMO6, Rio de Janeiro, Brasil*, 2005.

[21] *Optimization Toolbox*. MatLab, r2015b edition, September 2015.

[22] Peter Mercelis and Jean-Pierre Kruth. Residual stresses in selective laser sintering and selective laser melting. *Rapid Prototyping Journal*, 12(5):254–265, 2006.

[23] J París, F Navarrina, I Colominas, and M Casteleiro. Block aggregation of stress constraints in topology optimization of structures. *Advances in Engineering Software*, 41(3):433–441, 2010.

[24] Nicholas MK Poon and Joaquim RRA Martins. An adaptive approach to constraint aggregation using adjoint sensitivity analysis. *Structural and Multidisciplinary Optimization*, 34(1):61–73, 2007.

[25] Thomas A Poulsen. A new scheme for imposing a minimum length scale in topology optimization. *International Journal for Numerical Methods in Engineering*, 57(6):741–760, 2003.

[26] IA Roberts, CJ Wang, R Esterlein, M Stanford, and DJ Mynors. A three-dimensional finite element analysis of the temperature field during laser melting of metal powders in additive layer manufacturing. *International Journal of Machine Tools and Manufacture*, 49(12):916–923, 2009.

[27] Hakan Guray Senel. Gradient estimation using wide support operators. *Image Processing, IEEE Transactions on*, 18(4):867–878, 2009.

[28] M. Reuben Serphos. Incorporating am-specific manufacturing constraints into topology optimization. Master's thesis, Delft University of Technology, 2014.

[29] Ole Sigmund. Morphology-based black and white filters for topology optimization. *Structural and Multidisciplinary Optimization*, 33(4-5):401–424, 2007.

[30] Ole Sigmund and Joakim Petersson. Numerical instabilities in topology optimization: a survey on procedures dealing with checkerboards, mesh-dependencies and local minima. *Structural optimization*, 16(1):68–75, 1998.

[31] G. Strano, L. Hao, R. M. Everson, and K. E. Evans. A new approach to the design and optimisation of support structures in additive manufacturing. *The International Journal of Advanced Manufacturing Technology*, 2013.

[32] Krister Svanberg. The method of moving asymptotes - a new method for structural optimization. *International journal for numerical methods in engineering*, 24(2):359–373, 1987.

[33] Daniel Thomas. *The Development of Design Rules for Selective Laser Melting*. PhD thesis, University of Wales Institute, Cardiff, 2009.

[34] Matthew Tomlin and Jonathan Meyer. Topology optimization of an additive layer manufactured aerospace part. In *Proceeding of the 7th Altair CAE technology conference*, pages 1–9, 2011.

[35] J A van Toor. A knowledge based system to support design for selective laser meltiing. Master's thesis, Delft Univesity of Technology, 2014.

[36] Ben Vandenbroucke and Jean Pierre Kruth. Selective laser melting of biocompatible metals for rapid manufacturing of medical parts. *Rapid Prototyping Journal*, 13(4):196–203, 2007.

[37] Frederik Verhaeghe, Tom Craeghs, Jeroen Heulens, and Lieven Pandelaers. A pragmatic model for selective laser melting with evaporation. *Acta Materialia*, 57(20):6006–6012, 2009.

[38] Di Wang, Yongqiang Yang, Ziheng Yi, and Xubin Su. Research on the fabricating quality optimization of the overhanging surface in slm process. *The International Journal of Advanced Manufacturing Technology*, 65(9-12):1471–1484, 2013.

[39] Di Wang, Yongqiang Yang, Manhui Zhang, Jianbin Lu, Ruicheng Liu, and Dongming Xiao. Study on slm fabrication of precision metal parts with overhanging structures. In *Assembly and Manufacturing (ISAM), 2013 IEEE International Symposium on*, pages 222–225. IEEE, 2013.